GAIN SCHEDULING CONTROLLER FOR AIRCRAFT WITH MASS AND INERTIA VARIATION

by

EUNYOUNG KIM

Presented to the Faculty of the Graduate School of
The University of Texas at Arlington in Partial Fulfillment
of the Requirements
for the Degree of

DOCTOR OF PHILOSOPHY

THE UNIVERSITY OF TEXAS AT ARLINGTON

May 2017

To my parents

who set the example and who made me who I am.

ACKNOWLEDGEMENTS

I would like to thank the University of Texas at Arlington for giving me the opportunity to develop my research and further my knowledge in the field of Aerospace Engineering.

I would like to express both my gratitude and admiration to my supervising professor Dr. Atilla Dogan who took me under his wing and supported me with his guidance, patience, and insight during the course of my master and doctoral studies.

I am grateful to Dr. Alan Bowling, Dr. Chaoqun Liu, Dr. Kamesh Subbarao, and Dr. Wen Chan for their interest in my research and for agreeing to serve on my dissertation defense committee.

I would like to express special thanks to my family and friends who have supported me emotionally, intellectually, financially in pursuing my dreams.

May 08, 2017

ABSTRACT

GAIN SCHEDULING CONTROLLER FOR AIRCRAFT
WITH MASS AND INERTIA VARIATION

EunYoung Kim, Ph.D.

The University of Texas at Arlington, 2017

Supervising Professor: Atilla Dogan

Robustness is one of the main control design requirements for aircraft control. Robustness is sought in the stability and performance of closed loop system against various factors such as disturbance, measurement error, modeling error or un-modeled dynamics. In aircraft control design, it is common to assume that the mass and inertia properties of aircraft are constant. Further, aircraft is assumed to have symmetry in its mass distribution relative to its mid-vertical plane. There are, however, cases where the aircraft mass changes rapidly, most notably in aerial refueling operation. The mass change also results in changes in the inertia matrix. An aircraft may also lose its mass symmetry in the case of, for example, asymmetric fuel loading or internal fuel transfer between fuel tanks. If a control design is carried out based on a specific mass and inertia configuration, the stability and performance of the closed loop system may degrade when the aircraft flies with a different configuration. This research effort focuses on addressing this issue in aerial refueling and formation flight by employing gain scheduling based on the aircraft mass and inertia configuration. The fuel mass in each fuel tank is considered as gain scheduling variables in addition

to the ones associated with aircraft dynamics such as airspeed and turn rate. The first step of this research is to determine the number of nominal flight conditions to be included in the gain scheduling control design. Eigenvalue and Bode plot analyses are carried out based on the linearized equations of motion for various flight conditions, and symmetric and asymmetric fuel mass configurations. To reduce the number of cases included in the gain scheduling, "similar" cases are combined. An LQR-based MIMO (Multi Input Multi Output) integral control is designed for each nominal flight and mass configuration. An interpolation scheme based on the "mass distance" is developed to combine this linear controllers into the gain scheduling controller. The "mass distance" is defined as the norm of the differences between the current fuel tank amounts and those of each nominal mass configuration. This gain scheduling controller is implemented in aerial refueling simulation for a tailless delta wing aircraft with thrust vectoring capability. The simulation environment includes the 6-DOF models of both tanker and receiver, mass and inertial variation of the receiver aircraft in terms of the fuel mass in each fuel tank, aerodynamic coupling due to the tanker wake induced nonuniform wind. The controller of the tanker aircraft is to fly the aircraft at commanded altitude, speed, and turn rate. The gain scheduling controller of the receiver aircraft is to track the commanded position relative to the body frame of the tanker aircraft. The receiver controller was tuned in three control allocation cases: (1) no thrust vectoring; only aerodynamic control effects in use, (2) both aerodynamic effectors and thrust vectoring in use, and (3) no elevator or rudder used; only thrust vectoring and aileron in use. The performance of the gain scheduling controller is evaluated through the aerial refueling maneuver when the receiver moves between the observation position, point on the side and behind the tanker, and the refueling position, a point right behind and slightly below the tanker. The simulation results first of all demonstrates that a linear controller designed based on a nominal

flight condition and mass configuration cannot safely complete the refueling maneuver when the aircraft has a different mass configuration. The simulation results further shows that the gain scheduling controller employing mass configuration as additional scheduling variables can successfully carry out the refueling maneuver with various symmetric and asymmetric fuel tank configuration.

TABLE OF CONTENTS

ACKNOWLEDGEMENTS iv

ABSTRACT v

LIST OF ILLUSTRATIONS x

LIST OF TABLES xiv

Chapter Page

1. INTRODUCTION 1

1.1 Motivation 1

1.2 Problem Statement 1

1.3 Literature Review 2

1.3.1 Effect of Mass and Inertia Variation on Aircraft Control . . . 2

1.3.2 Gain Scheduling Methods in Aircraft Control 4

1.4 Prior Research 12

1.5 Original Contributions 13

1.6 Dissertation Organization 15

2. AIRCRAFT MODELS 16

2.1 Tanker Aircraft 16

2.1.1 Aircraft Description 16

2.1.2 Equations of Motion 17

2.1.3 Engine Model 22

2.2 Receiver Aircraft 22

2.2.1 Aircraft Description 23

2.2.2 Equations of Motion 24

2.2.3 Engine Model 28
2.2.4 Actuator Model 28
2.3 Modeling the Vortex and Its Effect 32
3. CONTROL DESIGN 34
3.1 Tanker Aircraft 34
3.1.1 Requirements 34
3.1.2 Flight Cases Analysis 35
3.1.3 Gain Scheduling Controller 37
3.2 Receiver Aircraft 40
3.2.1 Requirements 41
3.2.2 Nominal Condition Analysis 42
3.2.3 Linearization 44
3.2.4 Gain Scheduling Based on Flight Conditions 53
3.2.5 Determining Number of Nominal Conditions 58
4. MOTIVATION 64
5. GAIN SCHEDULING BASED ON FUEL MASS CONFIGURATION . . . 76
6. SIMULATION RESULTS 80
7. CONCLUSION AND FUTURE WORK 93
Appendix
A. NOMINAL CONDITIONS OF THE RECEIVER AIRCRAFT 97
B. EIGENVALUES OF THE RECEIVER AIRCRAFT 101
C. STRAIGHT LEVEL FLIGHT EIGENVALUES COMPARISON 114
D. TURNING FLIGHT EIGENVALUES COMPARISON 119
REFERENCES 128
BIOGRAPHICAL STATEMENT 135

LIST OF ILLUSTRATIONS

Figure		Page
2.1	Receiver aircraft with its fuel tanks [26]	29
2.2	Initial condition for lumped mass position vector [26]	30
2.3	Two-view diagram of fuel tank 1 [26]	31
2.4	Trailing vortex from the wings and horizontal tail	32
3.1	State feedback and integral control structure	44
3.2	Loci of the eigenvalues as the amount of fuel changes in tank 2, 3, and 4, and tank 1 is empty in cruise condition	45
3.3	Zoomed loci of the eigenvalues as the amount of fuel changes in tank 2, 3, and 4, and tank 1 is empty in cruise condition	46
3.4	Loci of the eigenvalues as the amount of fuel changes in tanks 1, 3, and 4, and tank 2 is empty in steady turn	46
3.5	Zoomed loci of the eigenvalues as the amount of fuel changes in tanks 1, 3, and 4, and tank 2 is empty in steady turn	47
3.6	Loci of the eigenvalues as the amount of fuel changes in all tanks in cruise	47
3.7	Zoomed loci of the eigenvalues as the amount of fuel changes in all tanks in cruise	48
3.8	Bode plot for case-56	48
3.9	Bode plot for case-12	49
3.10	Bode plot for case-64	49
3.11	Six Nominal Conditions Based on Flight Condition	54
3.12	Neighboring Nominal Design Conditions	55

3.13 Eigenvalue comparison for case-82 and case-66 60
3.14 Eigenvalue comparison for case-93 and case-91 61
3.15 Bode plots comparison for case-82 and case-66 62
3.16 Bode plots comparison for case-93 and case-91 62
4.1 Commanded and actual trajectory when fuel mass configuration is [0 0 0 0] in control design and [0 0 0 0] in simulation (CA-1) 66
4.2 Control variables when fuel mass configuration is [0 0 0 0] in control design and [0 0 0 0] in simulation (CA-1) 66
4.3 Airspeed, sideslip angle and angle of attack when fuel mass configuration is [0 0 0 0] in control design and [0 0 0 0] in simulation (CA-1) . . 67
4.4 Angular velocity and Euler angles when fuel mass configuration is [0 0 0 0] in control design and [0 0 0 0] in simulation (CA-1) 67
4.5 Translational and rotational wind components when fuel mass configuration is [0 0 0 0] in control design and [0 0 0 0] in simulation (CA-1) 68
4.6 Commanded and actual trajectory when fuel mass configuration is [0 0 0 0] in control design and [1 1 1 1] in simulation (CA-1) 68
4.7 Control variables when fuel mass configuration is [0 0 0 0] in control design and [1 1 1 1] in simulation (CA-1) 69
4.8 Commanded and actual trajectory when fuel mass configuration is [1 1 1 1] in control design and [1 1 1 1] in simulation (CA-2) 69
4.9 Control variables when fuel mass configuration is [1 1 1 1] in control design and [1 1 1 1] in simulation (CA-2) 70
4.10 Commanded and actual trajectory when fuel mass configuration is [1 1 1 1] in control design and [0 0 0 0] in simulation (CA-2) 70
4.11 Control variables when fuel mass configuration is [1 1 1 1] in control design and [0 0 0 0] in simulation (CA-2) 71

4.12 Control variables when fuel mass configuration is [1 1 1 1] in control design and [0 0.1 0.8 0.1] in simulation (CA-1) 71
4.13 Angular velocity and Euler angles when fuel mass configuration is [1 1 1 1] in control design and [0 0.1 0.8 0.1] in simulation (CA-1) 72
4.14 Angular velocity and Euler angles when fuel mass configuration is [1 0.1 0.8 0.1] in control design and [1 0.1 0.8 0.1] in simulation (CA-1) . 72
4.15 Commanded and actual trajectory when fuel mass configuration is [1 0.1 0.8 0.1] in control design and [1 1 1 1] in simulation (CA-1) 73
6.1 Commanded and actual trajectory when fuel mass configuration in simulation is [0 0 0 0], (CA-1) 82
6.2 Control variables when fuel mass configuration in simulation is [0 0 0 0], (CA-1) 83
6.3 Airspeed, sideslip angle and angle of attack when fuel mass configuration in simulation is [0 0 0 0], (CA-1) 84
6.4 Angular velocity and Euler angles when fuel mass configuration in simulation is [0 0 0 0], (CA-1) 85
6.5 Control variables when fuel mass configuration in simulation is [0 0 0 0], (CA-2) 86
6.6 Control variables when fuel mass configuration in simulation is [0 0 0 0], (CA-3) 86
6.7 Control variables when fuel mass configuration in simulation is [1 1 1 1], (CA-1) 87
6.8 Angular velocity and Euler angles when fuel mass configuration in simulation is [1 1 1 1], (CA-1) 87
6.9 Control variables when fuel mass configuration in simulation is [1 1 1 1], (CA-2) 88

6.10 Angular velocity and Euler angles when fuel mass configuration in simulation is [1 1 1 1], (CA-2) 88
6.11 Control variables when fuel mass configuration in simulation is [1 1 1 1], (CA-3) 89
6.12 Angular velocity and Euler angles when fuel mass configuration in simulation is [1 1 1 1], (CA-3) 89
6.13 Control variables when fuel mass configuration in simulation is [1 0.1 0.8 0.1], (CA-1) 90
6.14 Airspeed, sideslip angle and angle of attack when fuel mass configuration in simulation is [1 0.1 0.8 0.1], (CA-1) 90
6.15 Control variables when fuel mass configuration in simulation is [1 0 1 0], (CA-1) 91
6.16 Airspeed, sideslip angle and angle of attack when fuel mass configuration in simulation is [1 0 1 0], (CA-1) 91
6.17 Control variables when fuel mass configuration in simulation is [0 1 0 1], (CA-1) 92
6.18 Airspeed, sideslip angle and angle of attack when fuel mass configuration in simulation is [0 1 0 1], (CA-1) 92

LIST OF TABLES

Table		Page
2.1	ICE 101 Configuration and Aerodynamic Data [56]	23
3.1	Flight Cases by Turn rate and Airspeed	38
3.2	Nominal Conditions by Four Receiver Fuel Tanks	45
3.3	Sixteen Receiver Nominal Conditions	63
4.1	Coordinates of Observation and Refueling Position	64
4.2	Control Allocation (CA)	65
4.3	Flight Condition and Fuel Mass Configurations - Control Allocation (CA) case is 1.	65
4.4	Flight Condition and Fuel Mass Configurations - Control Allocation (CA) case is 1.	73
4.5	Flight Condition and Fuel Mass Configurations - Control Allocation (CA) case is 2.	74
4.6	Flight Condition and Fuel Mass Configurations - Control Allocation (CA) case is 2.	74
4.7	Flight Condition and Fuel Mass Configurations - Control Allocation (CA) case is 1.	74
6.1	Flight Condition and Fuel Mass Configurations	81

CHAPTER 1

INTRODUCTION

1.1 Motivation

Robustness is one of the main control design requirements for aircraft control. Robustness is sought in the stability and performance of closed loop system against various factors such as disturbance, measurement error, modeling error or un-modeled dynamics. In aircraft control design, it is common to assume that the mass and inertia properties of aircraft are constant. Further, aircraft is assumed to have symmetry in its mass distribution relative to its mid-vertical plane. There are, however, cases where the aircraft mass changes rapidly, most notably in aerial refueling operation. The mass change also results in changes in the inertia matrix. An aircraft may also lose its mass symmetry in the cases of, for example, asymmetric fuel loading or internal fuel transfer between fuel tanks. In formation flight when an aircraft flies in the wake of another aircraft, internal fuel transfer that changes the inertia properties of the aircraft may be utilized as an alternative trim mechanism. If a control design is carried out based on a specific mass and inertia configuration, the stability and performance of the closed loop system may degrade when the aircraft flies with a different configuration.

1.2 Problem Statement

This research is focused on the aircraft control design when the aircraft mass and inertia properties change rapidly. In this case, the mass and inertia properties of aircraft cannot be assumed to be constant. This research is focused on this issue

in aerial refueling and formation flight by employing gain scheduling based on the aircraft mass and inertia configuration. The gain scheduling controller for the receiver includes mass and inertia variation of the aircraft due to the change in fuel amounts in all fuel tanks, and covers all possible combinations of fuel levels and fuel tanks.

1.3 Literature Review

1.3.1 Effect of Mass and Inertia Variation on Aircraft Control

Standard control design techniques for aerial vehicles mostly have considered the aircraft as a rigid body when a dynamic model is developed. In aircraft control design, it is common to assume that the mass and inertia properties of aircraft are constant. There are, however, cases where the aircraft mass changes rapidly, most notably in aerial refueling operation. The mass change also results in changes in the inertia matrix. As the center of mass of the aerial vehicle changes, caused, for example, by fuel mass change, the difference between the center of mass and center of pressure due to the aerodynamics also changes. This affects the control capability of the aircraft. In prior aerial refueling studies, the mass transfer effect is ignored or treated as disturbance. However, in actual aerial refueling operation, when the aircraft empty body mass is compared to the fuel mass, the fuel mass accounts for a significant fraction and is changed very rapidly over time. Therefore, mass related research needs to be carefully investigated. In aircraft control design, another assumption is that aircraft has symmetry in its mass distribution with respect to its mid-vertical plane. An aircraft may also lose its mass symmetry in the case of, for example, asymmetric fuel loading or internal fuel transfer between fuel tanks. In formation flight when an aircraft flies in the wake of another aircraft, internal fuel transfer that changes the inertia properties of the aircraft may be utilized as an alternate trim mechanism. If

a control design is carried out based on a specific mass and inertia configuration, the stability and performance of the closed loop system may degrade when the aircraft flies with a different configuration. Mass and inertia variation are considered in aerial and space system dynamics and control such as spacecraft [1, 2], helicopter [3], airship [4, 5]. reentry vehicle [6], Unmanned Air Vehicle (UAV) [7], satellite [8], kinetic warhead [9, 10], multibody aeromaneuver vehicle [11], missile [12, 13], smart weapons [14, 15, 16], high supersonic speed vehicles [17], spinning vehicle [18], and underwater vehicles [19]. In [4, 6, 20], internal moving masses are used for weight distribution or mass center modification to influence the response of the airplane control. Moving mass related research is also found in [7, 9, 10, 11, 12, 21, 22, 23] with using center of mass offset. By causing center of mass offset to change the moment of inertia, aerial vehicle exerts inertial forces on the body frame and changes dynamic response. In [1, 2, 22, 23], by positioning the lumped mass within the vehicle, mass balancing is achieved to maintain center of mass position and ultimately to obtain attitude stabilization. Above studies demonstrate the control of aircraft using moving mass within the aircraft. However, this research is focused on the mass and inertia variation in aircraft changes the dynamic characteristics. In [1, 2, 3], mass center estimation is applied to control system to ensure adequate control of movable mass balance. Asymmetric mass distribution of aircraft are discussed in [22, 23, 24, 25, 26]. Ref. [24] described the asymmetry caused by internal fuel transfer in formation flight and Ref. [25] discussed the asymmetry caused by morphing aircraft. Ref. [24] aimed at eliminating the use of aerodynamic control effectors to reduce the induced drag, and proposed two different mechanisms which generate the moment: internal fuel transfer among fuel tanks and thrust variation. They created the rolling moment by transferring fuel among fuel tanks, reduced the aileron use, and saved fuel. Ref. [25] investigated the effect of symmetric and asymmetric span morphing in airplane

and tested it in an Unmanned Aerial Vehicle (UAV) for a loitering mission. Ref. [25] indicated that span morphing leads the aerodynamic and structural change, and these affect the force, moment, and mass properties of the aircraft. Ref. [25] further stated that flight dynamics and control are affected significantly by these changes.

1.3.2 Gain Scheduling Methods in Aircraft Control

1.3.2.1 Application of Gain Scheduling in Vehicle Control

Gain scheduling control methods are widely used for controlling nonlinear systems, especially aerospace vehicles. Some examples include the pitch axis of a missile [27], business jet aircraft control in a longitudinal flight [28], missile autopilot [29], large flexible Engineering Test Satellite VIII (ETS-VIII) [30], pitch-axis autopilot of an air-to-air missile [31], automated surface-to-air missile with dynamics influenced by Mach number and altitude during the flight [32], NASA's Orion control system design for launch abort vehicle [33], F-16 aircraft control with detailed aerodynamic data [34], attitude motion control of the pitch axis dynamics of the X-33 vehicle during ascent for velocities greater than Mach 2 [35], longitudinal motion of the F-18 aircraft [36], autopilot design for a missile pitch-channel control [37], longitudinal flight of Lockheed P2V-7 [38], and unmanned combat air vehicle (UCAV) model of Lockheed Martin's ICE (Innovative Control Effectors) 101-TV [39]. The modern/classical applications of gain scheduling are listed in [31] as jet engines, active suspensions, high-speed drives, missile autopilots, and VSTOL aircraft. Other application areas in addition to aerospace engineering are reel-winding mechanism [40], two-link flexible manipulator system including both rigid body and lightly damped structural mode [41], nonlinear continuous stirred tank reactor CSTR) chemical process [42] and three-level voltage-source inverters (VSI) for high power systems [43].

1.3.2.2 Types of Gain Scheduling Control Design Methods

Gain scheduling design technique has no strict theoretical basis. When gain scheduling technique is used as a nonlinear control method, there are two main approaches of parameterizing linear models: (i) linearization-based method [42, 39, 44, 45, 33, 46, 37] and (ii) linear parameter-varying (LPV) method [27, 30, 35, 36, 38, 40, 41, 45, 46, 47, 28, 31]. In the linearization-based method, the nonlinear model is approximated, through linearization, by multiple linear time invariant models at different operating conditions of choice. In LPV method, the nonlinear model is reformulated as a linear time-varying model [31]. As the first step of linearization-based method, several operating points need to be selected. Generally, these operating points are chosen from equilibrium points within the operating domain of the original nonlinear system. For each operating point, a linear controller is designed, which may require the linearization of the nonlinear model around each operating point. Then each linear controller is connected and formed into a single nonlinear controller. Lawrence and Rugh [45] use a family of linear controllers, each of which is designed based on the linearized plant at each operating point. One of the main requirements for gain scheduled controllers is that the linearized closed loop system at an operating point should have exactly the same properties as the linear controller designed for that operating point. Ref.[46] shows that this linearization property is retained when the discrete-equivalence of the gain scheduled controller via stop-invariant or bilinear transformation techniques is implemented in the sampled-data system implementation. The classical (static) gains are scheduled with variables which parameterize the equilibrium points through a series of equilibrium linearizations. The parameters can be control inputs or slowly-varying states. Dynamic gain seheduling uses fast-varying states. Ref. [39] does the dynamic gain scheduling by applying a trans-

formation to the classical gain schedules. In LPV method, the plant dynamics is reformulated to transform nonlinearities to linear time-varying parameters. These linear time-varying parameters are used as scheduling variables and scheduling is directly performed with the varying parameters of the system. For LPV system based gain scheduling [27, 30, 35, 36, 38, 40, 41, 45, 46, 48, 47, 28, 31], there are different methods to parameterize linear models. The linear models are represented by time-varying state-space matrices that are functions of varying parameters [30]. For LPV systems, the parameter variations is assumed to be independent of the system states. Ref. [35] applies the same method for quasi-LPV systems where the dependency of the parameter variation on the system states is ignored. In classical gain scheduling, it is hard to guarantee the global stability of the closed-loop system over the entire operating domain. The drawbacks of the classical gain scheduling design is found in both linearization-based method and LPV method. Saussie et al.[28] indicate the drawbacks of LPV method. According to them, in LPV technique, the controllers are directly obtained in a LPV format and this form is formulated as Linear Matrix Inequalities (LMI) optimization problems. They state that, with large operating domain, the LPV method cannot guarantee a global stability of the closed loop system because it is hard to conduct LMI optimization problem and the results show unrealistic answers. The linearization-based method has limitations such that the closed-loop stability and performance are assured only around the vicinity of the operating points and the parameter variation cannot be fast. Doyle III et al.[49] indicates that the traditional gain scheduling design takes fixed scheduling variables, so past values, time, and future transitions cannot influence the scheduling variables. When the operating conditions are changed, fixed variables cause the slow variations. Because of these limitations of classical gain scheduling techniques, modern gain scheduling design methods have been developed. Several modern techniques were added to improve the

LPV method. When an aircraft experiences rapid dynamic changes, the operating regions also need to be changed rapidly. However, slow variation condition cannot contain these operation regions in rapid manners [34]. To overcome this difficulty, dynamic gain scheduling with fast gain is proposed [39, 42, 49, 45]. Jones et al. [39] state that fast-varying states are ideal parameters for gain scheduling because aircraft responses are dominated mostly by fast modes and slow modes tend to be damped out by the pilot or automatic control system. Fast gain in dynamic gain scheduling copes with rapid changes throughout the range of operating conditions and overcome the limitation of slow variables. However, hidden coupling terms may appear and cause instability when fast-varying gain is used. In classical gain scheduling, the parameter is either a control input or a slowly-varying state. In dynamic gain scheduling, the fast-varying state is used as a parameter and may introduce unwanted additional dynamics during the partial derivative process in the linearization. Yang et al.[34] explain that dynamic gain scheduling is a control approach of scheduling controller gain with at least one fast-varying state associated with hidden coupling terms and compensating for nonlinearity during rapid maneuvers.

1.3.2.3 Methods to Determine the Number of Operating Points

The number of operating points for the gain scheduling controller requires a tradeoff between the needs for covering the whole operating domain and for keeping the number smaller to have a simpler controller. To determine the number of operating points, in Ref. [33], the variation of mass properties, aerodynamics, and atmosphere with the current nonlinear controller model are considered using Monte Carlo analysis, then design points are determined based on initial altitude, time, and Mach number. In Ref. [37], the Mach number and normal acceleration are chosen as the scheduling variables. The flight envelop is determined based on the limits of the

feasible ranges of the Mach number and normal acceleration. The operating points are determined by dividing the Mach number range into 16 segments and the normal acceleration range into 67 segments.

1.3.2.4 Selection of Scheduling Variables

To determine scheduling variable, Yoon et al.[27] used fixed parameters of normalized vertical acceleration and pitch rate,McNamara et al.[33] use Mach number, altitude and time to schedule parameters, and Fujimori et al.[38] use altitude and flight velocity as gain scheduling parameters. The gain scheduling parameters are selected from Mach number and angle of attack in controlling pitch angle of a missile [28]. Theodoulis and Duc [31] use vertical acceleration and Mach number to control pitch-axis autopilot of an air-air missile. In ref [36], gain scheduling control law is applied to dynamic equations of motion of F-18 aircraft, thus Mach number and altitude variations of the longitudinal flight are used for corresponding to different performance specifications. In [37], constant values of commanded normal acceleration and mach number are chosen as scheduling variables. Gao and Budman [42] consider four parameters for scheduling gain in PI controller. Shamma and Athans [48] present analysis for two types of gain scheduled control for nonlinear plant; scheduling on a reference trajectory and scheduling on the plant output. Stilwell et al. [46] examine the gain scheduling controller with sampled-data implementation. These sampled data is obtained from sample period of the controller input, output, and state. In Ref. [50], angle of attack, roll rate about the velocity vector, and sideslip are selected as gain scheduling variables to design flight control system for a model of the ICE (Innovative Control Effector) fighter aircraft. In Ref. [48] studies effect of the selection of scheduling variables based on reference trajectory versus plant outputs.

1.3.2.5 Linear Control Design Methods Used for Each Operating Point

Linear control design methods used for each operating point are proportional derivative (PD) controller [28, 44], μ-synthesis-based control law and DVDFB (direct velocity and displacement feedback) control law [30], linear quadratic regulator (LQR) approach [33], proportional-integral (PI) controllers [42, 51], linear quadratic regulator and gain scheduling PI controller [43], and state feedback controller [52]. In Ref. [30] use μ-synthesis-based control law to treat model variation due to paddle rotation as structured uncertainty of the satellite system, and DVDFB (direct velocity and displacement feedback) control law to improve tracking performance. In Ref. [31], proportional-integral/proportional-type controllers are applied to compute the pitch-axis autopilot of an air-air missile. In Ref. [32], Linear quadratic Gaussian with loop transfer recovery (LQG/LTR) gain scheduling controller is applied to design surface-to-air missile autopilot. In [33], once the simplified linear models at each design point have been created, the PID gain is tuned by using linear quadratic regulator (LQR) approach. In ref [42], proportional-integral (PI) controllers are used for nonlinear chemical processes. Alepuz et al. [43] suggest linear quadratic regulator to control any state variable of the converter in small and large signal operation. They explain that modeling error and input saturation are explicitly incorporated into the analysis with gain scheduling PI controller by reformulating a variable gain. For the linear control design for each operating point in Ref [37], first order transfer functions are chosen as controller transfer functions. The coefficients of the transfer functions are parameterized by the gain scheduling variables. Ref. [39] uses LQR-design method to determine the state-feedback gain while continuation tailoring is used to determine feed-forward gain schedule to achieve desired steady state behavior. In Ref. [45], an output feedback and integral-error controller is designed for each operating point to

have zero steady-state error. In Ref. [48], each operating point, a finite-dimensional compensator is assumed to be designed to stabilize the closed loop system.

1.3.2.6 Methods to Construct the Final Nonlinear Form of Gain Scheduling Controller

This section introduces several methods used to put all the linear controllers together to construct the final nonlinear form of gain scheduling controller. Since LPV method does not require interpolation process, these are only for the linearization-based method. Methods used to put all the linear controllers together to construct the final nonlinear form of gain scheduling controller, Ref. [33] constructs tables which are based on scheduling variables, tracking gain table and settling gain table, and gains are interpolated individually for different flight phases. In Ref. [37], the linear controller coefficients are designed at the boundaries of the design region, and determined by the upper and lower values of the gain scheduling variables. For the flight conditions inside the operating region, a second order polynomial of gain scheduling variables is used to interpolate the gains of the controller. In Ref. [43], the linear controllers are designed for each operating points corresponding to each design interval. The final gain scheduling controller consists of the linear controllers with a switching scheme, which is based on the boundaries between the design intervals. In Ref. [44], linear controller designed for each operating point is parameterized in terms of the scheduling variables. This leads to a gain scheduling controller that does not require interpolation between operating points. In Ref. [42], linear interpolation function based on four parameters is used to construct the final nonlinear form of gain scheduling controller. The values of those parameters are determined through the optimization method.

1.3.2.7 Methods to Analyze Stability and Performance Characteristics of the Closed Loop System

There are two approaches to guarantee the stability and performance of the closed loop system. One is using control design method [32, 39]. In this case, control design process guarantees the stability of the system. In Ref.[32], global robustness and performance of the system is guaranteed under parameter-varying conditions by applying time-varying Kalman filter (TVKF). Another is using simulation models[43, 45, 33, 37, 32]. Once the control design is completed, the closed-loop system performance at certain flight conditions within the flight envelope is demonstrated by simulation. In Ref. [32], two different simulations are carried out. In static simulations, the scheduling variables, Mach number and altitude, are fixed representing a specific operating condition, and the closed loop response is obtained to evaluate the performance of the gain scheduling controller. This simulation experiment is repeated for various values of Mach number and altitude, representing the four cornets of the flight envelope. In the dynamic simulations, the closed loop performance is demonstrated while the Mach number and altitude are varying according to defined functions of time. In Ref. [33], the gains are tested and performance requirements are evaluated in a non-linear simulation using flight software of Orion vehicle. In Ref. [37], the gain scheduling controller is implemented in a nonlinear simulation and various simulation cases within the operating ranges are run to show the performance of the closed loop system. In Ref. [39], the local stability achieved through LQR design method is expanded globally by using bifurcation diagrams of the nonlinear system in the continuation-based design method. In Ref. [43], Matlab and Simulink simulation results are used to validate controller design. In Ref. [44], the gain scheduling controller is guaranteed to preserve the closed-loop eigenvalues

and the input-output relation locally at each operating point. In Ref. [42], to analyze stability and performance characteristics of the closed loop system, conditions are set as linear matrix inequalities (LMIs) for nonlinear processes, and LMI-based tests are derived to analyze and guarantee the closed-loop stability and performance. Also, by comparing gain-scheduled PI controllers and linear PI controllers, gain-scheduled PI controllers show better performance.

1.4 Prior Research

In this research, gain scheduling based on mass variation is developed using the previously developed dynamic model [26] and control method [53]. The mathematical model of tanker is formulated relative to the inertial frame and the mathematical model of receiver is derived relative to the tanker aircraft. The separate dynamic models of tanker and receiver aircraft are implemented in the simulation of the standard racetrack maneuver in aerial refueling operation. An integrated simulation environment is developed to take into account tanker maneuvers, motion of the receiver relative to the tanker and the aerodynamic coupling due to the trailing wake-vortices of the tanker. The full 6-DOF nonlinear dynamics of the tanker aircraft is used in simulation. In the receiver's equations of motion, mathematical quantities contain the physical parameters of the receiver aircraft, and its fuel tanks and wind effects. These equations are used in simulation. Equations of motion for the receiver aircraft have the properties of time-varying mass and inertia associated with fuel transfer, and the vortex induced wind effect from the tanker. The equations of motion are implemented in an integrated simulation environment with feedback controllers for tanker and receiver aircraft. The feedback controller for the receiver is to fly the receiver aircraft along a desired trajectory defined relative to the tanker. The controller for the tanker is to fly the aircraft at the commanded altitude, airspeed, and turn

rate. Both controllers are designed with LQR-based MIMO state-feedback and integral control method. The tanker aircraft model represents KC-135R and the receiver aircraft model is for a tailless fighter aircraft with innovative control effectors (ICE) and thrust vectoring capability. Thus, the receiver aircraft has six control variables (three control effectors, throttle setting and two thrust vectoring angles) while the tanker has four standard control variables (three control surfaces and throttle setting). Since the receiver has redundant control variables, various control allocation schemes are investigated for trajectory tracking and station-keeping while the tanker flies in various racetrack maneuvers with different commanded turn rate. Mass and inertia variation of the receiver aircraft is modeled by point-masses with varying mass and positions, representing fuel in each of four fuel tanks. Gain scheduling in both receiver and tanker controllers are performed with scheduling variables of airspeed and turn rate based on six nominal cases of two different airspeeds and three turn rates while the mass/inertia properties are assumed to be fixed in control design [26],[53].

1.5 Original Contributions

This research effort focuses on addressing the issue of mass/inertia variation in aerial refueling and formation flight by expanding the gain scheduling scheme to include fuel mass in each fuel tank among the scheduling variables in addition to airspeed and turn rate. The fuel mass in each fuel tank is considered as state variable in addition to the standard states associated with aircraft dynamics. All possible fuel distributions, both symmetric and asymmetric, are considered in trim analyses of the aircraft in straight level and steady-turn flight conditions at constant altitude and constant airspeed. The gain scheduling controller design requires the definition of trim conditions in terms of the fuel amounts in fuel tanks for each set of turn rate and speed. The three turn rates (zero, right turn, and left turn) and two speed

values result in six nominal flight conditions, as done with the tanker aircraft. For the receiver aircraft, the number of mass/inertia configurations to be included in the set of trim conditions should be determined. The objective is to keep the number of such fuel tank configurations small while making sure that they will cover the whole span of the mass/inertia variation of the receiver aircraft. To reduce the number of cases included in the gain scheduling, similar cases are combined. In each possible case, the equations of motion are linearized to obtain the state and control matrices. From the state and control matrices, various transfer functions are computed. Similarity of the cases are determined based on the eigenvalue locations of the state matrix and Bode plots of the transfer functions. An LQR-based MIMO (Multi Input Multi Output) integral control is designed for each nominal flight and mass configuration. An interpolation scheme based on the "mass distance" is developed to combine this linear controllers into the gain scheduling controller. The "mass distance" is defined as the norm of the differences between the current fuel tank amounts and those of each nominal mass configuration. This gain scheduling controller is implemented in aerial refueling simulation for a tailless delta wing aircraft with thrust vectoring capability. The receiver controller was tuned in three control allocation cases: (1) no thrust vectoring; only aerodynamic control effects in use, (2) both aerodynamic effectors and thrust vectoring in use, and (3) no elevator or rudder used; only thrust vectoring and aileron in use. The performance of the gain scheduling controller is evaluated through the aerial refueling maneuver when the receiver moves between the observation position, point on the side and behind the tanker, and the refueling position, a point right behind and slightly below the tanker. The simulation results first of all demonstrates that the a linear controller designed based on a nominal flight condition and mass configuration cannot safely complete the refueling maneuver when the aircraft has a different mass configuration. The simulation results further

shows that the gain scheduling controller employing mass configuration as additional scheduling variables can successfully carry out the refueling maneuver with various symmetric and asymmetric fuel tank configuration.

1.6 Dissertation Organization

This Dissertation is organized as follows. Chapter 2 presents tanker and receiver aircraft models which include physical parameters, equations of motion, engine model, and actuator model. Also tanker aircraft's vortex model and its effect on the receiver dynamics will be explained in this section. Chapter 3 presents control design of receiver and tanker models. Requirements, nominal condition analysis and gain scheduling controller of both aircraft will be introduced. Determinations of the nominal conditions to be included in gain scheduling controller for receiver aircraft using eigenvalues and bode plot analysis will be explained. Chapter 4 demonstrates that the controller that is designed based on a specific mass configuration may not work when the aircraft flies with a different mass configuration. Chapter 5 presents the approach taken to expand the gain scheduling to include the mass configuration of the aircraft. Chapter 6 shows simulation results. Chapter 7 discusses conclusion and future work.

CHAPTER 2

AIRCRAFT MODELS

2.1 Tanker Aircraft

Evaluation of aerial refueling controllers in simulation needs to include full dynamic models of tanker and receiver aircraft. Generally, tanker aircraft flies in a pre-specified racetrack maneuver relative to an inertial frame during the standard aerial refueling operation. The tanker dynamics equations were developed previously [26] and a matrix form of the equations is presented in this section.

2.1.1 Aircraft Description

This section explains physical parameters of the tanker aircraft. A Boeing KC-135 model is used as tanker in this research. KC-135 aircraft has maximum take off weight 322.500 lbs and normal operating weight of 122.500 lbs [54]. KC-135 aircraft has aerial refueling boom which is located at the end of the tanker fuselage. The boom is connected at the tanker fuselage with the boom pivot, and this allows yaw and pitch motion of the boom relative to the fuselage [54]. The extendable portion of the boom is fully retracted inside the boom and extends up to 20 ft outside the boom [54]. At the end of the boom, two control surfaces, called ruddevators, are located. Each of the ruddevator has a 31 in chord and 61 in span, and it is mounted at a 42 deg dihedral angle with one another [54]. The functions of ruddevator are to allow the boom operator to move the boom toward the receptacle of receiver aircraft, and to help mitigate loads on the boom and bending during connected flight [54]. The boom fairing is of elliptical shape to reduce the drag in the free stream direction.

The boom can transfer fuel at the rate of up to 2,900 kg/min [54]. When deflected, the boom is located downward slope of 32.5 degrees relative to the fuselage reference plane [55].

2.1.2 Equations of Motion

2.1.2.1 Translational Kinematics

The translational kinematics equation is written in terms of the position vector of the tanker with respect to an inertial frame. Translational kinematics equation of the tanker aircraft in matrix form is

$$\dot{r}_{B_T} = \mathbf{R}^{\mathbf{T}}_{\mathbf{B_T I}} \mathbf{R}_{\mathbf{B_T W_T}} V_{\omega_T} + \mathbf{W} \tag{2.1}$$

where r_{B_T} is the position of the tanker relative to the inertial frame expressed in the inertial frame, $\mathbf{R_{B_T I}}$ is the rotation matrix from the inertial frame to the body frame of the tanker, $\mathbf{R_{B_T W_T}}$ is the rotation matrix from the tanker wind frame to body frame of the tanker, and V_{ω_T} is the velocity of the tanker relative to the surrounding air expressed in the wind frame of the tanker. Additionally, the vector W is the representation of the local wind velocity in the inertial frame, expanded as

$$W = \begin{bmatrix} W_x \\ W_y \\ W_x \end{bmatrix} \tag{2.2}$$

In addition to the matrix forms, the scalar forms of translational kinematics equations are

$$\begin{aligned} \dot{x}_T =& V_T \big[\cos\beta_T \cos\alpha_T \cos\theta_T \cos\psi_T + \sin\beta_T \left(-\cos\phi_T \sin\psi_T + \sin\phi_T \sin\theta_T \cos\psi_T \right) \\ &+ \cos\beta_T \sin\alpha_T \left(\sin\phi_T \sin\psi_T + \cos\phi_T \sin\theta_T \cos\psi_T \right) \big] + W_x \end{aligned} \tag{2.3}$$

$$\dot{y}_T = V_T\big[\cos\beta_T\cos\alpha_T\cos\theta_T\sin\psi_T + \sin\beta_T\left(\cos\phi_T\cos\psi_T + \sin\phi_T\sin\theta_T\cos\psi_T\right) + \cos\beta_T\sin\alpha_T\left(-\sin\phi_T\cos\psi_T + \cos\phi_T\sin\theta_T\sin\psi_T\right)\big] + W_y \tag{2.4}$$

$$\dot{z}_T = V_T\big[-\cos\beta_T\cos\alpha_T\sin\theta_T + \sin\beta_T\sin\phi_T\cos\theta_T + \cos\beta_T\sin\alpha_T\cos\phi_T\cos\theta_T\big] + W_z \tag{2.5}$$

where (x_T, y_T, z_T) is the position of the tanker aircraft relative the inertial frame, $(\psi_T, \theta_T, \phi_T)$ is the orientation of the tanker relative to the inertial frame in terms of the Euler angles, (V_T, β_T, α_T) are the airspeed, side slip angle and angle-of-attack of the tanker.

2.1.2.2 Translational Dynamics

Translational dynamics equation of the tanker aircraft in matrix form is

$$\begin{bmatrix} \dot{V}_{\omega_T} \\ \dot{\beta}_T \\ \dot{\alpha}_T \end{bmatrix} = \mathcal{E}_{\mathbf{T}}{}^{-1}\mathbf{S}(\omega_{\mathbf{B_T}})\mathbf{R}_{\mathbf{B_T W_T}}V_{\omega_T} + \mathcal{E}_{\mathbf{T}}{}^{-1}\mathbf{S}(\omega_{\mathbf{B_T}})\mathbf{W} - \mathcal{E}_{\mathbf{T}}{}^{-1}\dot{\mathbf{W}} + \frac{1}{m_T}\mathcal{E}_{\mathbf{T}}{}^{-1}(\mathbf{R}_{\mathbf{B_T I}}M_T + \mathbf{R}_{\mathbf{B_T W_T}}A_T + P_T) \tag{2.6}$$

where

$$\mathcal{E}_{\mathbf{T}}{}^{-1} = \begin{bmatrix} \cos\alpha_T\cos\beta_T & \sin\beta_T & \sin\alpha_T\cos\beta_T \\ -\frac{1}{V_{\omega_T}}\cos\alpha_T\sin\beta_T & \frac{1}{V_{\omega_T}}\cos\beta_T & -\frac{1}{V_{\omega_T}}\sin\alpha_T\sin\beta_T \\ -\frac{1}{V_{\omega_T}}\sin\alpha_T\sec\beta_T & 0 & \frac{1}{V_{\omega_T}}\cos\alpha_T\sec\beta_T \end{bmatrix} \tag{2.7}$$

V_{ω_T} is the airspeed, β_T is sideslip angle, α_T is angle-of-attack, m_T is the mass of the tanker, and $\mathbf{S}(\omega_{\mathbf{B_T}})$ is skew-symmetric matrix formed with representation of ω_{B_T}. The three different forces acting on the tanker aircraft are

$$M_T = \begin{bmatrix} 0 \\ 0 \\ m_T g \end{bmatrix} A_T = \begin{bmatrix} -D_T \\ -S_T \\ -L_T \end{bmatrix} P_T = \begin{bmatrix} T_T\cos\delta_T \\ 0 \\ -T_T\sin\delta_T \end{bmatrix} \tag{2.8}$$

where M_T is the gravitational force expressed in the inertial frame, A_T is the aerodynamic force expressed in the wind frame of the tanker, P_T is the propulsive force expressed in the body frame of the tanker, and g is the gravitational acceleration. Also, D_T is the drag, S_T is side force, L_T is lift, T_T is the thrust magnitude, and δ_T is the thrust inclination angle of the tanker. The scalar forms of the translational dynamics are

$$\begin{aligned}
\dot{V}_T &= g\left[\cos\theta_T \sin\beta_T \sin\phi_T + \cos\beta_T \left(\cos\phi_T \cos\theta_T \sin\alpha_T - \cos\alpha_T \sin\theta_T\right)\right] \\
&\quad + \frac{1}{m_T}\left[-D_T + T_T \cos\left(\alpha_T + \delta_T\right)\cos\beta_T\right] \qquad (2.9) \\
\dot{\beta}_T &= -r_T \cos\alpha_T + p_T \sin\alpha_T \\
&\quad + \frac{g}{V_T}\left[-\cos\phi_T \cos\theta_T \sin\alpha_T \sin\beta_T + \cos\beta_T \cos\theta_T \sin\phi_T + \cos\alpha_T \sin\beta_T \sin\theta_T\right] \\
&\quad - \frac{1}{m_T\, V_T}\left[S_T + T_T \cos\left(\alpha_T + \delta_T\right)\sin\beta_T\right] \qquad (2.10) \\
\dot{\alpha}_T &= q_T - \left(p_T \cos\alpha_T + r_T \sin\alpha_T\right)\tan\beta_T \\
&\quad + \frac{g\ \sec\beta_T}{V_T}\left[\cos\alpha_T \cos\phi_T \cos\theta_T + \sin\alpha_T \sin\theta_T\right] \\
&\quad - \frac{\sec\beta_T}{m_T\, V_T}\left[L_T + T_T \sin\left(\alpha_T + \delta_T\right)\right] \qquad (2.11)
\end{aligned}$$

where (p_T, q_T, r_T) is the angular velocity of the tanker expressed in the tanker's body frame. The standard expressions of the aerodynamic forces are

$$\begin{aligned}
D_T &= \frac{1}{2}\rho V_T^2 \mathcal{S}_T C_{D_T}\ , \qquad (2.12) \\
S_T &= \frac{1}{2}\rho V_T^2 \mathcal{S}_T C_{S_T}\ , \qquad (2.13) \\
L_T &= \frac{1}{2}\rho V_T^2 \mathcal{S}_T C_{L_T}\ , \qquad (2.14)
\end{aligned}$$

where $\mathcal{S}_T$ is the reference area of the tanker and ρ is the ambient air density. Also, the aerodynamic coefficients are

$$C_{D_T} = C_{D0} + C_{D\alpha^2}\ \alpha_T^2 \tag{2.15}$$

$$C_{S_T} = C_{S0} + C_{S\beta}\beta_T + C_{S\delta_r}\delta_{r_T} \tag{2.16}$$

$$C_{L_{wing}} = C_{L0} + C_{L\alpha}\alpha_T + C_{L\alpha 2}\ (\alpha_T - \alpha_{ref})^2 + C_{Lq}\frac{c_T}{2V_T}q_T \tag{2.17}$$

$$C_{L_{tail}} = C_{L\delta_e}\delta_{e_T} \tag{2.18}$$

$$C_{L_T} = C_{L_{wing}} + C_{L_{tail}} \tag{2.19}$$

where (δ_{a_T},δ_{e_T},δ_{r_T}) are the deflections of the control surfaces (aileron, elevator, rudder, respectively) and c_T is the chord length for the tanker.

2.1.2.3 Rotational Kinematics

The rotational kinematics equation of the tanker aircraft in matrix form is

$$\mathbf{R_{B_TI}}\dot{\mathbf{R}}_{\mathbf{B_TI}} = -\mathbf{S}(\omega_{\mathbf{B_T}}) \tag{2.20}$$

where ω_{B_T} is the angular velocity vector of the tanker relative to the inertial frame expressed in its own body frame as

$$\omega_{B_T} = \begin{bmatrix} p_T \\ q_T \\ r_T \end{bmatrix} \tag{2.21}$$

The rotational motion of the tanker aircraft in terms of Euler angles is, in scalar form,

$$\dot{\phi_T} = p_T + q_T \sin\phi_T \tan\theta_T + r\cos\phi_T \tan\theta_T \tag{2.22}$$

$$\dot{\theta_T} = q_T \cos\phi_T - r\sin\phi_T \tag{2.23}$$

$$\dot{\psi_T} = (q_T \sin\phi_T + r_T \cos\phi_T)\sec\theta_T \tag{2.24}$$

where note that both the orientation in terms of (ψ_T, θ_T, ϕ_T), and the angular velocity. (p_T, q_T, r_T), of the tanker are relative to the inertial frame.

2.1.2.4 Rotational Dynamics

The rotational dynamics equation of the tanker aircraft in matrix form is

$$\dot{\omega}_{B_T} = \underline{\underline{\mathbf{I}}}_{\mathbf{t}}^{-1} M_{B_T} + \underline{\underline{\mathbf{I}}}_{\mathbf{t}}^{-1} \mathbf{S}(\omega_{\mathbf{B_T}}) \underline{\underline{\mathbf{I}}}_{\mathbf{t}} \omega_{B_T} \tag{2.25}$$

where $\underline{\underline{\mathbf{I}}}_{\mathbf{t}}$ is the inertia matrix of the tanker aircraft. M_{B_T} is the moment of the external forces around the origin of the tanker's body frame and expressed in the body frame of the tanker as

$$M_{B_T} = \begin{bmatrix} \mathcal{L}_T \\ \mathcal{M}_T \\ \mathcal{N}_T \end{bmatrix} \tag{2.26}$$

where $\mathcal{L}_T$ is rolling moment, $\mathcal{M}_T$ is pitching moment, and $\mathcal{N}_T$ is yawing moment of the tanker. The scalar forms of the rotational dynamics equations are given as:

$$\begin{aligned} \dot{p_T} &= \frac{1}{(I_{xx}I_{zz} - I_{xz}^2)}[(I_{xx} - I_{yy} + I_{zz})I_{xz}p_T q_T + (I_{yy} - I_{zz} + I_{zz}^2 - I_{xz}^2)q_T r_T \\ &\quad + I_{zz}\mathcal{L}_T + I_{xz}\mathcal{N}_T] \qquad (2.27) \\ \dot{q_T} &= \frac{1}{I_{yy}}[(I_{zz} - I_{xx})p_T r_T + (r_T^2 - p_T^2)I_{xz} + \mathcal{M}_T] \qquad (2.28) \\ \dot{r_T} &= \frac{1}{(I_{xx}I_{zz} - I_{xz}^2)}[(I_{xx}^2 - I_{xx}I_{yy} + I_{xz}^2)p_T q_T + (-I_{xx} + I_{yy} - I_{zz})I_{xz}q_T r_T \\ &\quad + I_{xz}\mathcal{L}_T + I_{xx}\mathcal{N}_T] \qquad (2.29) \end{aligned}$$

where $I_{(\cdot)(\cdot)}$ is the moment or product of inertia of the tanker relative to the corresponding axis of the tanker's body frame. Note that the notation for $I_{(\cdot)(\cdot)}$ is the same for both tanker and the receiver while their values are obviously different. The rolling, pitching, and yawing moments of the tanker aircraft is,

$$\begin{aligned} \mathcal{L}_T &= \frac{1}{2}\rho V_{\omega_T}^2 \mathcal{S}_T b_T \mathcal{C}_{\mathcal{L}_T} \qquad (2.30) \\ \mathcal{M}_T &= \frac{1}{2}\rho V_{\omega_T}^2 \mathcal{S}_T c_T \mathcal{C}_{\mathcal{M}_T} + \triangle_{Z_T} T_T \qquad (2.31) \\ \mathcal{N}_T &= \frac{1}{2}\rho V_{\omega_T}^2 \mathcal{S}_T b_T \mathcal{C}_{\mathcal{N}_T} \qquad (2.32) \end{aligned}$$

where b_T is the wingspan of the tanker aircraft and $\triangle_{Z_T}$ is the moment arms of the thrust in the tanker's body frame. The aerodynamic moment coefficients are

$$\mathcal{C}_{\mathcal{L}_T} = \mathcal{C}_{\mathcal{L}_0} + \mathcal{C}_{\mathcal{L}\delta_a}\delta_{a_T} + \mathcal{C}_{\mathcal{L}\delta_r}\delta_{r_T} + \mathcal{C}_{\mathcal{L}\beta}\beta_T + \mathcal{C}_{\mathcal{L}_p}\frac{b_T}{2V_{\omega_T}}p_T + \mathcal{C}_{\mathcal{L}_r}\frac{b_T}{2V_{\omega_T}}r_T \quad (2.33)$$

$$\mathcal{C}_{\mathcal{M}_T} = \mathcal{C}_{\mathcal{M}_\alpha}\alpha_T + \mathcal{C}_{\mathcal{M}_{\delta_e}}\delta_{e_T} + \mathcal{C}_{\mathcal{M}_q}\frac{c_T}{2V_{\omega_T}}q_T \quad (2.34)$$

$$\mathcal{C}_{\mathcal{N}_T} = \mathcal{C}_{\mathcal{N}_0} + \mathcal{C}_{\mathcal{N}\delta_a}\delta_{a_T} + \mathcal{C}_{\mathcal{N}\delta_r}\delta_{r_T} + \mathcal{C}_{\mathcal{N}\beta}\beta_T + \mathcal{C}_{\mathcal{N}_p}\frac{b_T}{2V_{\omega_T}}p_T + \mathcal{C}_{\mathcal{N}_r}\frac{b_T}{2V_{\omega_T}}r_T \quad (2.35)$$

2.1.3 Engine Model

The thrust generated by the engine (T_T) is

$$T_T = \xi_T \, T_{max_T} \quad (2.36)$$

where ξ_T denotes the instantaneous throttle setting and T_{max_T} is the maximum available thrust of the tanker and assumed to be constant in this paper. The engine dynamics is modeled as that of a first order system with time constant τ_T. Therefore, we have

$$\dot{\xi}_T = \frac{\xi_T - \xi_{t_T}}{\tau_T} \ , \quad (2.37)$$

where ξ_{t_T} is the commanded throttle setting ($0 \leq \xi_t \leq 1$).

2.1.3.1 Actuator Model

For the present study, only the actuator saturation are considered. The deflection range attainable from each control surface is within (-20 deg, 20 deg).

2.2 Receiver Aircraft

In an efficient aerial refueling operation, the receiver aircraft needs to be controlled with respect to the tanker's position and orientation rather than with respect to the inertial reference frame. Moreover, the receiver aircraft will be exposed to a nonuniform wind field during the whole refueling operation when it is in the proximity

of the tanker due to the trailing vortices of the tanker. Nonlinear equations of receiver aircraft were derived [26] with respect to the tanker's position and orientation. During the aerial refueling operation, receiver aircraft moves to the contact position and stays relative to the tanker while tanker aircraft executes a pre-specified racetrack maneuver relative to the inertial frame [26], [53]. Matrix forms of the equations are given in this section as they are used in the simulation of the closed loop system.

2.2.1 Aircraft Description

This section explains the physical parameters of the receiver aircraft. The Innovative Control Effector (ICE) unmanned aircraft is used as the receiver aircraft in this research and being fueled from a KC 135 tanker aircraft. ICE aircraft was developed under a U.S. Air Force Research Laboratories (AFRL) sponsored program [50]. It is a tailless, single engine, and supersonic fighter aircraft with a 65 degree sweep delta wing [50]. It has conventional control effectors such as elevons, symmetric pitch flaps, and outboard leading-edge flaps, and has innovative control effectors which are pitch and yaw thrust vectoring, all-moving tips, and spoiler slop deflectors [50]. In ref. [56], vehicle configuration is depicted using the ICE101. Pitch flap is used for

Table 2.1. ICE 101 Configuration and Aerodynamic Data [56]

Reference Wing (Planform) Area	808.58 sq.ft
Wing Span	37 ft 6.0 in (450.00 in)
Reference Wing Aspect Ratio	1.74
Leading Edge Wing Sweep Angle	65.0 degree
Trailing Edge Sweep Angle	25 degree
Body Length (Centerline Chord)	517.49 in
Reference Wing Mean Aerodynamic Chord	335.33 in
Fuselage Station of Leading Edge of Wing Mean Aerodynamic Chord	165.67 in

pitch axis and elevon is used for roll control. Clam shells, which provide symmetrical deflection of top and bottom of the wing, are used for yaw control and speed brake function [56]. Some reference dimensions are given in Table 2.1.

2.2.2 Equations of Motion

2.2.2.1 Translational Kinematics

The translational kinematics equation is written in terms of the position vector of the receiver aircraft with respect to the tanker body frame. Translational kinematics equation of the receiver aircraft in matrix form is

$$\dot{\xi} = \mathbf{R}^{\mathbf{T}}_{\mathbf{B_R B_T}} \mathbf{R}_{\mathbf{B_R W_R}} U + \mathbf{R}^{\mathbf{T}}_{\mathbf{B_R B_T}} W - \mathbf{R}_{\mathbf{B_T I}}\, \dot{r}_{B_T} + \mathbf{S}(\omega_{\mathbf{B_T}})\xi \tag{2.38}$$

where ξ is the position vector of the receiver relative to the tanker expressed in the body frame of the tanker, U is the velocity of the receiver relative to the surrounding air expressed in the wind frame of the receiver (W_R-Frame), W is the velocity of the surrounding air relative to the ground expressed in the body frame of the receiver, and $\dot{r}_{B_T}$ is the velocity vector of the tanker relative to the inertial frame expressed in the inertial frame. $\mathbf{R}_{\mathbf{B_R B_T}}$ is the rotation matrix from tanker's body frame (B_T-Frame) to receiver's body frame (B_R-Frame), $\mathbf{R}_{\mathbf{B_R W_R}}$ is the rotation matrix from wind frame of the receiver (W_R-Frame) to body frame of the receiver (B_R-Frame) and parameterized by the angle of attack (α_R) and sideslip angle (β_R) of the receiver, and $\mathbf{R}_{\mathbf{B_T I}}$ is the rotation matrix from the inertial frame to body frame of the tanker (B_T-Frame).

2.2.2.2 Translational Dynamics

Translational dynamics of the receiver in matrix form is

$$\begin{aligned}
\dot{\mathcal{X}}_R &= \mathcal{E}_{\mathbf{R}}^{-1}\left[\mathbf{S}(\omega_{\mathbf{B_R B_T}}) + \mathbf{S}(\mathbf{R}_{\mathbf{B_R B_T}}\omega_{\mathbf{B_T}})\right](\mathbf{R}_{\mathbf{B_R W_R}}\, U + W) - \mathcal{E}_{\mathbf{R}}^{-1}\dot{W} \\
&+ \frac{1}{(M+m)}\mathcal{E}_{\mathbf{R}}^{-1}\big[\mathbf{R}_{\mathbf{B_R B_T}}\mathbf{R}_{\mathbf{B_T I}}\,(F + \dot{m}\,\dot{r}_{B_T}) \\
&- \dot{m}\left(\mathbf{R}_{\mathbf{B_R W_R}}\, U + W - \mathbf{R}_{\mathbf{B_R B_T}}\, V_{\dot{m}} + \mathbf{R}^{\mathbf{T}}_{\mathbf{B_R B_T}}\mathbf{S}(\omega_{\mathbf{B_T}})\rho c\right)\big] \\
&- \frac{1}{(M+m)}\mathcal{E}_{\mathbf{R}}^{-1}\sum_{j=1}^{k}\Bigg(\dot{m}_j\Big\{\dot{\rho}_{m_j} - \left[\mathbf{S}(\omega_{\mathbf{B_R B_T}}) + \mathbf{S}(\mathbf{R}_{\mathbf{B_R B_T}}\omega_{\mathbf{B_T}})\right]\rho_{m_j}\Big\} \\
&\quad + m_j\Big\{\ddot{\rho}_{m_j} + \mathbf{S}(\omega_{\mathbf{B_R B_T}})\left[\mathbf{S}(\omega_{\mathbf{B_R B_T}})\rho_{m_j} - 2\dot{\rho}_{m_j}\right] \\
&\quad + 2\mathbf{S}(\mathbf{R}_{\mathbf{B_R B_T}}\omega_{\mathbf{B_T}})\left[\mathbf{S}(\omega_{\mathbf{B_R B_T}})\rho_{m_j} - \dot{\rho}_{m_j}\right] \\
&\quad + \left[\mathbf{S^2}(\mathbf{R}_{\mathbf{B_R B_T}}\omega_{\mathbf{B_T}}) - \mathbf{S}(\mathbf{R}_{\mathbf{B_R B_T}}\dot{\omega}_{\mathbf{B_T}})\right]\rho_{m_j} + \mathbf{S}(\rho_{\mathbf{m_j}})\dot{\omega}_{B_R B_T}\Big\}\Bigg) \qquad (2.39)
\end{aligned}$$

where

$$\mathcal{X}_R = \begin{bmatrix} V_R & \beta_R & \alpha_R \end{bmatrix}^T \qquad (2.40)$$

$$U = \begin{bmatrix} V_R \\ 0 \\ 0 \end{bmatrix} \qquad (2.41)$$

$$\mathcal{E}_{\mathbf{R}} = \begin{bmatrix} \cos\beta_R\cos\alpha_R & -V_R\sin\beta_R\cos\alpha_R & -V_R\cos\beta_R\sin\alpha_R \\ \sin\beta_R & V_R\cos\beta_R & 0 \\ \cos\beta_R\sin\alpha_R & -V_R\sin\beta_R\sin\alpha_R & V_R\cos\beta_R\cos\alpha_R \end{bmatrix} \qquad (2.42)$$

and $\omega_{B_R B_T}$ is the angular velocity vector of the receiver relative to the tanker represented in body frame of the receiver, ω_{B_T} is the angular velocity vector of the tanker relative to the inertial frame, $\mathbf{S}(\omega_{\mathbf{B_R B_T}})$ is skew symmetric matrix constructed with representation $\omega_{B_R B_T}$, M is mass of solid part of the receiver, m is total mass of fuel, F is total external force acting on the receiver aircraft, $V_{\dot{m}}$ is velocity of fuel flow into the receiver aircraft relative to the tanker, m_j is mass of fuel in j^{th} fuel tank of the

receiver, and ρ_{m_j} is the position vector of the center of mass of the fuel mass in the j^{th} tank expressed in body frame of the receiver (B_R-Frame).

2.2.2.3 Rotational Kinematics

The standard rotational kinematics equations are used both in tanker and receiver aircraft. However, their interpretations are different because angular position and angular velocity of the receiver aircraft are relative to tanker body frame, an accelerating and rotating reference frame. The rotational kinematics equations of the receiver aircraft in matrix form take the form of Poisson's equation as

$$\dot{\mathbf{R}}_{\mathbf{B_R B_T}} = \mathbf{S}(\omega_{\mathbf{B_R B_T}})\mathbf{R}_{\mathbf{B_R B_T}} \tag{2.43}$$

where $\omega_{B_R B_T}$ is the representation of the angular velocity vector of the receiver aircraft relative to the tanker body frame expressed in its own body frame as

$$\omega_{B_R B_T} = \begin{bmatrix} p_{R_T} \\ q_{R_T} \\ r_{R_T} \end{bmatrix} \tag{2.44}$$

The scalar form of this matrix equation in terms of Euler angles are

$$\dot{\phi} = p + q\sin\phi\tan\theta + r\cos\phi\tan\theta \tag{2.45}$$

$$\dot{\theta} = q\cos\phi - r\sin\phi \tag{2.46}$$

$$\dot{\psi} = (q\sin\phi + r\cos\phi)\sec\theta \tag{2.47}$$

where note that both the orientation, (ψ, θ, ϕ), and the angular velocity, (p, q, r), of the receiver are relative to the tanker.

2.2.2.4 Rotational Dynamics Equation

The rotational dynamics equation of the receiver aircraft in matrix form is

$$
\begin{aligned}
\dot{\omega}_{B_R B_T} &= \underline{\underline{\mathbf{I}}}_{\mathbf{t}}^{-1} M_{B_R} + \underline{\underline{\mathbf{I}}}_{\mathbf{t}}^{-1} \mathbf{S}(\omega_{\mathbf{B_R B_T}} + \mathbf{R}_{\mathbf{B_R B_T}} \omega_{\mathbf{B_T}}) \underline{\underline{\mathbf{I}}}_{\mathbf{M}} \left(\omega_{B_R B_T} + \mathbf{R}_{\mathbf{B_R B_T}} \omega_{B_T}\right) \\
&+ \underline{\underline{\mathbf{I}}}_{\mathbf{t}}^{-1} \sum_{j=1}^{k} \mathbf{S}(\rho_{\mathbf{m_j}}) \Big[m_j \ \left(\omega_{B_R B_T}^T + \omega_{B_T}^T \mathbf{R}_{\mathbf{B_R B_T}}^{\mathbf{T}}\right) \rho_{m_j} \left(\omega_{B_R B_T} + \mathbf{R}_{\mathbf{B_R B_T}} \omega_{B_T}\right) \\
&\quad + m_j \ \ddot{\rho}_{m_j} + \dot{m}_j \ \dot{\rho}_{m_j} \Big] \\
&+ \underline{\underline{\mathbf{I}}}_{\mathbf{t}}^{-1} \left[\sum_{j=1}^{k} \mathbf{S}(\rho_{\mathbf{m_j}}) \ m_j \right] \ \Big\{ - \left[\mathbf{S}(\omega_{\mathbf{B_R B_T}}) + \mathbf{S}(\mathbf{R}_{\mathbf{B_R B_T}} \ \omega_{\mathbf{B_T}}) \right] \left(\mathbf{R}_{\mathbf{B_R W_R}} \ U + W \right) \\
&\quad + \mathcal{E}_{\mathbf{R}} \ \dot{\mathcal{X}}_R + \dot{W} \ \Big\} \\
&+ \underline{\underline{\mathbf{I}}}_{\mathbf{t}}^{-1} \left[\mathbf{S}(\rho_{\mathbf{m_j}}) \ \dot{m}_j \right] \ \left(\mathbf{R}_{\mathbf{B_R w_R}} \ U + W \right) \\
&- 2 \ \underline{\underline{\mathbf{I}}}_{\mathbf{t}}^{-1} \sum_{j=1}^{k} m_j \ \left[\left(\rho_{m_j}^T \ \dot{\rho}_{m_j} \right) \mathbf{I}_{\mathbf{3\times 3}} - \dot{\rho}_{m_j} \rho_{m_j}^T \right] \left(\omega_{B_R B_T} + \mathbf{R}_{\mathbf{B_R B_T}} \omega_{B_T} \right) \\
&- \underline{\underline{\mathbf{I}}}_{\mathbf{t}}^{-1} \sum_{j=1}^{k} \dot{m}_j \ \left[\left(\rho_{m_j}^T \ \rho_{m_j} \right) \mathbf{I}_{\mathbf{3\times 3}} - \rho_{m_j} \rho_{m_j}^T \right] \left(\omega_{B_R B_T} + \mathbf{R}_{\mathbf{B_R B_T}} \omega_{B_T} \right) \\
&- \mathbf{S}(\omega_{\mathbf{B_R B_T}}) \ \mathbf{R}_{\mathbf{B_R B_T}} \omega_{B_T} - \mathbf{R}_{\mathbf{B_R B_T}} \dot{\omega}_{B_T} \\
&- \underline{\underline{\mathbf{I}}}_{\mathbf{t}}^{\ -1} \dot{m} \mathbf{S}(\rho_R) \left(\mathbf{R}_{\mathbf{B_R B_T}} \mathbf{R}_{\mathbf{B_T I}} \dot{r}_{B_T} + \mathbf{R}_{\mathbf{B_R B_T}} V_{\dot{m}} - \mathbf{R}_{\mathbf{B_R B_T}} \mathbf{S}(\omega_{B_T}) \rho c \right) \qquad (2.48)
\end{aligned}
$$

where $\underline{\underline{\mathbf{I}}}_{\mathbf{t}}$ is the total inertia matrix of the entire system (receiver and fuel) at a given time in body frame of the receiver (B_R-Frame), always non-singular, and $\underline{\underline{\mathbf{I}}}_{\mathbf{M}}$ is the inertia matrix of the receiver, excluding fuel transferred. M_{B_R} is the total moment of the external forces acting on the receiver due to the source of gravity, aerodynamics, and propulsion about the origin of body frame of the receiver. In Eq. (2.48), only $\dot{r}_{B_T}$ (the velocity of the tanker relative to the inertial frame) is with respect to the inertial frame. Other representations are in either body frame of tanker or in body frame of receiver aircraft. In rotational dynamics, refueling effect is represented by the concentrated fuel mass and its center of mass location in each fuel tank. In present work, receiver airplane has four fuel tanks and the effect of fuel flow into each

tank is taken into account separately. A center of mass change during refueling is incorporated in the equation by writing the equation with respect to a point fixed geometrically in the B_R-frame. Similarly, aerodynamic variables such as airspeed, angle of attack, side-slip angle, and aerodynamic stability derivatives are determined by the geometric shape of the aircraft, and thus standard definitions can be applied directly without modification [26].

2.2.3 Engine Model

As in the case of the tanker, the engine model ofthe receiver is also a first order transfer function with constant maximum thrust, obviously with different maximum thrust and different time constant.

2.2.4 Actuator Model

For the present study, only the actuator saturation and rate limit effects are considered for the receiver. The deflection range attainable from the elevon is (-30 deg, 30 deg), from the pitch flap (-30 deg, 30 deg) and from the clamshells (-60 deg, 60 deg). All three control effectors have a rate limit of ±90 deg/sec. Likewise, the thrust vectoring has a limit of ± 30 deg in both directions and a rate limit of ±30 deg/sec.

2.2.4.1 Fuel Tank Configuration

This section describes how the receiver aircraft's fuel tanks are incorporated with mathematical quantities in the equations of motion. Fig. 2.1 depicts the fuel tanks and control surfaces of ICE aircraft. ICE aircraft has four different fuel tanks symmetrically located with respect to xz-plane. During fuel transfer in standard aerial refueling operation, the fuel flown into the receiver is equally distributed among the

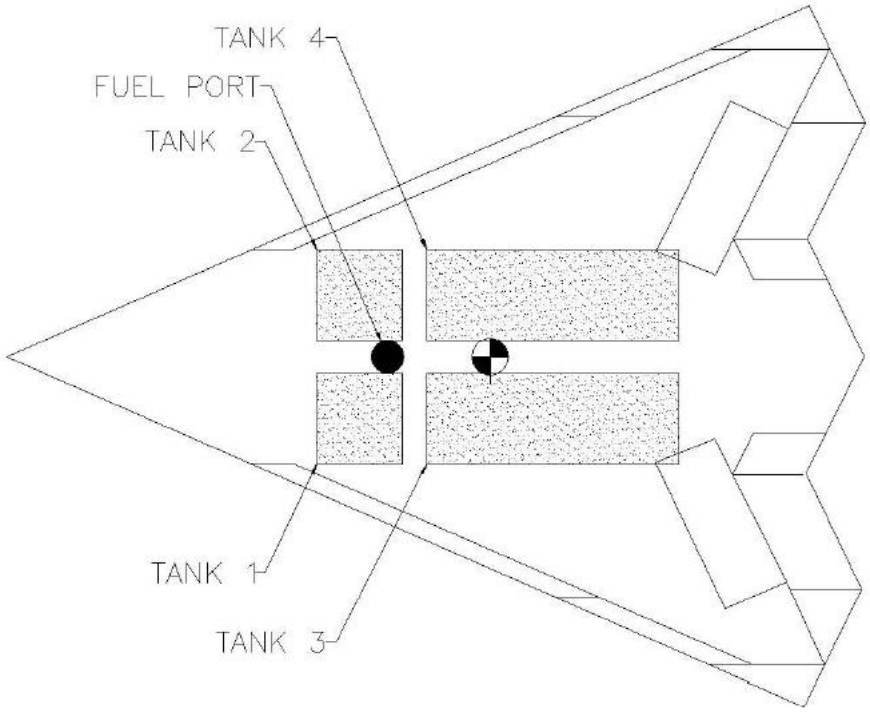

Figure 2.1. Receiver aircraft with its fuel tanks [26].

four fuel tanks. In the ICE receiver aircraft, 35% of fuel capacity is from the front tanks, tank 1 and tank 2. 65% of fuel capacity is from the tank 3 and tank 4. The overall fuel flow rate ($\dot{m}$) from the tanker to the receiver aircraft is considered as an external input. The actual mass contained in the j^{th} fuel tank at any instance of time is computed by integrating fuel flow rate for j^{th} fuel tank ($\dot{m}_j$) over time. The fuel mass amount in the j^{th} fuel tank at any instant of time is formulated as

$$m_j(t) = \int_0^t \dot{m}_j(\tau)\mathtt{d}\tau \tag{2.49}$$

where t is time. In case of any residual fuel remains in the tank before the refueling started, the residual fuel is considered as part of the receiver aircraft. Therefore, when the refueling is not yet conducted, $m_j(0) = 0$. The position vector of the fuel mass concentrated at the j^{th} point is denoted by $\underline{\rho}_{m_j}$, and expressed in B_R-frame. Note that it is assumed that all fuel tanks are rectangular shape, fuel remains level within

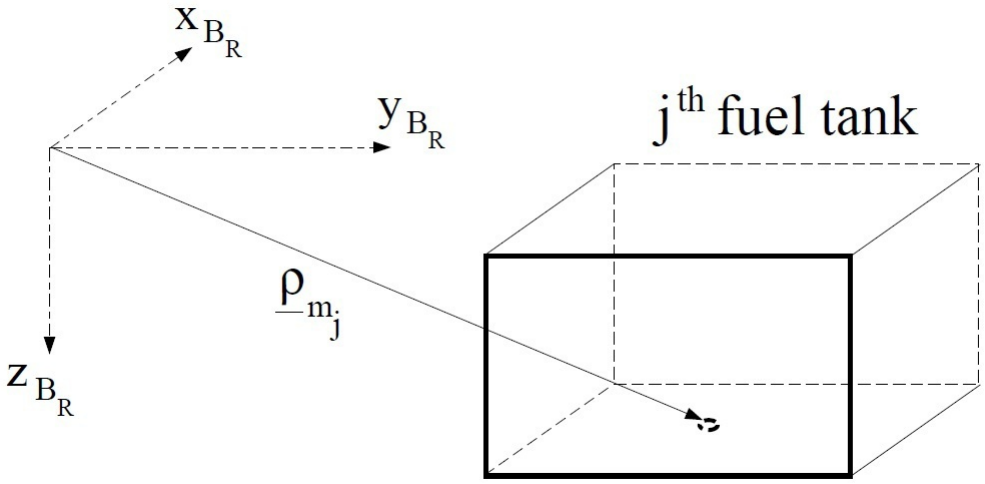

Figure 2.2. Initial condition for lumped mass position vector [26].

each fuel tank and fuel in each fuel tank is concentrated at the center of mass (CM) position. Because of this, initial position of $\rho_{m_j}(0)$ is considered to be the mid-point of the base of j^{th} fuel tank (Fig. 2.2) or the surface of the remaining fuel (Fig. 2.3). Fig. 2.3 shows the example of two-view diagram of fuel tank 1.

$$\underline{\rho}_{m_1}(0) = [\underline{\hat{B}}_R]^T \begin{bmatrix} x_1(0) \\ y_1(0) \\ z_1(0) \end{bmatrix} \tag{2.50}$$

Based on the assumption that fuel tanks are rectangular and the fuel remains level in each tank, $x_1(t)$ and $y_1(t)$ values do not change during the refueling. Only $z_1(t)$ varies with time as the level of the fuel rises. Accumulated fuel mass in the fuel tank 1 is formulated as

$$m_1(t) = \int_0^t \dot{m}_1(\tau)\mathtt{d}\tau \tag{2.51}$$

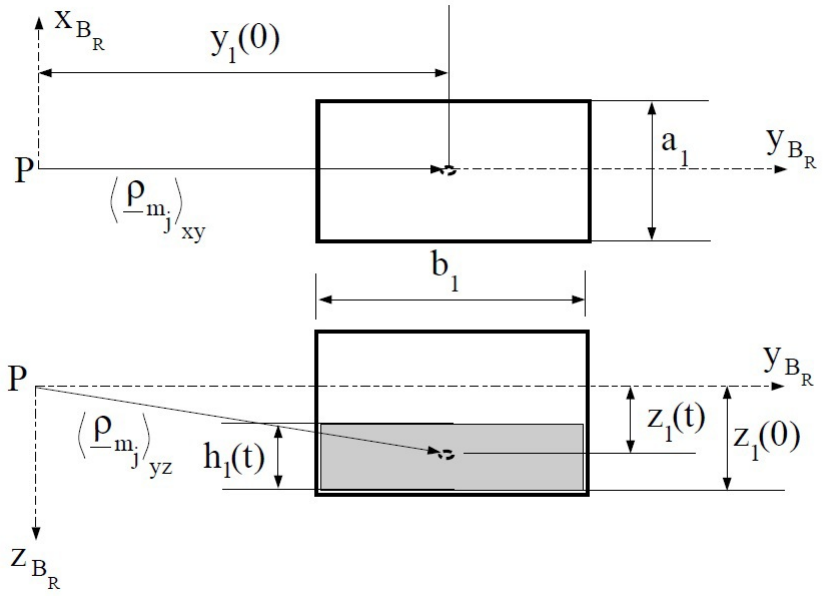

Figure 2.3. Two-view diagram of fuel tank 1 [26].

where $\dot{m}_1(t)$ is the fuel flow rate into tank 1. The fuel's height of the CM from the base of the fuel tank as fuel is flowing in is calculated as

$$h_1(t) = \frac{m_1(t)}{\rho_{fuel} a_1 b_1} \tag{2.52}$$

where a_1 is the length, b_1 is the breadth of fuel tanks 1, and ρ_{fuel} is the density of the fuel. Time-varying position vector of fuel mass concentrated at the fuel CM in the fuel tank 1 is

$$\underline{\rho}_{m_1}(t) = [\underline{\hat{B}}_R]^T \begin{bmatrix} x_1(0) \\ y_1(0) \\ z_1(0) - \frac{h_1(t)}{2} \end{bmatrix} \tag{2.53}$$

This time-varying position vector for other fuel tanks are similarly formulated and the position vectors of all fuel tanks are applied in the receiver's equations of motion.

2.3 Modeling the Vortex and Its Effect

The tanker vortex-induced wind field acting on the receiver aircraft is non-uniform in nature. To apply this in the receiver dynamics equations without doing any modifications, the non-uniform induced wind components and gradients need to be approximated to equivalent uniform wind components and gradients. After a fairly reasonable approximation is achieved, aerodynamic coupling between the tanker and the receiver is implemented in a direct and computationally efficient way. In the receiver's equation, the wind effect terms are denoted as W, $\dot{W}$ and considered to be based on the uniform wind distribution acting at the receiver's center of mass, expressed in the receiver's body frame. In the aerial refueling dynamic model

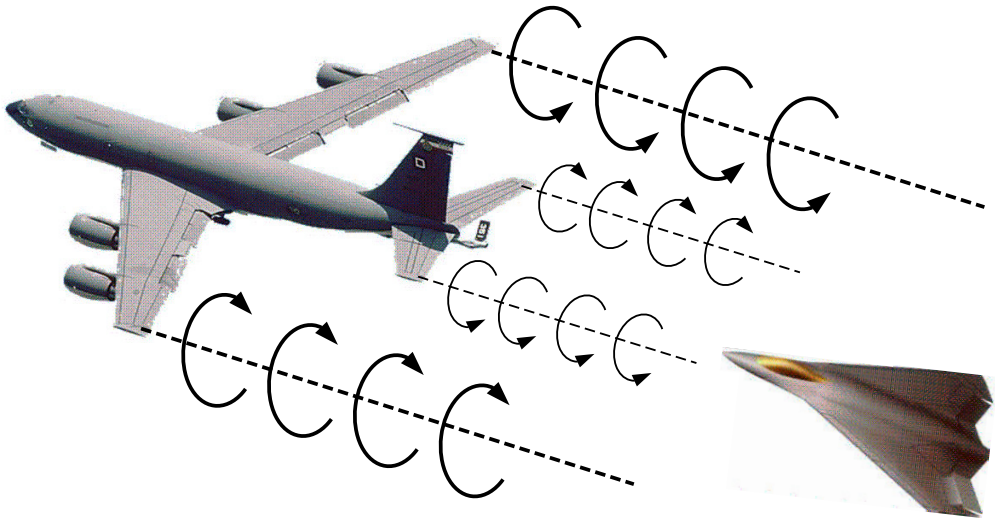

Figure 2.4. Trailing vortex from the wings and horizontal tail.

for this research, tanker is considered to generate two horseshoe vortices, one from the wings and one from the horizontal tail. These vortices induce additional wind velocities on the body of the receiver aircraft. These vortex-induced wind velocities cause change in the forces and moments experienced by the receiver. The induced

wind velocities the receiver aircraft experiences are written as a function of the relative separation as well as the relative orientation between the tanker and the receiver using a modified horseshoe vortex model based on the Helmholtz profile. Induced wind and wind gradients are non-uniform along the body dimensions of the receiver aircraft. Therefore, instead of attempting to directly estimate the induced forces and moments on the receiver aircraft, the induced wind velocities and wind gradients are computed by using an averaging technique as uniform approximation. By introducing the effective wind components and gradients into the nonlinear aircraft equations, wind components and wind temporal variation of wind in the body frame of receiver aircraft are used to determine the effects on the receiver's dynamics. Besides the actual vortex model and the averaging technique, this model has the effect of vortex decay over time, different geometrical dimensions for the tanker and the receiver aircraft, and many useful geometrical parameters of the aircraft such as the wing sweep angle, the dihedral angle, and the relative distance between the center of mass of the UAV and the aerodynamic center of the wing.

CHAPTER 3

CONTROL DESIGN

3.1 Tanker Aircraft

In an aerial refueling operation, the tanker aircraft flies in a pre-specified course while a receiver aircraft is refueled, and other receiver aircraft fly in formation waiting for their turn for refueling. Generally, the tanker aircraft flies at a constant altitude with a constant speed. The refueling flight course for the tanker aircraft is composed of steady straight level flight and steady constant altitude turns, and those two combined flights generate a "racetrack" maneuver.

3.1.1 Requirements

Even though tanker aircraft in aerial refueling is flown by a human pilot, in computer simulation, a controller for the tanker aircraft should be designed and implemented to fly any desired racetrack maneuver. In this work, steady turns are specified by yaw rates of the aircraft. The tanker aircraft is required to satisfy commanded yaw rates with small transient and zero steady-state error. While starting and ending a turn, and during the turn, deviation in altitude and speed from their respective nominal values should be small and decay to zero at steady-state. In the simulation environment, the closed-loop performance of the tanker aircraft should be similar to the flight of manned tanker aircraft in an actual racetrack maneuver.

3.1.2 Flight Cases Analysis

Specification of the flight cases and the solution of the equations of motion for determining the flight cases values of the tanker aircraft states and control variables at each flight case condition are presented in this section. The trimmed steady-state flight case varies with the parameterized values of V_{T0} and $\dot{\psi}_{T0}$. During the entire racetrack maneuver, desired side slip is zero ($\beta_{T0} = 0$), airspeed, angle-of-attack, and altitude are constants ($V_T = V_{T0}$, $\alpha_T = \alpha_{T0}$ and $\dot{z}_{T0} = 0$). For a given steady-state flight condition whether it is a straight-level or turning flight, angular velocity components are constants ($p_T = p_{T0}$, $q_T = q_{T0}$ and $r_T = r_{T0}$), pitch and roll angles are constants ($\theta_T = \theta_{T0}$ and $\phi_T = \phi_{T0}$), and $\dot{\psi}_T = \dot{\psi}_{T0}$. Then the rotational kinematics equations at any nominal conditions yield

$$p_{T0} = -\sin\theta_{T0}\,\dot{\psi}_{T0} \tag{3.1}$$

$$q_{T0} = \sin\phi_{T0}\cos\theta_{T0}\,\dot{\psi}_{T0} \tag{3.2}$$

$$r_{T0} = \cos\phi_{T0}\cos\theta_{T0}\,\dot{\psi}_{T0} \tag{3.3}$$

Three steady-state trimmed flight conditions yield from the translational dynamics equations.

$$\begin{aligned} 0 = {} & g\big(\cos\phi_{T0}\cos\theta_{T0}\sin\alpha_{T0} - \cos\alpha_{T0}\sin\theta_{T0}\big) + \frac{1}{m_T}\big[-\frac{1}{2}\rho V_{T0}^2 S_T(C_{D0} \\ & + C_{D\alpha}\alpha_{T0} + C_{D\alpha^2}\alpha_{T0}^2 + C_{D\delta_e}\delta_{e_{T0}}) + T_{T0}\cos(\alpha_{T0}+\delta_T)\big] \end{aligned} \tag{3.4}$$

$$\begin{aligned} 0 = {} & \cos\phi_{T0}\cos\theta_{T0}\cos\alpha_{T0}\dot{\psi}_{T0} + \sin\theta_{T0}\sin\alpha_{T0}\dot{\psi}_{T0} - \frac{g}{V_{T0}}\cos\theta_{T0}\sin\phi_{T0} \\ & + \frac{1}{2m_T}\rho V_{T0} S_T(C_{S0} + C_{S\delta_r}\delta_{r_{T0}} + C_{S\delta_a}\delta_{a_{T0}}) \end{aligned} \tag{3.5}$$

$$\begin{aligned} 0 = {} & \sin\phi_{T0}\cos\theta_{T0}\dot{\psi}_{T0} + \frac{g}{V_{T0}}(\cos\alpha_{T0}\cos\phi_{T0}\cos\theta_{T0} + \sin\alpha_{T0}\sin\theta_{T0}) \\ & - \frac{1}{2m_T}\rho V_{T0} S_T(C_{L0} + C_{L\alpha}\alpha_{T0} + C_{L\alpha^2}(\alpha_{T0} - \alpha_{ref}^2) \\ & + C_{Lq}\frac{c}{2V_{T0}}\sin\phi_{T0}\cos\theta_{T0}\dot{\psi}_{T0} + C_{L\delta_e}\delta_{e_{T0}}) - \frac{1}{m_T V_{T0}}T_{T0}\sin(\alpha_{T0}+\delta_T) \end{aligned} \tag{3.6}$$

Other three steady-state trimmed flight conditions yield from the rotational dynamics equations and the constitutive equations.

$$
\begin{aligned}
0 &= \frac{1}{I_{xx}I_{zz}-I_{xz}^2}\big[-I_{xz}(I_{xx}-I_{yy}+I_{zz})\sin\theta_{T0}\cos\theta_{T0}\sin\phi_{T0}\dot{\psi}_{T0}^2 \\
&\quad +(I_{yy}I_{zz}-I_{zz}^2-I_{xz}^2)\sin\phi_{T0}\cos\phi_{T0}\cos\theta_{T0}^2\dot{\psi}_{T0}^2 \\
&\quad +\frac{1}{2}\rho V_{T0}^2 S_T b_T I_{zz}(C_{\mathcal{L}_0}+C_{\mathcal{L}\delta_a}\delta_{a_{T0}}+C_{\mathcal{L}\delta_r}\delta_{r_{T0}}-C_{\mathcal{L}_p}\frac{b_T}{2V_{T0}}\sin\theta_{T0}\dot{\psi}_{T0} \\
&\quad +C_{\mathcal{L}_r}\frac{b_T}{2V_{T0}}\cos\phi_{T0}\cos\theta_{T0}\dot{\psi}_{T0}) \\
&\quad +\frac{1}{2}\rho V_{T0}^2 S_T b_T I_{xz}(C_{\mathcal{N}_0}+C_{\mathcal{N}\delta_a}\delta_{a_{T0}}+C_{\mathcal{N}\delta_r}\delta_{r_{T0}}-C_{\mathcal{N}_p}\frac{b_T}{2V_{T0}}\sin\theta_{T0}\dot{\psi}_{T0} \\
&\quad +C_{\mathcal{N}_r}\frac{b_T}{2V_{T0}}\cos\phi_{T0}\cos\theta_{T0}\dot{\psi}_{T0})\big] \qquad (3.7)\\
0 &= \frac{1}{I_{yy}}\big[(I_{xx}-I_{zz})\sin\theta_{T0}\cos\theta_{T0}\cos\phi_{T0}\dot{\psi}_{T0}^2+I_{xz}\cos\theta_{T0}^2\dot{\psi}_{T0}^2(\cos\phi_{T0}^2-1) \\
&\quad +\frac{1}{2}\rho V_{T0}^2 S_{T0}^2 c(C_{\mathcal{M}0}+C_{\mathcal{M}\alpha}\alpha_{T0}+C_{\mathcal{M}\delta_e}\delta_{e_{T0}}+C_{\mathcal{M}_q}\frac{c}{2V_{T0}}\sin\phi_{T0}\cos\theta_{T0}\dot{\psi}_{T0}) \\
&\quad +\Delta_{z_T}T_{T0}\cos\delta_T+\Delta_{x_T}T_{T0}\sin\delta_T\big] \qquad (3.8)\\
0 &= \frac{1}{I_{xx}I_{zz}-I_{xz}^2}\big[-(I_{xx}^2-I_{xx}I_{yy}+I_{xz}^2)\sin\theta_{T0}\cos\theta_{T0}\sin\phi_{T0}\dot{\psi}_{T0}^2 \\
&\quad +I_{xz}(-I_{xx}+I_{yy}-I_{zz})\sin\phi_{T0}\cos\phi_{T0}\cos\theta_{T0}^2\dot{\psi}_{T0}^2 \\
&\quad +\frac{1}{2}\rho V_{T0}^2 S_T b_T I_{xz}(C_{\mathcal{L}_0}+C_{\mathcal{L}\delta_a}\delta_{a_{T0}}+C_{\mathcal{L}\delta_r}\delta_{r_{T0}}-C_{\mathcal{L}_p}\frac{b_T}{2V_{T0}}\sin\theta_{T0}\dot{\psi}_{T0} \\
&\quad +C_{\mathcal{L}_r}\frac{b_T}{2V_{T0}}\cos\phi_{T0}\cos\theta_{T0}\dot{\psi}_{T0}) \\
&\quad +\frac{1}{2}\rho V_{T0}^2 S_T b_T I_{xx}(C_{\mathcal{N}_0}+C_{\mathcal{N}\delta_a}\delta_{a_{T0}}+C_{\mathcal{N}\delta_r}\delta_{r_{T0}}-C_{\mathcal{N}_p}\frac{b_T}{2V_{T0}}\sin\theta_{T0}\dot{\psi}_{T0} \\
&\quad +C_{\mathcal{N}_r}\frac{b_T}{2V_{T0}}\cos\phi_{T0}\cos\theta_{T0}\dot{\psi}_{T0})\big] \qquad (3.9)
\end{aligned}
$$

Additionally, since altitude is constant, $\dot{z}_T$ equation in Eq.(2.5) at a steady-state trimmed flight condition yields

$$
0 = \sin\alpha_{T0}\cos\phi_{T0}\cos\theta_{T0}-\cos\alpha_{T0}\sin\theta_{T0} \qquad (3.10)
$$

Note that in these seven algebraic equations, there are seven unknowns: α_{T0}, θ_{T0}, ϕ_{T0}, T_{T0}, $\delta_{a_{T0}}, \delta_{e_{T0}}, \delta_{r_{T0}}$. By solving these seven equations, the nominal values of the

unknowns are computed. Further, using Eqs. (3.1), (3.2), and (3.3), the nominal values of the angular velocity components, p_{T0}, q_{T0} and r_{T0}, are calculated. Note that this flight case analysis is parameterized by $\dot{\psi}_{T0}$. Therefore, when a straight-level flight is to be analyzed, $\dot{\psi}_{T0}$ is set to 0. If a specific turn is to be analyzed, then $\dot{\psi}_{T0}$ is set to the desired turn rate.

3.1.3 Gain Scheduling Controller

A multi-input-multi-output state-feedback LQR and integral control technique are combined to design controller which is to maintain altitude and speed, and to track yaw rates. The control variables available for the tanker aircraft are three conventional control surfaces and throttle setting. The outputs to be controlled are the airspeed, altitude, and yaw rates. A gain scheduling scheme is implemented based on the commanded speed and yaw rates. The tanker's equations of motion which are given in the previous section are linearized at six different steady-state trimmed nominal conditions. Two of the nominal conditions correspond to the tanker flying straight level at constant altitude with two different airspeeds. Other two correspond to the tanker turning with a specified turn rate to positive direction at constant altitude with two different airspeeds. And the other two correspond to tanker turning with a specified turn rate to negative direction at constant altitude with two different airspeeds. These six flight cases are summarized in Table 3.1. Note that the flight cses are parameterized by the tanker yaw rates and airspeed. Thus, the flight case values of the states and the control variables are also functions of the three parameters. Once a set of flight case values for each of six nominal conditions are determined, the equations of motion of the tanker are linearized at each flight case using the respective set of flight case values.

Table 3.1. Flight Cases by Turn rate and Airspeed

Flight Case	Tanker Yaw Rate	Tanker Airspeed
1	$\dot{\psi}_{T,1}$	$V_{T,1}$
2	$\dot{\psi}_{T,1}$	$V_{T,2}$
3	$\dot{\psi}_{T,2}$	$V_{T,1}$
4	$\dot{\psi}_{T,2}$	$V_{T,2}$
5	$\dot{\psi}_{T,3}$	$V_{T,1}$
6	$\dot{\psi}_{T,3}$	$V_{T,2}$

Followings are the six different sets of linearized equation of motion, in state-space form, for the tanker.

$$\Delta\dot{\underline{x}}_T = \mathbf{A}_{T,i}\ \Delta\underline{x}_T + \mathbf{B}_{T,i}\ \Delta\underline{u}_T \tag{3.11}$$

where $\mathbf{A}_{T,i} \in \Re^{9\times 9}$, $\mathbf{B}_{T,i} \in \Re^{9\times 4}$, $i \in \{1,2,3,4,5,6\}$, for the six nominal conditions described in Table 3.1, respectively. The state vector for the tanker aircraft is

$$\Delta\underline{x}_T = [\Delta V_T\ \ \Delta\beta_T\ \ \Delta\alpha_T\ \ \Delta p_T\ \ \Delta q_T\ \ \Delta r_T\ \ \Delta\theta_T\ \ \Delta\phi_T\ \ \Delta z_T\ ]^T \tag{3.12}$$

The control input vector is

$$\Delta\underline{u}_T = [\Delta\delta_{a_T}\ \ \Delta\delta_{e_T}\ \ \Delta\delta_{r_T}\ \ \Delta\xi_{t_T}\ ]^T \tag{3.13}$$

where $(\delta_{a_T}, \delta_{e_T}, \delta_{r_T})$ are the control surface deflections of the tanker and ξ_{t_T} is the throttle setting for the tanker. In all equations above, Δ indicates that the corresponding variable is the deviation from its nominal value. Since the requirements of the controller are to track commanded speed, altitude and yaw rate, the following output vector of the tanker aircraft is chosen

$$\underline{y}_T = \left[\Delta V_T\ \ \Delta z_T\ \ \Delta\dot{\psi}_T\right]^T \tag{3.14}$$

To ensure zero tracking error at steady state condition, the state space equations are augmented by three integrators for speed error, altitude error and yaw rate error:

$$\dot{\underline{e}}_T = \underline{y}_T - \underline{y}_{T,c} \tag{3.15}$$

where $\underline{y}_{T,c} = [\Delta V_{T,c}\ \Delta z_{T,c}\ \Delta\dot{\psi}_{T,c}]^T$ is the commanded output vector of the tanker. Thus, in scalar form

$$\begin{aligned} \dot{e}_{V_T} &= \Delta V_T - \Delta V_{T,c} \\ \dot{e}_{z_T} &= \Delta z_T - \Delta z_{T,c} \\ \dot{e}_{\dot{\psi}_T} &= \Delta\dot{\psi}_T - \Delta\dot{\psi}_{T,c} \end{aligned} \tag{3.16}$$

By including the augmentation states in the state–space equations, the augmented state equation becomes

$$\begin{bmatrix} \Delta\dot{\underline{x}}_T \\ \dot{\underline{e}}_T \end{bmatrix} = \begin{bmatrix} \mathbf{A}_{T,i} & \mathbf{0_{9\times 3}} \\ \mathbf{C_T} & \mathbf{0_{3\times 3}} \end{bmatrix} \begin{bmatrix} \Delta\underline{x}_T \\ \underline{e}_T \end{bmatrix} + \begin{bmatrix} \mathbf{B}_{T,i} \\ \mathbf{0_{3\times 4}} \end{bmatrix} \Delta\underline{u}_T - \begin{bmatrix} \mathbf{0_{9\times 3}} \\ \mathbf{I_{3\times 3}} \end{bmatrix} \underline{y}_{T,c} \tag{3.17}$$

Using LQR design technique, the state feedback gain matrix $[\mathbf{K_{T,x}}\ \mathbf{K_{T,e}}]$ is obtained to minimize the cost function:

$$J(\underline{u}_T) = \int_0^\infty \left\{ [\ \Delta\underline{x}_T^T \quad \underline{e}_T^T\ ] \mathbf{Q}_{T,i} \begin{bmatrix} \Delta\underline{x}_T \\ \underline{e}_T \end{bmatrix} + \Delta\underline{u}_T^T \mathbf{R}_{T,i}\, \Delta\underline{u} \right\} \mathrm{d}t \tag{3.18}$$

where $\mathbf{Q}_{T,i} \in \Re^{12\times 12}$ are symmetric positive semidefinite, $\mathbf{R}_{T,i} \in \Re^{4\times 4}$ are symmetric positive definite. Note that matrices $\mathbf{Q}_{T,i}$, and $\mathbf{R}_{T,i}$ can be selected separately for each flight case. Thus, the state feedback control laws with the integral control are

$$\Delta\underline{u}_{T,i} = -\mathbf{K_{x_{T,i}}}\, \Delta\underline{x}_T - \mathbf{K_{e_{T,i}}}\, \underline{e}_T \tag{3.19}$$

where $i \in \{1, 2, 3, 4, 5, 6\}$, corresponding to the six flight cases. In the implementation of these controllers, a "scheduling" scheme should be employed, based on scheduling

parameters, $\dot{\psi}_T$ and V_T to determine effective values of the gains at a given flight condition. To formulate the overall non-linear controller based on the linear designs at the six flight cases, Lagrange interpolation scheme is utilized. Thus, the gain scheduling control law is

$$\begin{aligned}
\Delta\underline{u} = & \frac{\left(\dot{\psi}_{T,c}-\dot{\psi}_{T,2}\right)\left(\dot{\psi}_{T,c}-\dot{\psi}_{T,3}\right)(V_{T,c}-V_{T,2})}{\left(\dot{\psi}_{T,1}-\dot{\psi}_{T,2}\right)\left(\dot{\psi}_{T,1}-\dot{\psi}_{T,3}\right)(V_{T,1}-V_{T,2})}\,\underline{u}_1 \\
& + \frac{\left(\dot{\psi}_{T,c}-\dot{\psi}_{T,2}\right)\left(\dot{\psi}_{T,c}-\dot{\psi}_{T,3}\right)(V_{T,c}-V_{T,1})}{\left(\dot{\psi}_{T,1}-\dot{\psi}_{T,2}\right)\left(\dot{\psi}_{T,1}-\dot{\psi}_{T,3}\right)(V_{T,2}-V_{T,1})}\,\underline{u}_2 \\
& + \frac{\left(\dot{\psi}_{T,c}-\dot{\psi}_{T,1}\right)\left(\dot{\psi}_{T,c}-\dot{\psi}_{T,3}\right)(V_{T,c}-V_{T,2})}{\left(\dot{\psi}_{T,2}-\dot{\psi}_{T,1}\right)\left(\dot{\psi}_{T,2}-\dot{\psi}_{T,3}\right)(V_{T,1}-V_{T,2})}\,\underline{u}_3 \\
& + \frac{\left(\dot{\psi}_{T,c}-\dot{\psi}_{T,1}\right)\left(\dot{\psi}_{T,c}-\dot{\psi}_{T,3}\right)(V_{T,c}-V_{T,1})}{\left(\dot{\psi}_{T,2}-\dot{\psi}_{T,1}\right)\left(\dot{\psi}_{T,2}-\dot{\psi}_{T,3}\right)(V_{T,2}-V_{T,1})}\,\underline{u}_4 \\
& + \frac{\left(\dot{\psi}_{T,c}-\dot{\psi}_{T,1}\right)\left(\dot{\psi}_{T,c}-\dot{\psi}_{T,2}\right)(V_{T,c}-V_{T,2})}{\left(\dot{\psi}_{T,3}-\dot{\psi}_{T,1}\right)\left(\dot{\psi}_{T,3}-\dot{\psi}_{T,2}\right)(V_{T,1}-V_{T,2})}\,\underline{u}_5 \\
& + \frac{\left(\dot{\psi}_{T,c}-\dot{\psi}_{T,1}\right)\left(\dot{\psi}_{T,c}-\dot{\psi}_{T,2}\right)(V_{T,c}-V_{T,1})}{\left(\dot{\psi}_{T,3}-\dot{\psi}_{T,1}\right)\left(\dot{\psi}_{T,3}-\dot{\psi}_{T,2}\right)(V_{T,2}-V_{T,1})}\,\underline{u}_6
\end{aligned} \tag{3.20}$$

Note that the control law assumes the availability of full state measurement or estimation for feedback. The control variables available for the tanker aircraft are the three conventional control surfaces and the throttle setting. The outputs to be controlled are the airspeed, altitude and yaw rate.

3.2 Receiver Aircraft

To successfully perform an aerial refueling operation, the receiver is required to approach to the tanker, stay at the refueling contact position during the actual fuel transfer, and fly away when the refueling is completed. These three phases should be

conducted in a safe manner despite various sources of disturbances such as trail wake vortex, fuel transfer effect, and motion of the tanker. The receiver aircraft motion is defined in the tanker's body frame, thus the reference trajectory for the receiver can simply be defined relative to the tanker simply. When the receiver is in the station-keeping phase, that is, receiver needs to be stay at the refueling contact position, the reference trajectory for the receiver aircraft becomes a point in the body-frame of the tanker. The receiver's trajectory-tracking controller is built to follow the safe reference trajectory in time after ensuring the trajectory from the observation position to the contact position, and from the contact position to the fly-away path. For the receiver aircraft, controller is strongly required to fly close to the reference trajectory.

3.2.1 Requirements

The primary requirement of the control design is the tracking of the generated trajectories, with zero steady-state error in the x, y, z coordinates in the tanker's body frame, under the disturbance of trailing vortex, time variation of the inertia properties of the receiver and the possible steady maneuvers of the tanker's body frame. Meanwhile, the control inputs generated by the controller should not cause significant saturation on the magnitudes and rates of the actuators. Moreover, during the transient, overshoot or undershoot on trajectory response should be minimized to ensure the safety of the refueling. At the same time, the response of the closed loop system should be fast enough so that the approach and fly–away maneuvers are completed as planned and the high-wind regions of the trailing vortex field are exited in a timely fashion. Additionally, during the approach, fly–away and station-keeping maneuvers, the angle-of-attack and the airspeed should not be close to their corresponding stall values. In this regard, very big pitch angle should not be commanded. Finally, to ensure the safety of the aircraft, the bank angle should be small relative to its nomi-

nal value. As stated earlier, the controller should perform satisfactorily in all phases of the "racetrack" maneuver, i.e. while the tanker is in a straight wing-level flight, in a steady turn, in transition from straight flight to turn and in transition back to straight flight. Control design of the receiver aircraft should also consider the mass and inertia variations. That is, the gain scheduling scheme should include mass and inertia variation of the aircraft due to the change in fuel amounts in all fuel tanks, and should cover all possible combinations of fuel levels in fuel tanks.

3.2.2 Nominal Condition Analysis

In aerial refueling operation, the receiver aircraft is required to maintain its position and orientation relative to the tanker aircraft. As in the case of tanker, wind terms are ignored in the trim analysis and lumbarization. Since the objective of the receiver is to maintain relative position and orientation with respect to the tanker, translational and angular velocity components of the receiver should be the same as those of the tanker. Thus, for nominal condition analysis; $V_0 = V_{T0}$, $p_0 = p_{T0}$, $q_0 = q_{T0}$ and $r_0 = r_{T0}$. Also yaw rates of the tanker and the receiver should be the same ($\dot{\psi}_0 = \dot{\psi}_{T0}$). Similar to the tanker, side slip angle of the receiver at the nominal condition is set to zero ($\beta_0 = 0$) and the receiver maintain its altitude ($\dot{z}_0 = 0$). At nominal condition, the thrust vectoring angles are preferred to be zero ($\delta y_0 = 0$ and $\delta z_0 = 0$). While the dynamic equations of motion of the receiver are written relative to the tanker as given in Eps. (3.30) and (2.48), for the trim analysis, the equations relative to the inertial frame are used. Further, at the steady-state, the mass and

the center of mass of fuel in each fuel tank are considered to be constant. These simplifications yield

$$\begin{aligned}
\dot{\mathcal{X}}_R &= \mathcal{E}_{\mathbf{R}}^{-\mathbf{1}}[\mathbf{R}_{\mathbf{B_R I}}\frac{1}{m_t}F - \mathbf{S}(\rho_{\mathbf{cm,t}})\dot{\omega}_{B_R} + \mathbf{S}(\omega_{\mathbf{B_R}})\mathbf{R}_{\mathbf{B_R W_R}}U - \mathbf{R}_{\mathbf{B_R I}}\dot{W}_I \\
&\quad -\mathbf{S^2}(\omega_{\mathbf{B_R}})\rho_{cm,t}] \qquad (3.21)\\
\dot{\omega}_{B_R} &= \underline{\underline{\mathbf{I}}}_{\mathbf{t}}^{-1}[M_{B_R} + \mathbf{S}(\omega_{\mathbf{B_R}})\underline{\underline{\mathbf{I}}}_{\mathbf{t}}\omega_{B_R} + m_t\mathbf{S}(\rho_{\mathbf{cm,t}})\mathcal{E}_{\mathbf{R}}\dot{\mathcal{X}}_R + m_t\mathbf{S}(\rho_{\mathbf{cm,t}})\mathbf{R}_{\mathbf{B_R I}}\dot{W}_I \\
&\quad -m_t\mathbf{S}(\rho_{\mathbf{cm,t}})\mathbf{R}_{\mathbf{B_R I}}\dot{W}_I - m_t\mathbf{S}(\rho_{\mathbf{cm,t}})\mathbf{S}(\omega_{\mathbf{B_R}})\mathbf{R}_{\mathbf{B_R W_R}}U] \qquad (3.22)\\
\dot{\xi} &= \mathbf{R}^{\mathbf{T}}_{\mathbf{B_R B_T}}\mathbf{R}_{\mathbf{B_R W_R}}U + \mathbf{R}^{\mathbf{T}}_{\mathbf{B_R B_T}}W - \mathbf{R}_{\mathbf{B_T I}}\,\dot{r}_{B_T} + \mathbf{S}(\omega_{\mathbf{B_T}})\xi \qquad (3.23)
\end{aligned}$$

where

$$\mathcal{X}_R = \begin{bmatrix} V_R \\ \beta_R \\ \alpha_R \end{bmatrix} \qquad (3.24)$$

$$\omega_{B_R} = \begin{bmatrix} p_R \\ q_R \\ r_R \end{bmatrix} \qquad (3.25)$$

and $\mathcal{X}_R$ is written with respect to the wind frame and ω_{B_R} is written with respect to the inertial frame. At nominal flight condition, $\mathcal{X}_R$ = constant, ω_{B_R} = constant and no wind. At a steady-state trimmed flight conditions, translational dynamics and rotational dynamics yield

$$\mathbf{R}_{\mathbf{B_R I}}\frac{1}{m_t}F + \mathbf{S}(\omega_{\mathbf{B_R}})\mathbf{R}_{\mathbf{B_R W_R}}U - \mathbf{S^2}(\omega_{\mathbf{B_R}})\rho_{cm,t} = \begin{bmatrix} 0 \\ 0 \\ 0 \end{bmatrix} \qquad (3.26)$$

$$M_{B_R} + \mathbf{S}(\omega_{\mathbf{B_R}})\underline{\underline{\mathbf{I}}}_{\mathbf{t}}\omega_{B_R} - m_t\mathbf{S}(\rho_{\mathbf{cm,t}})\mathbf{S}(\omega_{\mathbf{B_R}})\mathbf{R}_{\mathbf{B_R W_R}}U = \begin{bmatrix} 0 \\ 0 \\ 0 \end{bmatrix} \qquad (3.27)$$

Since altitude is constant, $\dot{z}$ equation from translational kinematics yield

$$\dot{z} = -V_R \cos\alpha \cos\beta \sin\theta + V_R \sin\beta \sin\phi \cos\theta + V_R \sin\alpha \cos\beta \cos\phi \cos\theta \qquad (3.28)$$

Note that in these seven equations, there are seven unknowns. By solving these seven equations, the nominal values of the unknowns are computed. Recall that in the equations of motion of the receiver aircraft, euler angles are relative to the tanker. While all the other nominal values are directly computed, the relative euler angles need to be computed.

3.2.3 Linearization

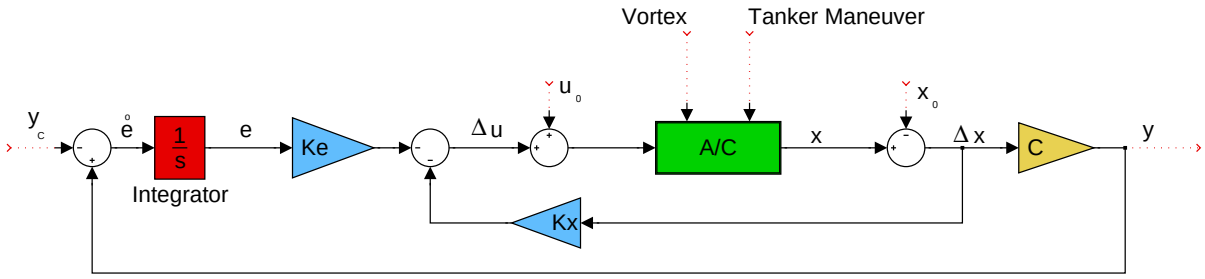

Figure 3.1. State feedback and integral control structure.

As stated earlier, the gain scheduling controller for the receiver should include the variation of mass/inertia of the aircraft. This can be done by using the amount of fuel in each fuel tanks as scheduling parameters in additions to the turn rate and speed of the aircraft. The gain scheduling controller design requires the definition of trim conditions in terms of the fuel amounts in fuel tanks for each set of turn rate and speed. The three turn rates (zero, right turn and left turn) and two speed values result in six flight cases, as done with the tanker aircraft. For the receiver aircraft, the number of mass/inertia configurations to be included in the set of trim

Table 3.2. Nominal Conditions by Four Receiver Fuel Tanks

Nominal Condition	Fuel Filled Tanks
1	$None$
2	$Tank_4$
3	$Tank_3$
4	$Tank_4, Tank_3$
5	$Tank_2$
6	$Tank_4, Tank_2$
7	$Tank_3, Tank_2$
8	$Tank_4, Tank_3, Tank_2$
9	$Tank_1$
10	$Tank_4, Tank_1$
11	$Tank_3, Tank_1$
12	$Tank_4, Tank_3, Tank_1$
13	$Tank_2, Tank_1$
14	$Tank_4, Tank_2, Tank_1$
15	$Tank_3, Tank_2, Tank_1$
16	$Tank_1, Tank_2, Tank_3, Tank_4$

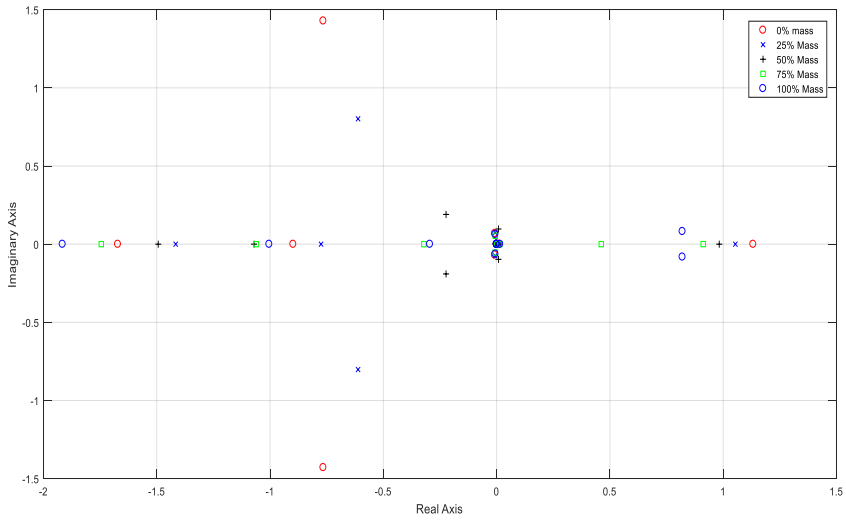

Figure 3.2. Loci of the eigenvalues as the amount of fuel changes in tank 2, 3, and 4, and tank 1 is empty in cruise condition.

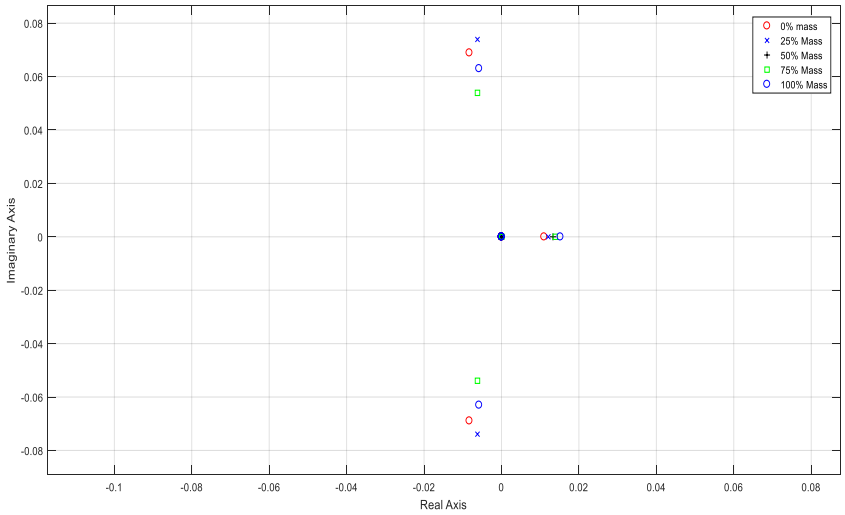

Figure 3.3. Zoomed loci of the eigenvalues as the amount of fuel changes in tank 2, 3, and 4, and tank 1 is empty in cruise condition.

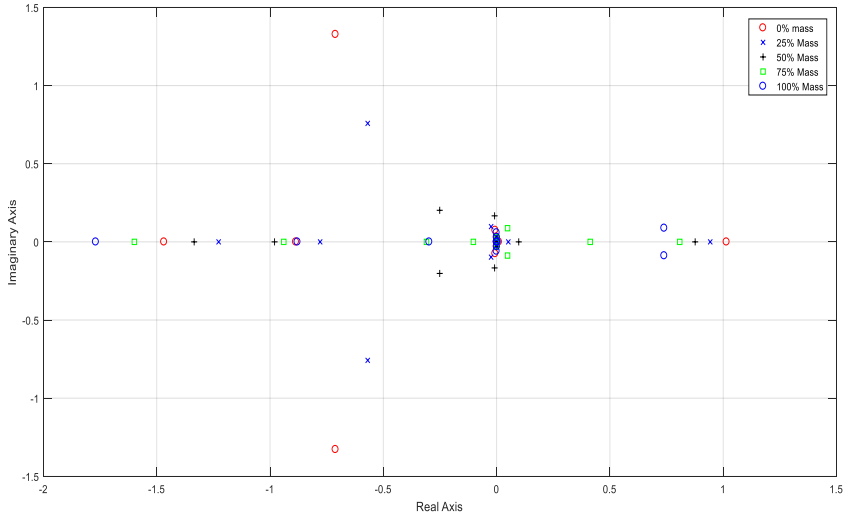

Figure 3.4. Loci of the eigenvalues as the amount of fuel changes in tanks 1, 3, and 4, and tank 2 is empty in steady turn.

conditions should be determined. The objective is to keep the number of such fuel tank configurations small while making sure that they will cover the whole span of

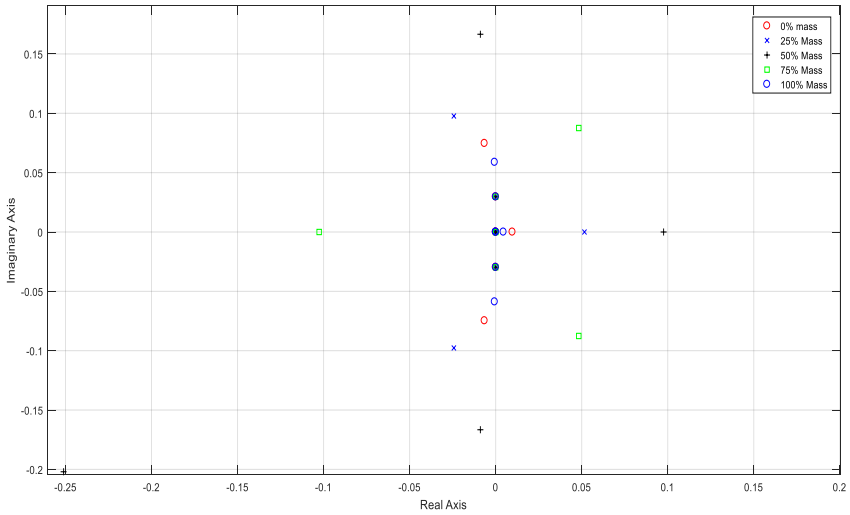

Figure 3.5. Zoomed loci of the eigenvalues as the amount of fuel changes in tanks 1, 3, and 4, and tank 2 is empty in steady turn.

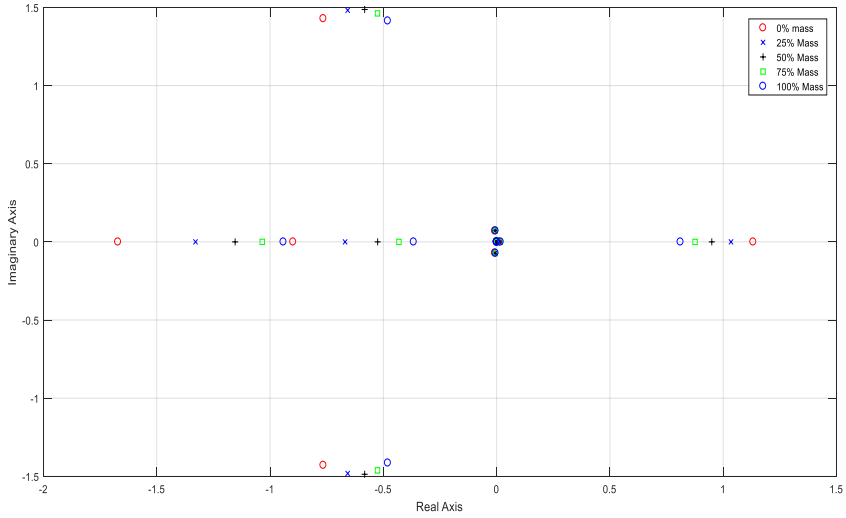

Figure 3.6. Loci of the eigenvalues as the amount of fuel changes in all tanks in cruise.

the mass/inertia variation of the receiver aircraft. The ICE receiver aircraft has four fuel tanks. For each fuel tank, initially five different mass amounts considered are 0%, 25%, 50%, 75%, and 100% full. This leads to $5^4 = 625$ permutations for the four

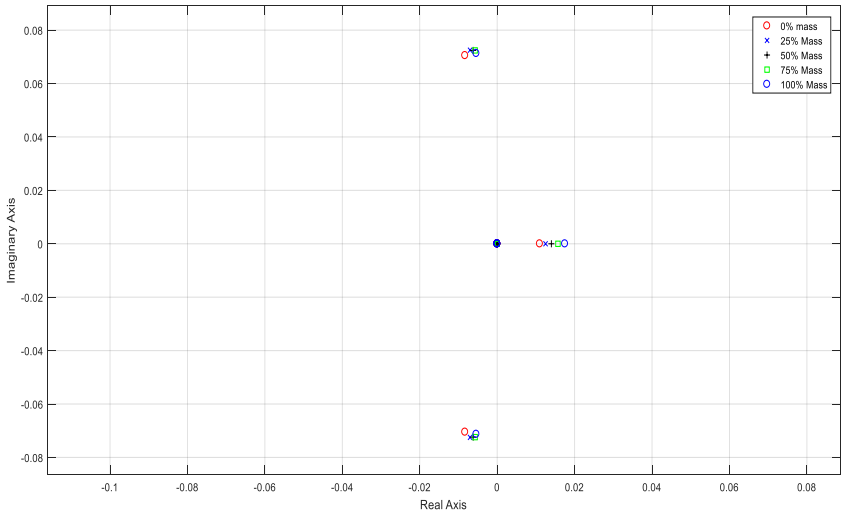

Figure 3.7. Zoomed loci of the eigenvalues as the amount of fuel changes in all tanks in cruise.

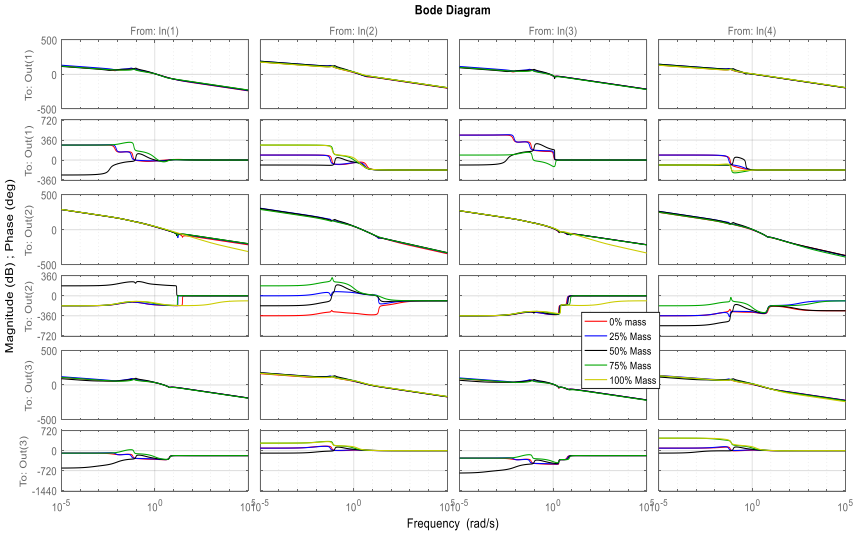

Figure 3.8. Bode plot for case-56.

fuel tanks in each of the 6 flight cases. This is obviously too many trim conditions for a gain scheduling controller. Two different analyses are carried out to determine how many of these permutations need to be kept and how many can be excluded from

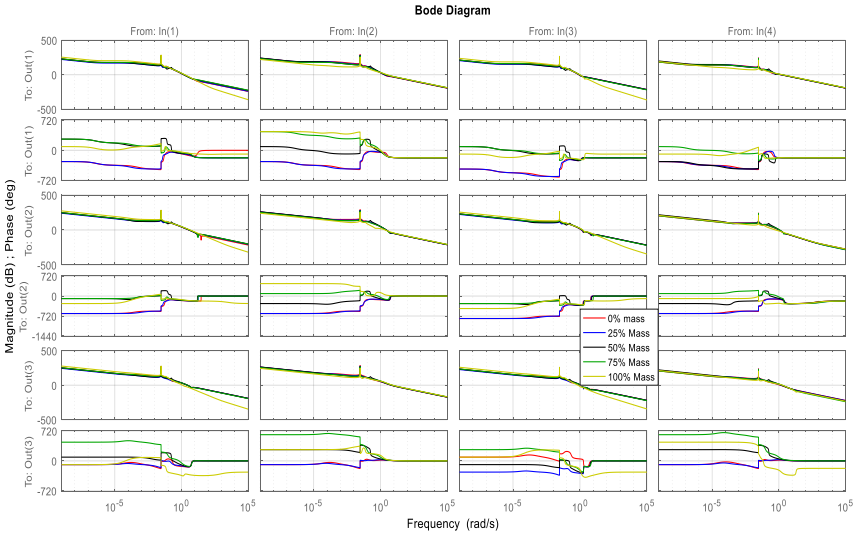

Figure 3.9. Bode plot for case-12.

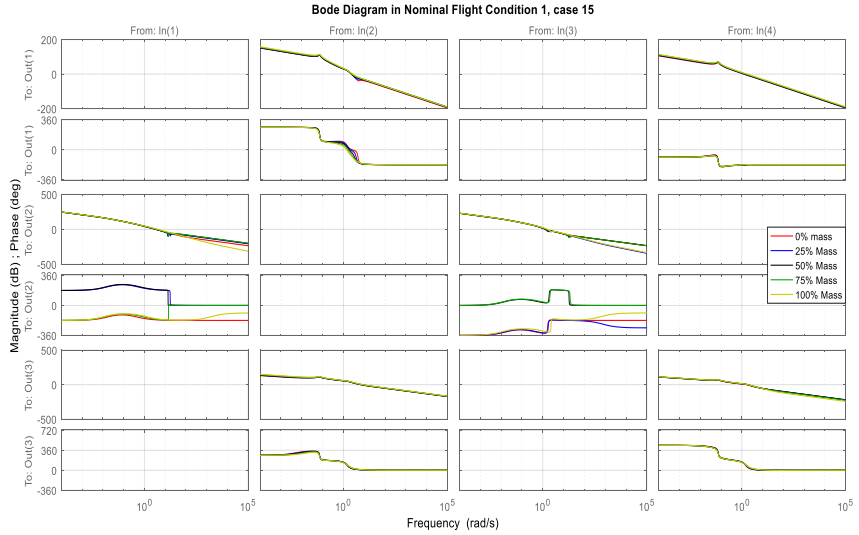

Figure 3.10. Bode plot for case-64.

the gain scheduling controller design: (1) Eigenvalue analysis, and (2) Frequency domain analysis. In each fuel tank permutation at each nominal flight condition, the trim analysis and linearization are carried out and the matrices of the state space representation are constructed. In the eigenvalue analysis, eigenvalues of the open

loop state space model are placed on complex domain. If the eigenvalues of multiple permutations are within a specified proximity, then, all these permutations will be represented by one of the permutations within the group. In the case of frequency domain analysis, Bode plots of the open loop system based on the state space matrices are compared and again the permutations with Bode plots "close to each other" are represented by one permutations within the group. This approaches are justified by the fact that linear systems with eigenvalues or Bode plots close to each other have similar dynamic characteristics. Through eigenvalue and Bode analyses, it is demonstrated that, in all six flight cases, fuel tank permutation with 0%, 25%, and 50% full fuel tanks have similar dynamic responses. Similarly, fuel tank permutations with 75% and 100% fuel have similar dynamical responses. Thus, only 0% and 100% fuel cases are included in fuel tank permutations considered for gain scheduling control design. For example, three fuel tanks, 2, 3, and 4, are filled at various levels and tank 1 is empty while the aircraft is in a cruise condition with airspeed $V_{T,2}$. The eigenvalue locations of the state matrix of the linearized model at each of the trim conditions are plotted on the complex domain, as shown in Fig. 3.2. The plot clearly shows that the eigenvalues of the open loop system moves on the complex domain as the fuel amount changes in the three fuel tanks. The question here is whether the changes in the eigenvalue locations are significant to require considerations of all these trim conditions in the gain scheduling controller. Note that most clusters of eigenvalues show small movement as the fuel amount changes except the eigenvalues scattered around -2.0 to -0.7 on or close to the real axis. Fig. 3.3 shows the details about Fig. 3.2 around the clusters near the intersection between real and imaginary axis. When the tanks are 100% full, the eigenvalues are complex while in the three other cases, eigenvalues break into the real axis. Similar trend is seen in Fig. 3.4 and Fig. 3.5 when eigenvalue locations are analyzed when fuel tanks 1, 3, and 4 are filled

at different levels and tank 2 is empty while the aircraft is in a steady-state turn. Another example, as shown in Fig. 3.6 and Fig. 3.7, is when all fuel tanks are filled at various levels in a cruise condition. Fig. 3.8 and Fig. 3.2 are in the same condition such as most deviated cases for the cruise condition. Fig. 3.9 and Fig. 3.4 are in the condition of most deviated cases for the steady turn. Fig. 3.10 and Fig. 3.6 show the condition of all four fuel tanks are fully filled in a cruise condition. In Fig. 3.8, Fig. 3.9 and Fig. 3.10, frequency domain has 4 categories for control input values as in Eq. (3.31). However in this analysis $\Delta\delta_y$ and $\Delta\delta_z$ are not considered because these values are set to be zero at the trim analysis. So only four values are showing in these figures such as $\Delta\delta_a$, $\Delta\delta_e$, $\Delta\delta_r$, and $\Delta\xi$. In the figure magnitude and phase angle have three outputs. These three represent output vector in Eq. (3.33) as in Δx, Δy, Δz. These analyses show that not all fuel levels at 0%, 25%, 50%, 75%, and 100% need to be considered in gain scheduling as the dynamics of the linear models are "close" according to eigenvalue locations. This reduces the number of permutations from 625 to 16 for each nominal flight condition. These 16 cases are tabulated in Table B.2. Sixteen mass/inertia configurations for each of the six flight case added up to 96 trim conditions for the gain scheduling controller. These 96 trim conditions are tabulated in Table A.1 - Table A.3 in Appendix A. Linearizing the equations of motion at each of the 96 cases leads to 96 different state space representations.

$$\Delta\underline{\dot{x}} = \mathbf{A}_i\ \Delta\underline{x} + \mathbf{B}_i\ \Delta\underline{u} + \mathbf{H}_i\ \Delta\underline{w} \tag{3.29}$$

where $\mathbf{A}_i \in \Re^{12\times12}$, $\mathbf{B}_i \in \Re^{12\times6}$, $\mathbf{H}_i \in \Re^{12\times6}$, $i \in \{1, ..., 96\}$, for the combinations of the six flight cases described in Table 3.1 and 16 conditions listed in Table B.2. The state vector is

$$\Delta\underline{x} = [\Delta V\ \ \Delta\beta\ \ \Delta\alpha\ \ \Delta p\ \ \Delta q\ \ \Delta r\ \ \Delta\psi\ \ \Delta\theta\ \ \Delta\phi\ \ \Delta x\ \ \Delta y\ \ \Delta z]^T \tag{3.30}$$

The control input vector is

$$\Delta\underline{u} = [\Delta\delta_a \ \Delta\delta_e \ \Delta\delta_r \ \Delta\xi \ \Delta\delta_y \ \Delta\delta_z]^T \tag{3.31}$$

The disturbance vector due to the motion of the tanker is

$$\Delta\underline{w} = [\Delta V_{xT} \ \Delta V_{yT} \ \Delta V_{zT} \ \Delta p_T \ \Delta q_T \ \Delta r_T \ \Delta\dot{p}_T \ \Delta\dot{q}_T \ \Delta\dot{r}_T \ \Delta\psi_T \ \Delta\theta_T \ \Delta\phi_T]^T \tag{3.32}$$

In all equations above, Δ indicates that the corresponding variable is the perturbation from its nominal value. Note that, since the nonlinear equations of motion are derived in terms of the states of the receiver relative to the tanker, in the linearized equations, the effect of the motion of the tanker on the relative motion is clearly identified by H_i matrices. However, H_i matrices are not utilized in the control design carried out in this research. Since the position tracking controller is to be designed for the receiver relative to the tanker, the outputs to be tracked are (Δx, Δy,Δz). Thus, output vector is chosen to be

$$\underline{y} = [\Delta\beta \ \Delta x \ \Delta x \ \ \Delta y \ \ \Delta z]^T \tag{3.33}$$

To ensure zero tracking error at steady state condition, the state space equations are augmented by three integrators, one for each position error:

$$\underline{\dot{e}} = \underline{y} - \underline{y_c} \tag{3.34}$$

where $\underline{y_c} = [\Delta\beta_c \ \ \Delta x_c \ \ \Delta y_c \ \ \Delta z_c]^T$ is zero sideslip command and the commanded trajectory for the receiver in the body frame of the tanker for approaching the refueling contact position. Thus, in scalar form

$$\begin{aligned} \dot{e}_\beta &= \Delta\beta - \Delta\beta_c \\ \dot{e}_x &= \Delta x - \Delta x_c \\ \dot{e}_y &= \Delta y - \Delta y_c \\ \dot{e}_z &= \Delta z - \Delta z_c \end{aligned} \tag{3.35}$$

By including the augmentation states in the state-space equations, the augmented state equation becomes

$$\begin{bmatrix} \Delta\underline{\dot{x}} \\ \underline{\dot{e}} \end{bmatrix} = \begin{bmatrix} \mathbf{A}_i & \mathbf{0_{12\times 3}} \\ \mathbf{C} & \mathbf{0_{3\times 3}} \end{bmatrix} \begin{bmatrix} \Delta\underline{x} \\ \underline{e} \end{bmatrix} + \begin{bmatrix} \mathbf{B}_i \\ \mathbf{0_{3\times 6}} \end{bmatrix} \Delta\underline{u} + \begin{bmatrix} \mathbf{H}_i \\ \mathbf{0_{3\times 6}} \end{bmatrix} \Delta\underline{w} - \begin{bmatrix} \mathbf{0_{12\times 3}} \\ \mathbf{I_{3\times 3}} \end{bmatrix} \underline{y_c} \tag{3.36}$$

Using LQR design technique, the state feedback gain matrix $[\mathbf{K_x}\ \mathbf{K_e}]$ is obtained to minimize the cost function:

$$J(\underline{u}) = \int_0^\infty \left\{ [\ \Delta\underline{x}^T \quad \underline{e}^T\ ] \mathbf{Q}_i \begin{bmatrix} \Delta\underline{x} \\ \underline{e} \end{bmatrix} + \Delta\underline{u}^T \mathbf{R}_i\, \Delta\underline{u} \right\} \mathrm{d}t \tag{3.37}$$

where $\mathbf{Q}_i \in \Re^{15\times 15}$ are symmetric positive semidefinite and $\mathbf{R}_i \in \Re^{6\times 6}$ are symmetric positive definite. Note that matrices $\mathbf{Q}_i$ and $\mathbf{R}_i$ can be selected separately for each nominal condition. Thus, the state feedback control laws with the integral control are

$$\Delta\underline{u_i} = -\mathbf{K_{x_i}}\, \Delta\underline{x} - \mathbf{K_{e_i}}\, \underline{e} \tag{3.38}$$

where $i \in \{1, ..., 96\}$, corresponding to the 96 nominal conditions.

3.2.4 Gain Scheduling Based on Flight Conditions

As discussed in Section 3.1.3, the tanker aircraft control design considers six nominal flight conditions (see Fig. 3.11) based on two different nominal speeds and three different turn rates. The tanker gain scheduling controller uses a Lagrange interpolation scheme, formulated in Eq. (3.20) which encompasses all six nominal conditions. For the gain scheduling controller of the receiver aircraft, a slightly different interpolation scheme is used, mostly to facilitate the expansion of gain scheduling to fuel mass configuration, later in this research. The interpolation for gain scheduling is now done only among the "neighboring" nominal conditions. This implies that

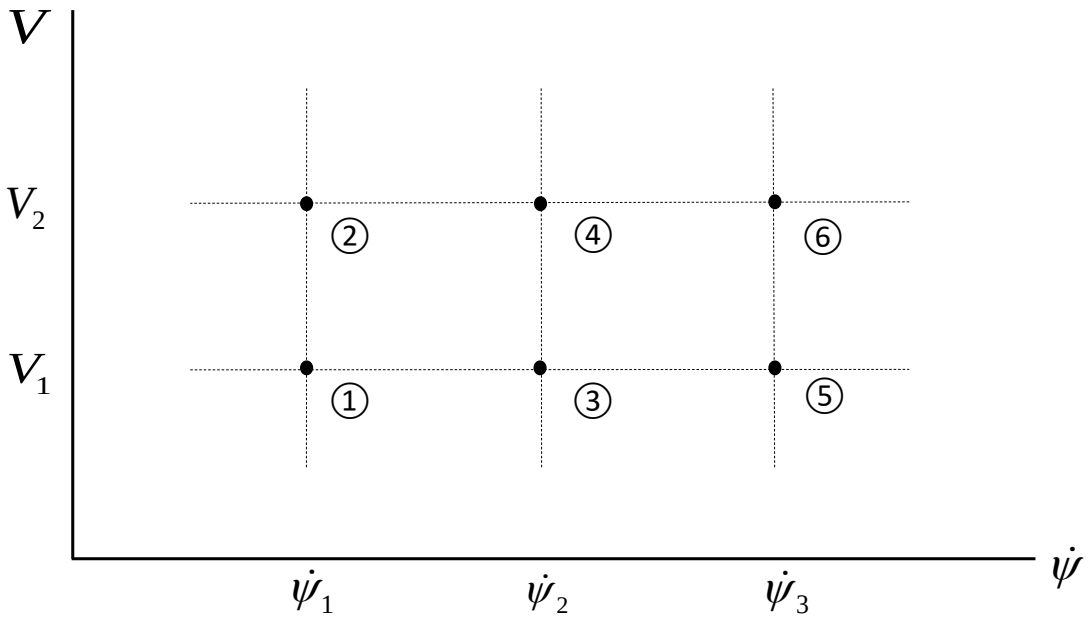

Figure 3.11. Six Nominal Conditions Based on Flight Condition.

the neighboring nominal design conditions need to be determined for a given flight condition. For this, the speed V and turn rate $\dot{\psi}$ are normalized as

$$V_N = \frac{V}{(V_2 - V_1)}$$
$$\dot{\psi}_N = \frac{\dot{\psi}}{(\dot{\psi}_3 - \dot{\psi}_1)}$$

such that

$$\dot{\psi}_{N1} = 0, \;\; \dot{\psi}_{N2} = 0.5, \;\; \dot{\psi}_{N3} = 1$$

$$V_{N1} = 0, \;\; V_{N2} = 1$$

Let $\mathbf{S}_{BC}(\dot{\psi}_N, V_N)$ be the set of "neighboring" nominal design points for $\dot{\psi}_N$ and V_N. The algorithm used to determine the neighboring points is depicted in Fig. 3.12.

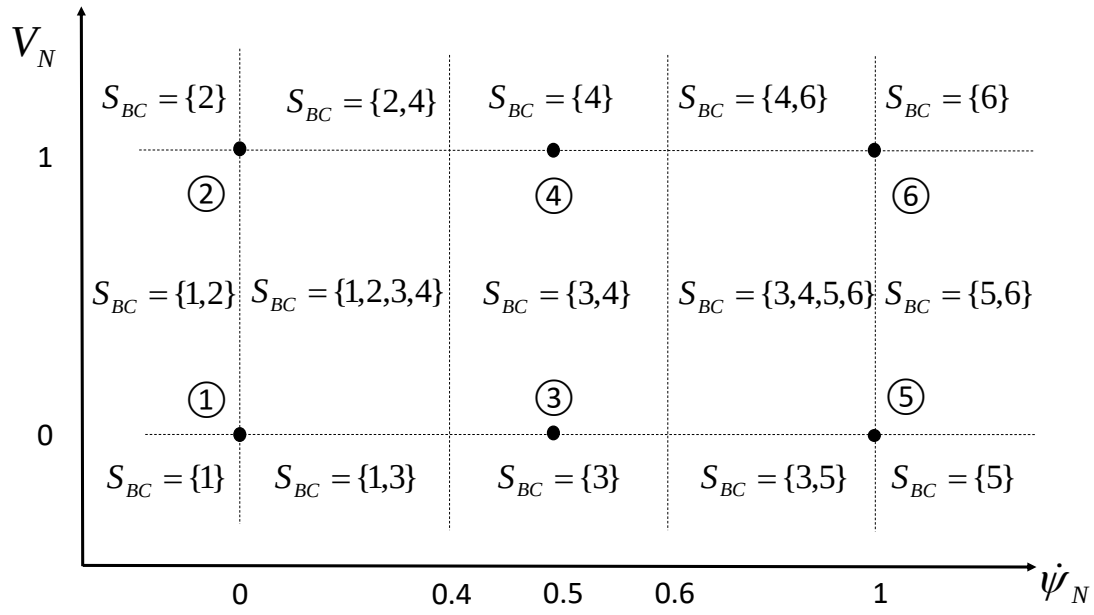

Figure 3.12. Neighboring Nominal Design Conditions.

Given a flight condition with $(V_C, \dot{\psi}_C)$, "distance" to each "neighboring" nominal design point should be computed. This is done along each scheduling variable separately. Let $(V_{BC_i}, \dot{\psi}_{BC_i})$ be the speed and the turn rate of the given neighboring point, BC-i. The sets of the nominal values of the scheduling variables used in defining the nominal design conditions are

$$\mathbf{S}_V = \{V_1,\ V_2\}$$

$$\mathbf{S}_{\dot{\psi}} = \left\{\dot{\psi}_1,\ \dot{\psi}_2,\ \dot{\psi}_3\right\}$$

Note $V_{BCi} \in \mathbf{S}_V$ and $\dot{\psi}_{BCi} \in \mathbf{S}_{\dot{\psi}}$. For the nominal point, the subsets of the scheduling variables are defined as

$$\mathbf{S}_V^i = \mathbf{S}_V - \{V_{BCi}\} \tag{3.39}$$

$$\mathbf{S}_{\dot{\psi}}^i = \mathbf{S}_{\dot{\psi}} - \left\{\dot{\psi}_{BCi}\right\} \tag{3.40}$$

Then, the Lagrange interpolation coefficients for each scheduling variable is defined as

$$a_V^i = \prod_{j=1}^{n(\mathbf{S}_V^i)} \frac{V_C - V_j}{V_{BC_i} - V_j} \tag{3.41}$$

where $V_j \in \mathbf{S}_V^i$, and $n(\mathbf{S}_V^i)$ is the cardinal of (number of element in) Set $\mathbf{S}_V^i$. Similarly

$$a_{\dot{\psi}}^i = \prod_{j=1}^{n(\mathbf{S}_{\dot{\psi}}^i)} \frac{\dot{\psi}_C - \dot{\psi}_j}{\dot{\psi}_{BCi} - \dot{\psi}_j} \tag{3.42}$$

where $\dot{\psi}_j \in \mathbf{S}_{\dot{\psi}}^i$. The Lagrange coefficient for BC-i is defined to be the product of the individual coefficients as

$$a^i = a_V^i \;\; a_{\dot{\psi}}^i \tag{3.43}$$

The last step is to normalize the coefficients over all the neighboring points considered as

$$\bar{a}^i = \frac{a^i}{\sum_{j=1}^{n(\mathbf{S}_{BC})} a_j}$$

where $n(\mathbf{S}_{BC})$ is the cardinal of the set of the neighboring nominal design points. Finally, the gain scheduling controller is formulated as the linear combination of the controllers designed for each neighboring point as

$$u = \sum_{i=1}^{n(\mathbf{S}_{BC})} \bar{a}^i u_i$$

where u_i is the linear controller designed for the nominal flight condition BC-i.

The above discussion is further explained in an example. Consider a flight condition with $(V_C, \dot{\psi}_C)$ such that the normalized values are

$$0 < V_{NC} < 1$$

$$0.4 < \dot{\psi}_{NC} < 0.6$$

which implies, as depicted in Fig. 3.12, that the neighboring points are BC-3 and BC-4, i.e.,

$$\mathbf{S}_{BC} = \{3, 4\}$$

The Lagrange interpolation coefficient with respect to nominal design conditions BC-3 and BC-4 are to be computed. Starting with BC-3, note from Fig. 3.11 that $V_{BC_3} = V_1$ and $\dot{\psi}_{BC_3} = \dot{\psi}_2$. By Eqs. (3.39) and (3.40), subsets of scheduling variable values are

$$\mathbf{S}_V^3 = \{V_2\}$$

$$\mathbf{S}_{\dot{\psi}}^3 = \left\{\dot{\psi}_1, \dot{\psi}_3\right\}$$

Then, Eqs. (3.41) and (3.42) imply

$$a_V^3 = \frac{V_C - V_2}{V_1 - V_2}$$

$$a_{\dot{\psi}}^3 = \frac{\dot{\psi}_C - \dot{\psi}_1}{\dot{\psi}_2 - \dot{\psi}_1} \cdot \frac{\dot{\psi}_C - \dot{\psi}_3}{\dot{\psi}_2 - \dot{\psi}_3}$$

Thus, the Lagrange coefficient of design condition BC-3 is

$$a^3 = a_V^3 \, a_{\dot{\psi}}^3$$

Similarly, the Lagrange coefficient of BC-4 is formulated as follows. Note that $V_{BC_4} = V_2$ and $\dot{\psi}_{BC_4} = \dot{\psi}_2$. By Eqs. (3.39) and (3.40), the subsets of scheduling variable values are

$$\mathbf{S}_V^4 = \{V_1\}$$

$$\mathbf{S}_{\dot{\psi}}^4 = \left\{\dot{\psi}_1, \dot{\psi}_3\right\}$$

Then, Eqs. (3.41) and (3.42) imply

$$a_V^4 = \frac{V_C - V_1}{V_2 - V_1}$$

$$a_{\dot{\psi}}^4 = \frac{\dot{\psi}_C - \dot{\psi}_1}{\dot{\psi}_2 - \dot{\psi}_1} \cdot \frac{\dot{\psi}_C - \dot{\psi}_3}{\dot{\psi}_2 - \dot{\psi}_3}$$

Thus, the Lagrange coefficient of design condition BC-4 is

$$a^4 = a_V^4 \, a_{\dot{\psi}}^4$$

Normalization of a^3 and a^4, by Eq. (3.44), yields

$$\bar{a}^3 = \frac{a^3}{a^3 + a^4}$$

$$\bar{a}^4 = \frac{a^4}{a^3 + a^4}$$

Finally, the gain scheduling controller is

$$u = \bar{a}^3 u_3 + \bar{a}^4 u_4$$

where u_3 and u_4 are the linear controllers designed specifically for nominal conditions BC-3 and BC-4, respectively.

3.2.5 Determining Number of Nominal Conditions

3.2.5.1 Eigenvalue Analysis

The process of reducing the number of nominal conditions included in the gain scheduling controller further from 96 are detailed in this section. The main idea is to replace a group of nominal conditions with a representative one when the linearized models around those nominal conditions are "close" to each other in some sense. Examples of using eigenvalues locations and Bode plots are presented. The eigenvalues of state matrix A_i in the linearized equation for each of the 96 nominal conditions in Eq. (3.29) are plotted on the complex domain. If the eigenvalues of multiple cases are "close" on the complex domain, then the corresponding linear models are considered to be dynamically similar, and thus only one of those nominal condition is used in the gain scheduling. The first sets of cases to analyze are the ones with symmetric fuel tank loading when the aircraft is in straight-level flight condition. For example, case-57 and case-53 have only fuel tank 1 and 2 full, respectively when $\dot{\psi}_{T,2}$ and $V_{T,2}$. When the eigenvalues of the corresponding state matrices are compared, it is seen that the eigenvalues are located at exactly the same positions, as expected. This means that

only one of these nominal cases will be sufficient to be included in the gain scheduling. The second sets of cases are the ones with symmetric fuel tank loading when the aircraft is in turning flight condition. For example, case-89 when $\dot{\psi}_{T,3}$ and $V_{T,2}$ with tank 1 full, and case-21 when $\dot{\psi}_{T,1}$ and $V_{T,2}$ with tank 2 full are compared. These cases are symmetrically similar and eigenvalues are located at exactly the same position when eigenvalues of the corresponding state matrices are compared, as expected. The third case are the ones with "close" to each other to group them together. For example, case-82 when $\dot{\psi}_{T,3}$ and $V_{T,2}$ with tank 4 full, and case-66 when $\dot{\psi}_{T,3}$ and $V_{T,1}$ with tank 4 full are compared. These cases are not symmetrically similar, however when comparing eigenvalues, they are very close together to group them together as in Fig. 3.13. The last case shows not all the cases fit in the grouping process. When comparing case-93 and case-91, those are not symmetrically similar and the pattern of eigenvalue location is different as in Fig 3.14. Case-93 when $\dot{\psi}_{T,3}$ and $V_{T,2}$ with tank 1,and 2 full and case-91 when $\dot{\psi}_{T,3}$ and $V_{T,2}$ with tank 1,and 3 full need to be treated individually.

3.2.5.2 Bode Plot Analysis

To generate Bode plots, input-output pair should be defined and then corresponding transfer function needs to be derived from A_i and B_i matrices. Bode plots are helping the eigenvalue discussion by showing cases how they are close together each other or not. Figure 3.15 shows the third case of eigenvalue example for case-82 and case-66 comparison and figure 3.16 demonstrates the last case of eigenvalue example for case-93 and case-91 comparison.

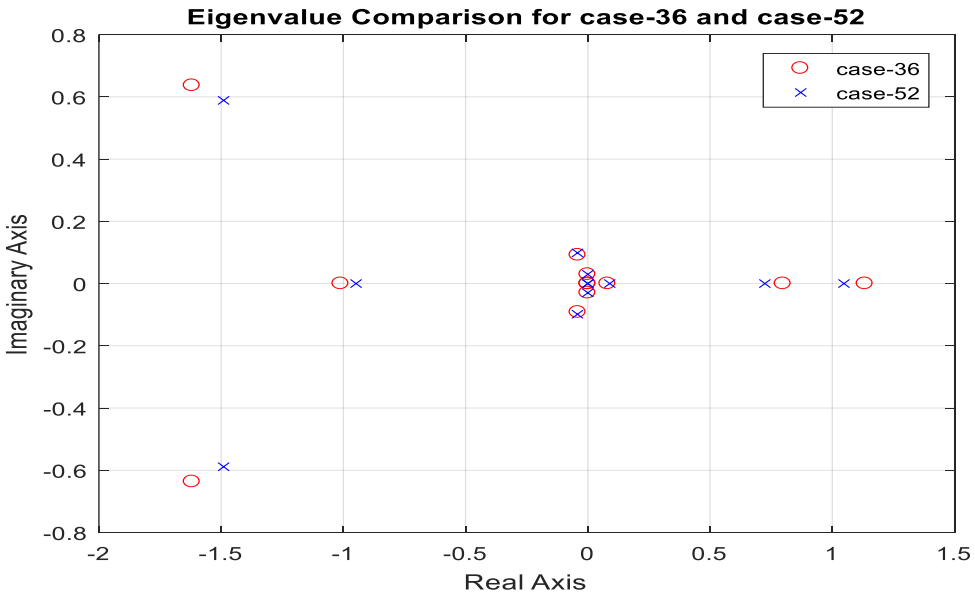

Figure 3.13. Eigenvalue comparison for case-82 and case-66.

3.2.5.3 Simplified Receiver Gains

Using eigenvalue and Bode analyses the nominal design conditions for the gain scheduling are reduced from 96 to 16 mass configuration cases. In the gain scheduling algorithm, 16 nominal cases of fuel tank configurations for each of the 6 flight conditions will be used.

3.2.5.4 Gain Scheduling Controller

Once the nominal cases to be included in the gain scheduling scheme are determined, as detailed in the previous section, the LQR controllers for each of the nominal cases are designed as explained in Section 3.2.3. These linear controllers should be put together for the final implementation based on the scheduling variables of airspeed, yaw rate and fuel tank configurations. An interpolation function formulated

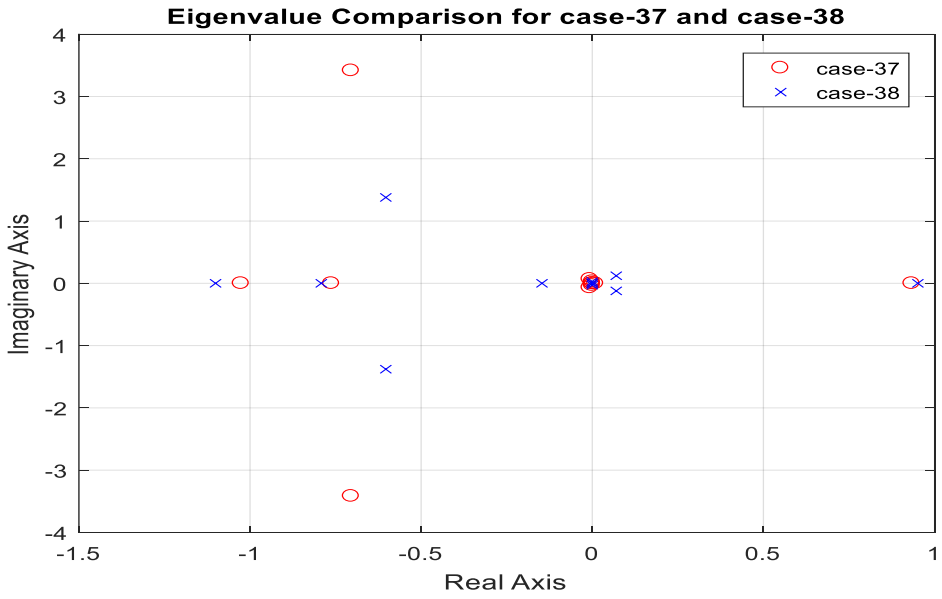

Figure 3.14. Eigenvalue comparison for case-93 and case-91.

for the tanker controller in Eq. (3.20) because of the discrete nature of the scheduling variable of fuel configuration. This formulation is part of the plan for completion.

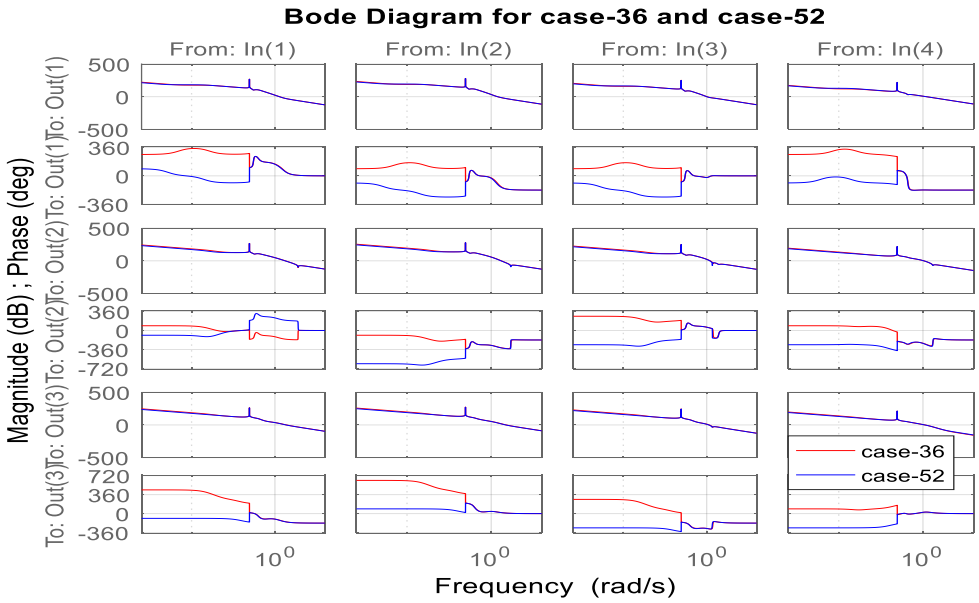

Figure 3.15. Bode plots comparison for case-82 and case-66.

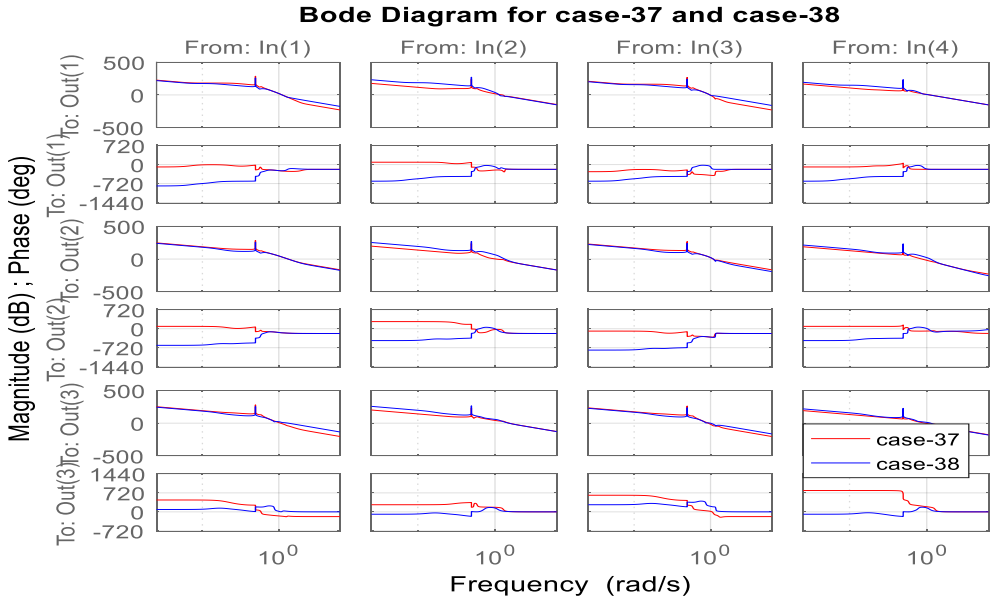

Figure 3.16. Bode plots comparison for case-93 and case-91.

Table 3.3. Sixteen Receiver Nominal Conditions

Nominal Condition	Flight Condition	Tank 1	Tank 2	Tank 3	Tank 4
4	1	0	0	1	1
11	1	1	0	1	0
16	1	1	1	1	1
19	2	0	0	1	0
24	2	0	1	1	1
29	2	1	1	0	0
33	3	0	0	0	0
36	3	0	0	1	1
51	4	0	0	1	0
57	4	1	0	0	0
60	4	1	0	1	1
69	5	0	1	0	0
75	5	1	0	1	0
83	6	0	0	1	0
89	6	1	0	0	0
95	6	1	1	1	0

CHAPTER 4

MOTIVATION

This section shows the results of several simulation cases when the receiver aircraft moves between the observation position and refueling (contact) positions while the tanker aircraft flies at constant altitude and constant speed in cruise condition. Table 4.1 gives the coordinates of the observation and refueling position relative to the tanker aircraft body frame. The observation position is the right side and behind the tanker aircraft. The refueling position is in the wake, right behind and below the tanker aircraft where the receiver is subject to downwash. The receiver aircraft is at the observation position when the simulation starts. To move to the refueling position, the receiver first moves down to the altitude of the refueling position, then moves laterally until behind the tanker. In the last phase, the receiver moves forward to the refueling position. During these maneuvers, the receiver experiences different aerodynamic forces and moments induced by the wake of the tanker. After staying at the refueling position for a while, the receiver moves back to the observation position by following the three phases in the receiver order. As described in the control design chapter, the control design process uses state and control/input matrices computed for a specified fuel tank configuration as well as trim values of the state and control

Table 4.1. Coordinates of Observation and Refueling Position

	x	y	z
Observation Position [m]	-59.13	56.33	0
Refueling Position [m]	-35.50	0	8.5

Table 4.2. Control Allocation (CA)

Cases	CA Description
1	No thrust vectoring, only control surfaces used
2	Mix of thrust vectoring and control surfaces used
3	Thrust vectoring and δ_a used, no δ_e, and no δ_r

Table 4.3. Flight Condition and Fuel Mass Configurations - Control Allocation (CA) case is 1.

	V [m/s]	$\dot{\psi}[deg/s]$	Tank 1	Tank 2	Tank 3	Tank 4
Control Design	204.39	0	0	0	0	0
Simulation	204.39	0	0	0	0	0

variables, again computed for a specific fuel tank configuration. Weighting matrices Q and R are also tuned based on the matrices of the linear state-space model of the aircraft. In this chapter, the performance of the closed loop system will be evaluated in simulation as described above for fuel tank configurations that are different from the one the control design is based on. This is to evaluate the robustness of the closed-loop system against the mass and inertia variations. The receiver aircraft simulation has thrust vectoring capability. In control design, by setting control weighting matrix R, the levels of thrust vectoring versus of aerodynamic control surfaces, δ_e and δ_r, are specified. Three main control allocation cases are designed and simulated. Table 4.2 gives description of these three cases. The first simulation case is summarized in Table 4.3. The fuel amounts in the tanks are expressed as percent of the maximum fuel capacity of the corresponding tank, i.e., 0% implies empty fuel tank and 100% means full fuel tank. In this simulation, aircraft has the same fuel tank configuration in simulation as in the control design.

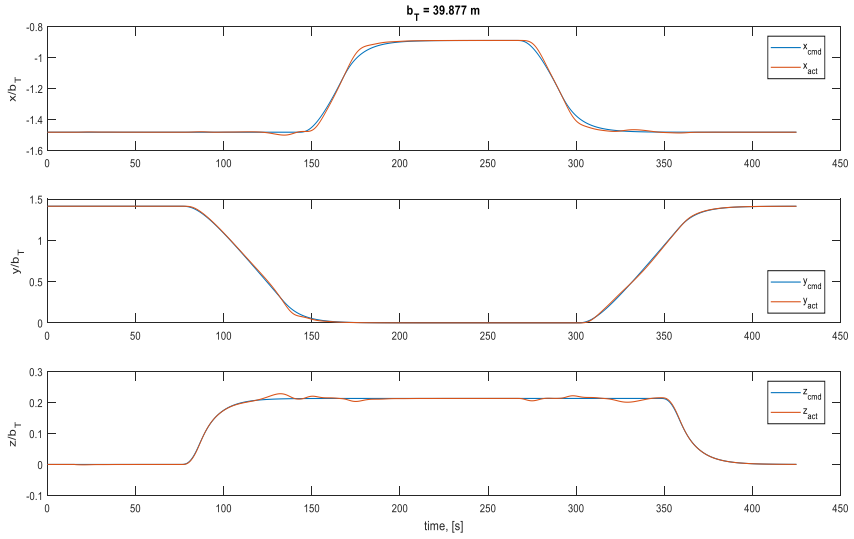

Figure 4.1. Commanded and actual trajectory when fuel mass configuration is [0 0 0 0] in control design and [0 0 0 0] in simulation (CA-1).

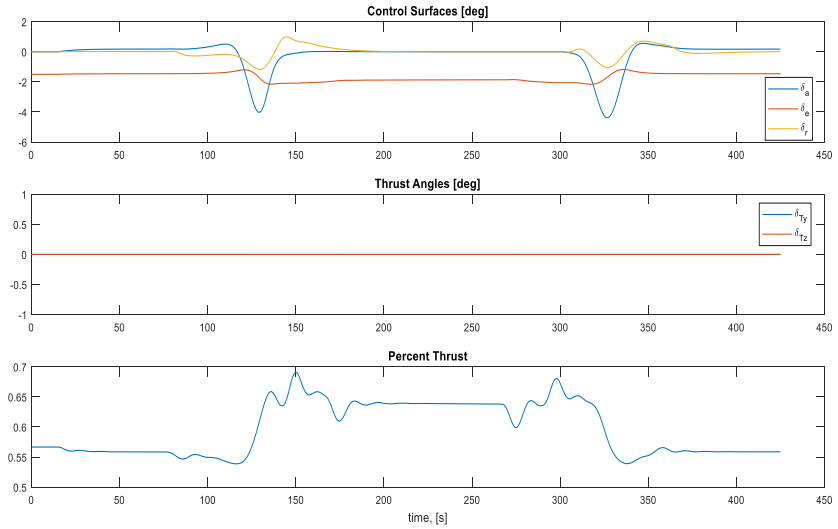

Figure 4.2. Control variables when fuel mass configuration is [0 0 0 0] in control design and [0 0 0 0] in simulation (CA-1).

Simulation results are shown in Figs. 4.1- 4.5. Fig. 4.1 shows that the controller successfully moves the receiver aircraft through the commanded trajectory. Fig. 4.2

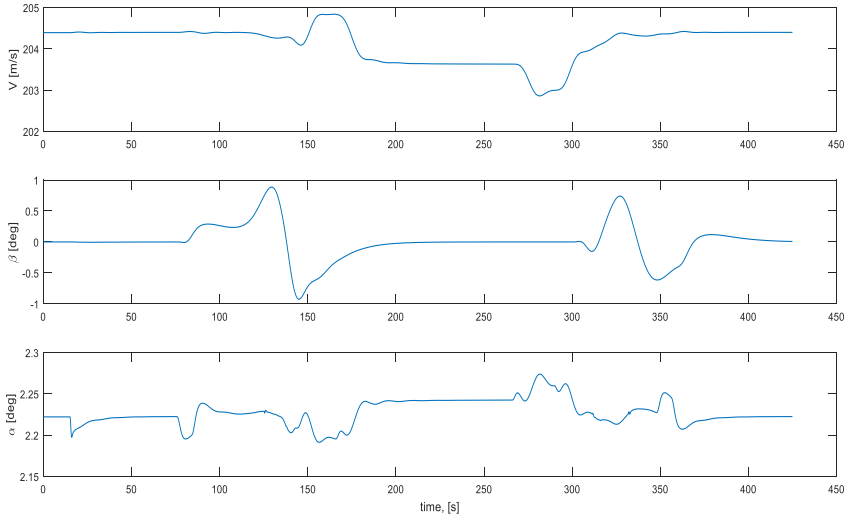

Figure 4.3. Airspeed, sideslip angle and angle of attack when fuel mass configuration is [0 0 0 0] in control design and [0 0 0 0] in simulation (CA-1).

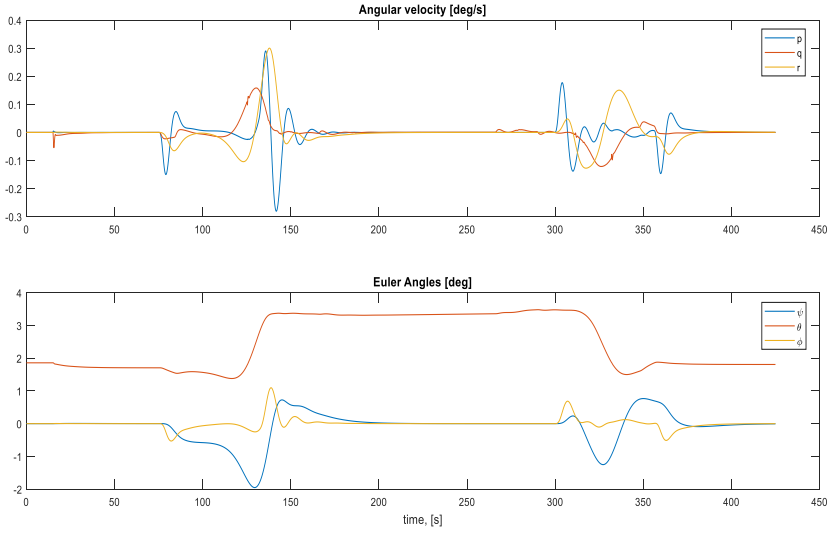

Figure 4.4. Angular velocity and Euler angles when fuel mass configuration is [0 0 0 0] in control design and [0 0 0 0] in simulation (CA-1).

shows the variation of the control variables through the maneuver. Since the control allocation case in this simulation is CA-1, no thrust vectoring is used as δ_y and δ_z stay

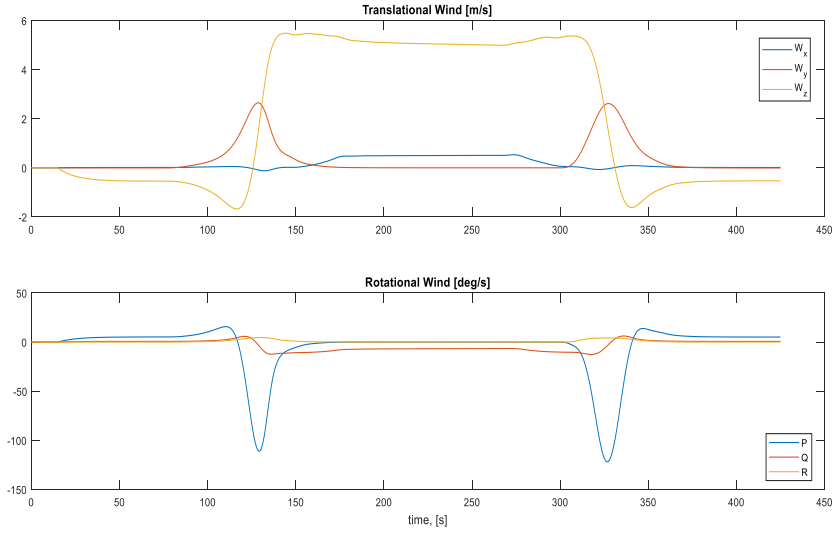

Figure 4.5. Translational and rotational wind components when fuel mass configuration is [0 0 0 0] in control design and [0 0 0 0] in simulation (CA-1).

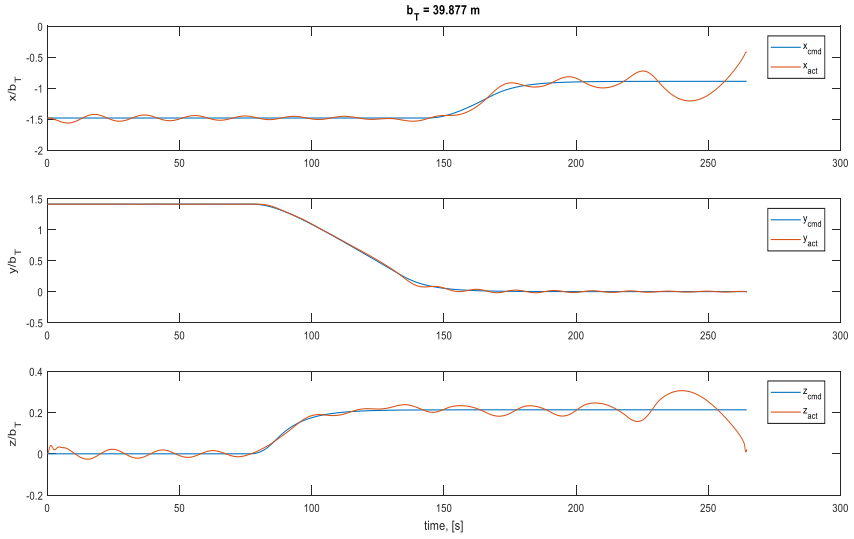

Figure 4.6. Commanded and actual trajectory when fuel mass configuration is [0 0 0 0] in control design and [1 1 1 1] in simulation (CA-1).

at zero. Fig. 4.3 shows the variations of airspeed, sideslip angle and angle of attack. In Fig. 4.4, angular velocity components and Euler angles are presented. Fig. 4.5

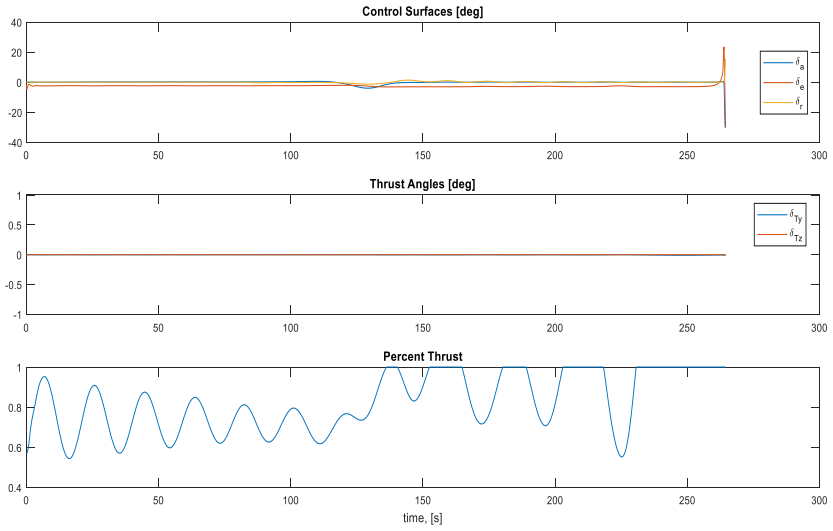

Figure 4.7. Control variables when fuel mass configuration is [0 0 0 0] in control design and [1 1 1 1] in simulation (CA-1).

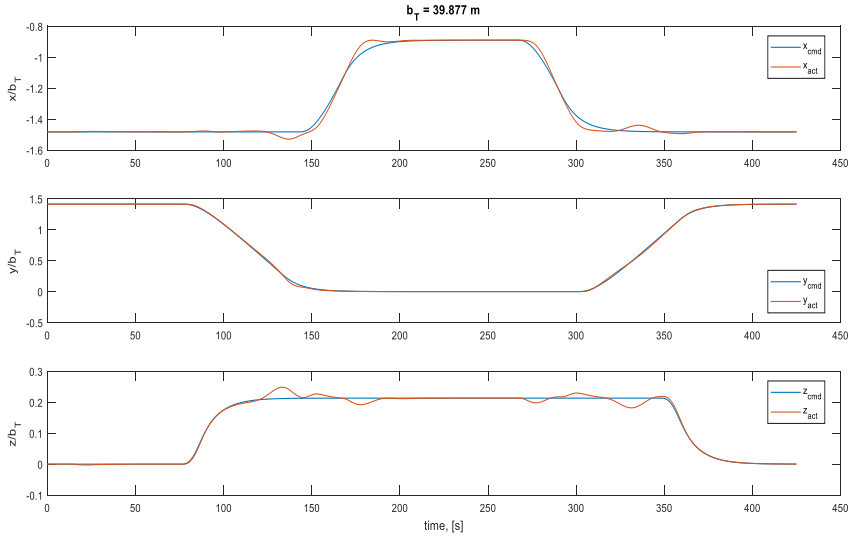

Figure 4.8. Commanded and actual trajectory when fuel mass configuration is [1 1 1 1] in control design and [1 1 1 1] in simulation (CA-2).

shows the translational and rotational wind components the aircraft experiences as it moves in and out of the tanker wake. Table 4.4 describes the second simulation

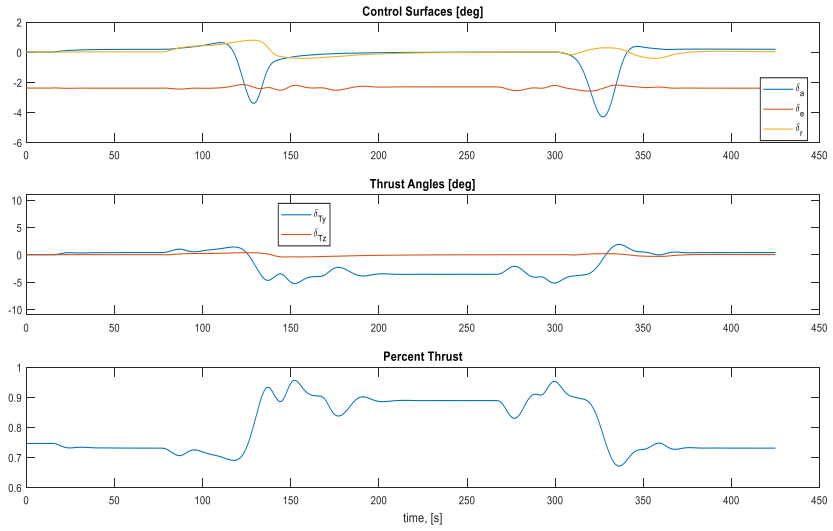

Figure 4.9. Control variables when fuel mass configuration is [1 1 1 1] in control design and [1 1 1 1] in simulation (CA-2).

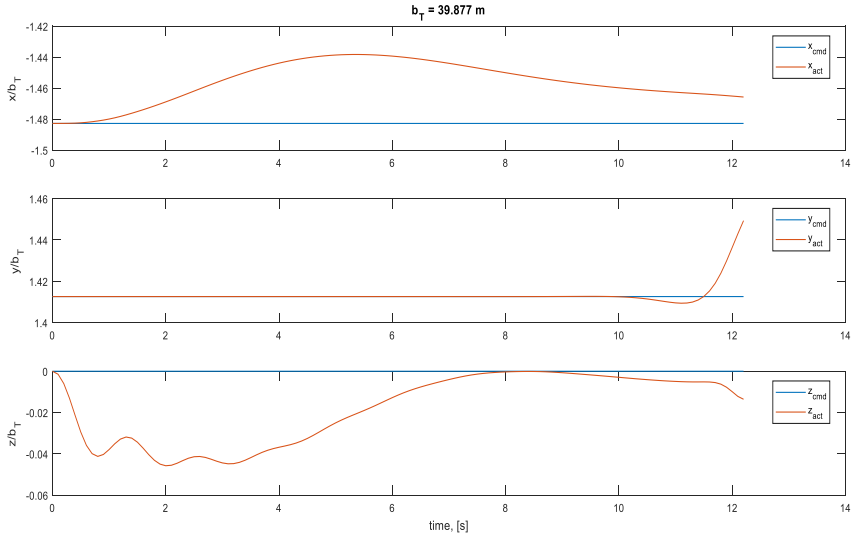

Figure 4.10. Commanded and actual trajectory when fuel mass configuration is [1 1 1 1] in control design and [0 0 0 0] in simulation (CA-2).

case. The control design is the same as the first case above, i.e., all fuel tanks are considered empty. In the simulated flight, the fuel tanks are all full. That is, the fuel

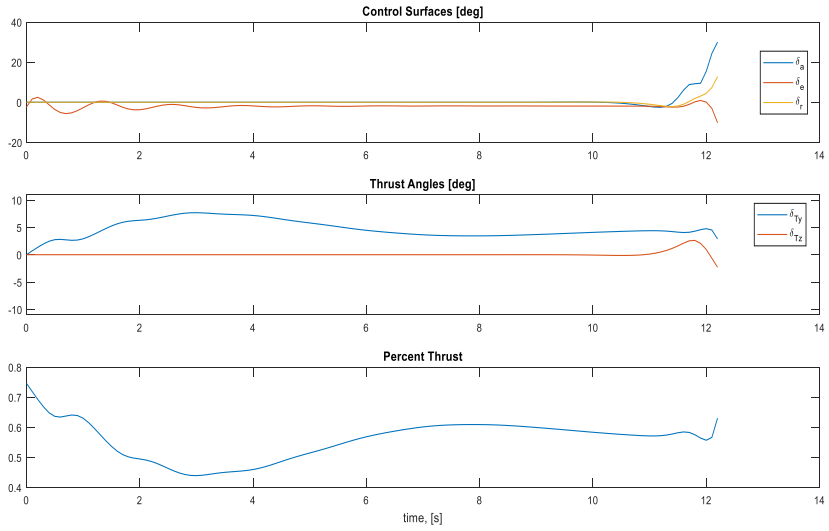

Figure 4.11. Control variables when fuel mass configuration is [1 1 1 1] in control design and [0 0 0 0] in simulation (CA-2).

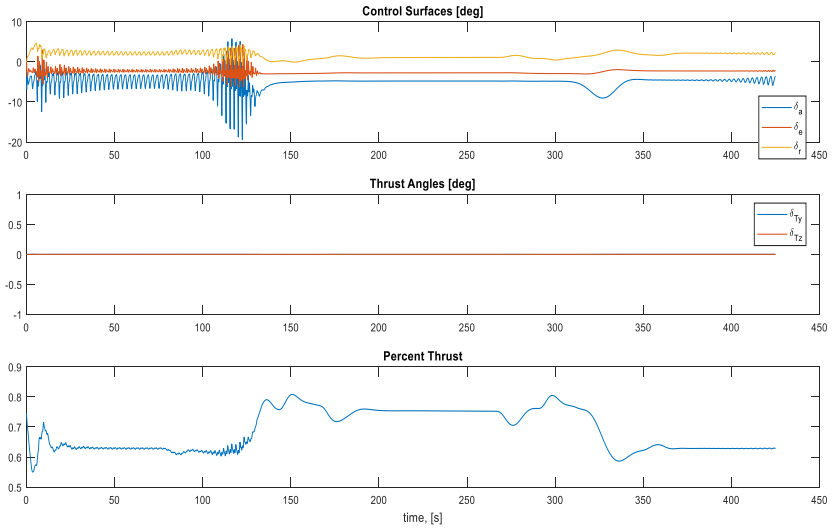

Figure 4.12. Control variables when fuel mass configuration is [1 1 1 1] in control design and [0 0.1 0.8 0.1] in simulation (CA-1).

mass configuration in flight is different from the design configuration. Figs. 4.6 and 4.7 show the result of this simulation. Note that the maneuver cannot be completed.

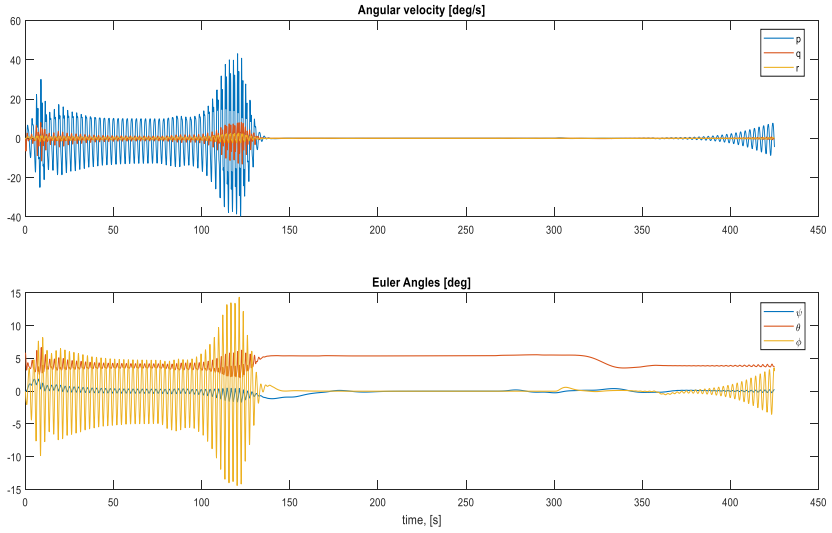

Figure 4.13. Angular velocity and Euler angles when fuel mass configuration is [1 1 1 1] in control design and [0 0.1 0.8 0.1] in simulation (CA-1).

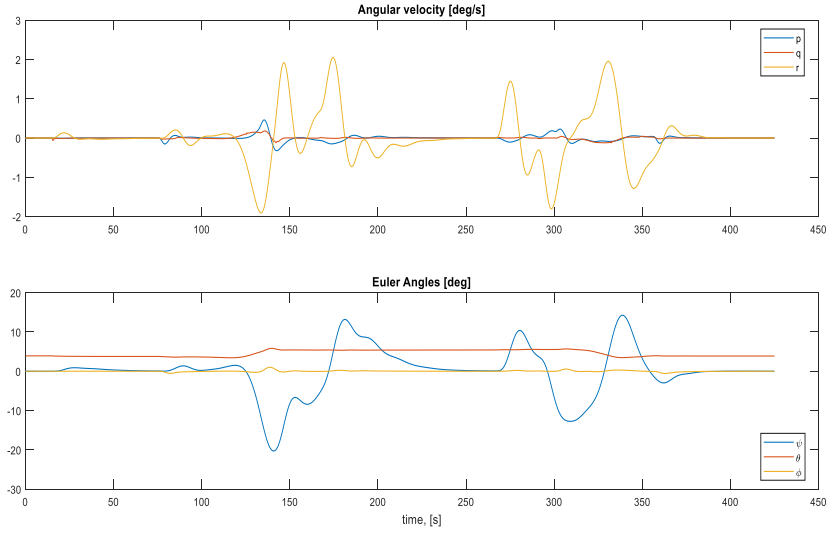

Figure 4.14. Angular velocity and Euler angles when fuel mass configuration is [1 0.1 0.8 0.1] in control design and [1 0.1 0.8 0.1] in simulation (CA-1).

The controller designed with all empty fuel tank configuration fails to fly the aircraft with all fuel tanks full. Since the controller in the above case could not fly the aircraft

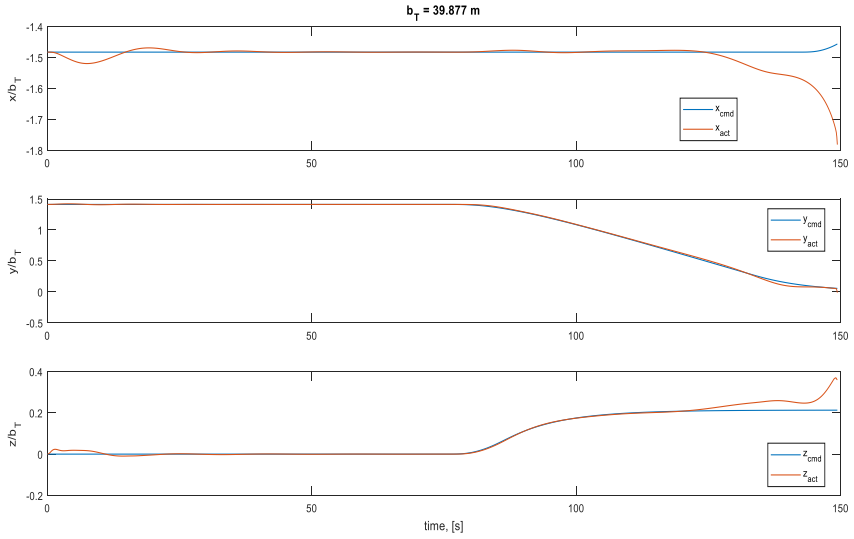

Figure 4.15. Commanded and actual trajectory when fuel mass configuration is [1 0.1 0.8 0.1] in control design and [1 1 1 1] in simulation (CA-1).

Table 4.4. Flight Condition and Fuel Mass Configurations - Control Allocation (CA) case is 1.

	V [m/s]	$\dot{\psi}[deg/s]$	Tank 1	Tank 2	Tank 3	Tank 4
Control Design	204.39	0	0	0	0	0
Simulation	204.39	0	1	1	1	1

with all fuel tanks full, the controller is redesigned, this time, with all fuel tanks set to full configuration in control design. The aircraft with all fuel tanks full is simulated with this controller, as described in Table 4.5. This time, control allocation CA-2, as described in Table 4.2, is used. The simulation results are given in Figs. 4.8 and 4.9. This controller successfully executes the maneuver while all the fuel tanks are full. The first two simulation cases show that the controller designed with all fuel tanks considered empty could not fly the aircraft when the fuel tanks are all full. Now, the question is whether the controller designed based on the configuration of all full fuel tanks can fly the aircraft when the fuel tanks are empty. This case is

Table 4.5. Flight Condition and Fuel Mass Configurations - Control Allocation (CA) case is 2.

	V [m/s]	$\dot{\psi}[deg/s]$	Tank 1	Tank 2	Tank 3	Tank 4
Control Design	204.39	0	1	1	1	1
Simulation	204.39	0	1	1	1	1

Table 4.6. Flight Condition and Fuel Mass Configurations - Control Allocation (CA) case is 2.

	V [m/s]	$\dot{\psi}[deg/s]$	Tank 1	Tank 2	Tank 3	Tank 4
Control Design	204.39	0	1	1	1	1
Simulation	204.39	0	0	0	0	0

summarized in Table 4.6 and the simulation results are shown in Figs. 4.10 and 4.11. The results show that controller designed for the heaviest configuration cannot fly the lightest configuration through the refueling maneuver. Another simulation case, described in Table 4.7, shows the performance when the aircraft fuel configuration is asymmetric. The controller designed based on the mass configuration of all fuel tanks full is enable to complete the maneuver in this asymmetric fuel loading. However, as shown in Figs. 4.12 and 4.13, the aircraft experiences high frequency, oscillation in its response, especially in roll motion and aileron deflection. If the controller is designed based on this specific asymmetric fuel configuration, the response is much better, without any oscillation, as shown in Fig. 4.14. This controller, however, fails

Table 4.7. Flight Condition and Fuel Mass Configurations - Control Allocation (CA) case is 1.

	V [m/s]	$\dot{\psi}[deg/s]$	Tank 1	Tank 2	Tank 3	Tank 4
Control Design	204.39	0	1	1	1	1
Simulation	204.39	0	1	0.1	0.8	0.1

to complete the maneuver when the aircraft fuel configuration in flight is different from the design configuration.

CHAPTER 5

GAIN SCHEDULING BASED ON FUEL MASS CONFIGURATION

In Section 3.2.4, the gain scheduling was done based on flight condition, which is defined in terms of speed V and turn rate $\dot{\psi}$. The previous section has shown that the controller that is designed based on a specific mass configuration may not work when the aircraft flies with a different mass configuration. The mass configuration is defined in terms of amount of fuel in the fuel tanks; more specifically, in terms of the percent of fuel amount in each fuel tank relative to the fuel capacity of the corresponding fuel tank. This section presents the approach taken to expand the gain scheduling to include the mass configuration of the aircraft. The specific aircraft considered has four fuel tanks. Percent fuel in each fuel tank is denoted by m_1, m_2, m_3 and m_4, which are considered gain scheduling variables in addition to V and $\dot{\psi}$, which are the gain scheduling variables to define the flight condition. Since the four fuel tank percentages are part of the gain scheduling variables, the nominal value set for each fuel mass is defined, similar to $\mathbf{S}_V$ and $\mathbf{S}_{\dot{\psi}}$ in Section 3.2.4 as

$$\begin{aligned} \mathbf{S}_{m_1} &= \{0, 1\} \\ \mathbf{S}_{m_2} &= \{0, 1\} \\ \mathbf{S}_{m_3} &= \{0, 1\} \\ \mathbf{S}_{m_4} &= \{0, 1\} \end{aligned} \tag{5.1}$$

where note that only empty and full fuel amounts are considered based on the eigenvalue and Bode analyses, presented in Section 3.2.5. A mass configuration is defined as

$$\mathbf{C}_m = \{(m_1, m_2, m_3, m_4) : m_1 \in \mathbf{S}_{m_1},\ \ m_2 \in \mathbf{S}_{m_2},\ \ m_3 \in \mathbf{S}_{m_3},\ \ m_4 \in \mathbf{S}_{m_4}\}$$

The nominal design points are redefined for this section to include mass configuration in addition to flight condition $(V, \dot{\psi})$ as $(V, \dot{\psi}, \mathbf{C}_m)$. Let $(V_{BCi}, \dot{\psi}_{BCi}, \mathbf{C}_{m_{BCi}})$ be the flight condition and mass configuration of nominal design point BC-i. Let $(V_C, \dot{\psi}_C, \mathbf{C}_{m_C})$ be the current flight condition and mass configuration. The first step is to determine the "neighboring" nominal design conditions $\mathbf{S}_{BC}$ based on the current flight condition $(V_C, \dot{\psi}_C)$. This is done using the algorithm introduced in Section 3.2.4, and depicted in Fig. 3.12. This approach requires that there are at least two nominal points in $\mathbf{S}_{BC}$ with the same nominal flight condition, and with distinct mass configurations. The "mass distance" from the current mass configuration to each of the nominal point in $\mathbf{S}_{BC}$ is computed as

$$\begin{aligned} d\mathbf{C}_{m_{BCi}} &= \| \mathbf{C}_{m_C} - \mathbf{C}_{m_{BCi}} \| \\ &= \sqrt{\sum_{j=1}^{4} (m_{j_{BCi}} - m_{j_C})^2} \end{aligned} \tag{5.2}$$

Based on the "mass distance", the subset of $\mathbf{S}_{BC}$ with two "closest" ones to the current mass configuration for each flight condition is established. This subset is denoted as $\bar{\mathbf{S}}_{BC}$. For nominal condition $BC - i \in \bar{\mathbf{S}}_{BC}$, the Lagrange interpolation coefficients for speed V and turn rate $\dot{\psi}_C$, a_V^i and $a_{\dot{\psi}}^i$, are computed as before, by Eqs. (3.41) and (3.42), respectively. The Lagrange interpolation coefficient for mass configuration can similarly be computed as

$$a_m^i = \prod_{j=1}^{4} \frac{m_{j_C} - m_j}{m_{j_{BCi}} - m_j} \tag{5.3}$$

where $m_j \in \left\{\mathbf{S}_{m_j} - m_{j_{BCi}}\right\}$. That is, when $m_{j_{BCi}} = 0$, $m_j = 1$, and when $m_{j_{BCi}} = 1$, $m_j = 0$, since $\mathbf{S}_{m_j} = \{1, 0\}$ as defined in Eq. (5.1).

Based on the eigenvalue and Bode analyses, only empty and full fuel tank configurations are considered for nominal design conditions. Since there are four fuel tanks, $2^4 = 16$ combinations of fuel tank configurations for each of the 6 flight conditions. However, as the eigenvalue and Bode analyses further suggested, not all 16 mass configurations are included in the set of nominal design conditions for the gain scheduling. In fact, as stated above, the gain scheduling approach taken in this research requires only at least 2 mass configurations per nominal flight condition. While this is done to reduce the computational complexity, it brings about a potential issue with the Lagrange interpolation scheme formulated in Eq. (5.3). If the current mass configuration happens to be one of the 16 possible mass configurations, then a_m^i in Eq. (5.3) will be 1 for that mass configuration, and a_m^i will be 0 for all 15 others. When this specific mass configuration is not one of the nominal design points in $\mathbf{S}_{BC}$, i.e., $\mathbf{S}_{BC}$ consists of design points with $a_m^i = 0$, then the scheduling coefficients for all design points in $\mathbf{S}_{BC}$ and thus in $\bar{\mathbf{S}}_{BC}$ will be zero. Thus, the gain scheduling controller will fail by simply generating zeros for all control variables. For such cases, an alternative a_m^i calculation is developed. This approach employs the "mass distance" as formulated in Eq. (5.2).

$$a_m^i = 1 - \frac{d\mathbf{C}_{m_{BCi}}}{\sum_{j=1}^{2} d\mathbf{C}_{m_{BCj}}(V_{BCi}, \dot{\psi}_{BCi})} \tag{5.4}$$

where $d\mathbf{C}_{m_{BCj}}(V_{BCi}, \dot{\psi}_{BCi})$ indicates the "mass distances" of the design points with the same flight conditions as BC-i. The formulation in Eq. (5.4) defines the mass gain scheduling coefficient in a way similar to the Lagrange interpolation coefficient in Eq. (5.3) in that as the mass configuration approaches that of BC-i, a_m^i increases toward 1.

Once the speed, turn rate, and mass configuration coefficients are computed individually, the gain scheduling interpolation coefficients for each nominal design is computed by their product as

$$a^i = a^i_V \;\; a^i_{\dot{\psi}} \;\; a^i_m$$

As done in Section 3.2.4, the next step is normalization of these coefficients over all design points considered as

$$\bar{a}^i = \frac{a^i}{\sum_{j=1}^{n(\bar{\mathbf{S}}_{BC})} a^j}$$

where $n(\bar{\mathbf{S}}_{BC})$ is the cardinal of set $\bar{\mathbf{S}}_{BC}$.

Finally, as done in Section 3.2.4, the gain scheduling controller is formulated as the linear combination of the controllers designed for each neighboring point as

$$u = \sum_{i=1}^{n(\bar{\mathbf{S}}_{BC})} \bar{a}^i \;\; u_i$$

where u_i is the linear controller designed for the nominal flight condition BC-i.

CHAPTER 6

SIMULATION RESULTS

In the earlier section, it was shown that the controller designed based on a specific fuel mass configuration may not work for the aircraft flying with different fuel mass configurations. That is why the gain scheduling controller was expanded to include various sets of mass configurations. This chapter is to demonstrate the performance of this controller, first for fuel mass configurations with which the aerial refueling maneuvers could not be (satisfactorily) completed with one single mass configuration based controller. Further, various other simulation cases will be prosecuted to demonstrate the performance and robustness of the controller. Table 6.1 lists the simulation cases presented in this section. The flight condition chosen is flight condition 4, i.e., $V_{T,2} = 204.39m/s$ and $\dot{\psi}_{T,2} = 0deg/s$. Note that in the gain scheduling controller, for this flight condition, three fuel mass configurations are included. These are [0 0 1 0], [1 0 0 0], and [1 0 1 1]. The cases simulated here are none of these three configurations, and thus the gain scheduling performance is demonstrated for mass configurations not included in the control design. In Table 6.1, the first three cases are when the aircraft performs the aerial refueling maneuver when the fuel tanks are empty. Each case uses one of the three control allocation cases. Figs. 6.1- 6.4 show the simulation results when the control allocation is CA-1. The controller successfully completes the maneuver even if the fuel mass configuration is not one of the nominal design cases. Note that, especially, δ_e is not zero initially before the refueling maneuver starts. This is because the control variables use trim values from the nominal design cases and all three nominal design cases for this flight condition (zero turn rate

Table 6.1. Flight Condition and Fuel Mass Configurations

CA	V [m/s]	$\dot{\psi}[deg/s]$	Tank 1	Tank 2	Tank 3	Tank 4
1	204.39	0	0	0	0	0
2	204.39	0	0	0	0	0
3	204.39	0	0	0	0	0
1	204.39	1	1	1	1	1
2	204.39	1	1	1	1	1
3	204.39	1	1	1	1	1
1	204.39	0	1	0.1	0.8	0.1
2	204.39	0	1	0.1	0.8	0.1
3	204.39	0	1	0.1	0.8	0.1
1	204.39	0	1	0	1	0
2	204.39	0	1	0	1	0
3	204.39	0	1	0	1	0
1	204.39	0	0	1	0	1
2	204.39	0	0	1	0	1
3	204.39	0	0	1	0	1

and speed is 204.39 m/s) have asymmetrical fuel loading. The aircraft even flying in straight level is trimmed with nonzero aileron and rudder deflections. As can be seen in Fig. 6.2, the thrust vectoring angles are kept at zero since control allocation case CA-1 does not use thrust vectoring. The translational and the rotational wind components the aircraft is exposed to during the maneuver are similar as before since the aircraft follows very closely the same commanded trajectory relative to the tanker. Thus, the wind component plots are not shown in this section.

Figs. 6.5 and 6.6 show the control variable responses when control allocation cases CA-2 and CA-3 are used, respectively, when the aircraft fuel tanks are all empty as in the previous case. As shown in Fig. 6.5, in CA-2 case, both aerodynamic control surfaces and thrust vectoring are used. When control allocation CA-3 is used, elevator and rudder are kept constant, and only thrust vectoring is used to generate pitching and yawing moments. In CA-3, aileron is still in use. As with CA-1, in CA-2 and

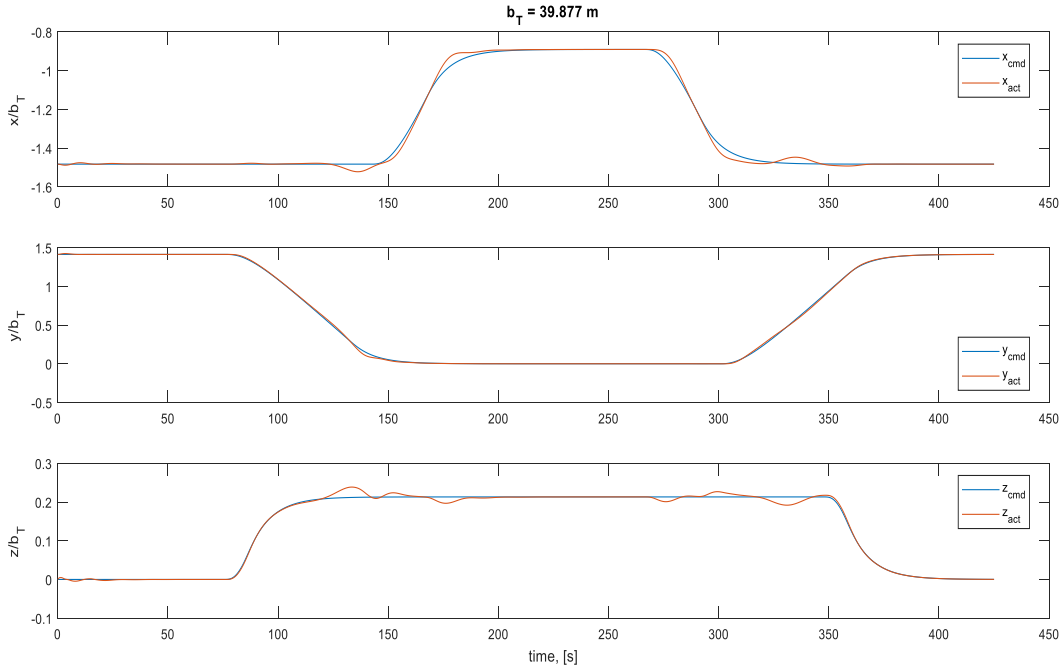

Figure 6.1. Commanded and actual trajectory when fuel mass configuration in simulation is [0 0 0 0], (CA-1).

CA-3, the aircraft can successfully completes the refueling maneuver with empty fuel tank configuration even if this fuel configuration is not one of the nominal design cases. The gain scheduling controller is also evaluated when the aircraft is at its heaviest configuration, i.e., all fuel tanks are full. This is done with all control allocation cases. The results are presented in Figs. 6.7- 6.12. Figs. 6.7- 6.8 show CA-1; Figs. 6.9- 6.10 show CA-2; Figs. 6.11- 6.12 show CA-3. The other variables are not shown as their responses are similar to previously discussed corresponding cases. Note that this mass configuration is also different from any of the mass configuration included in the control design. In all three control allocation cases, the aircraft completes the maneuver successfully. The aileron responses are similar in all three cases. The elevator and rudder use is reduced while thrust vectoring use is increased

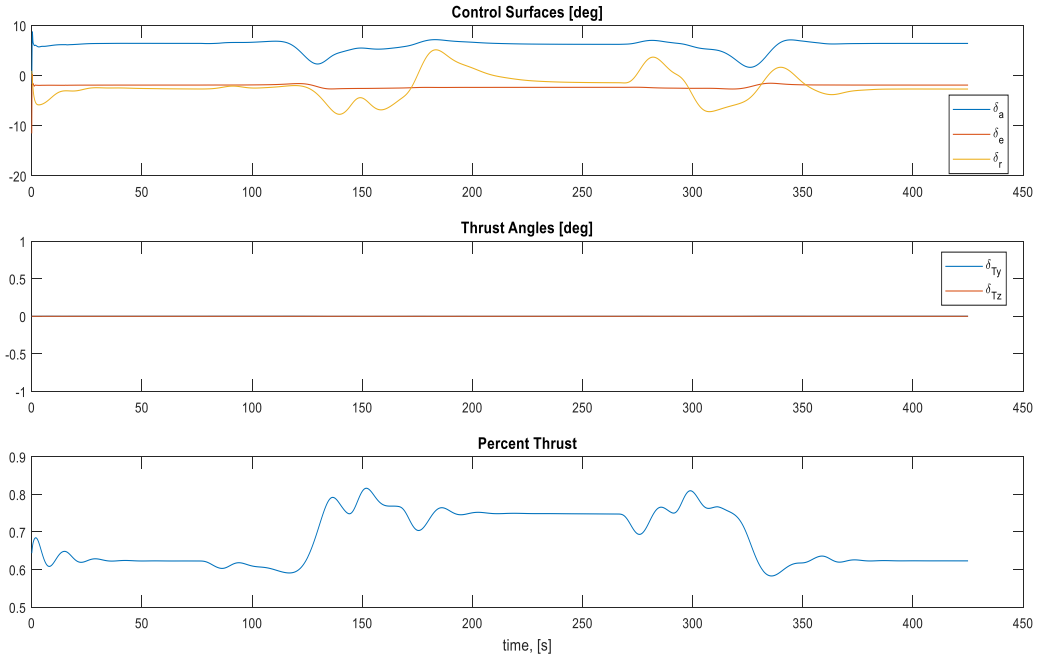

Figure 6.2. Control variables when fuel mass configuration in simulation is [0 0 0 0], (CA-1).

as the control allocation shifts from CA-1 to CA-2, to CA-3. The thrust responses in all three cases are very similar. Since the aircraft is heaviest, the thrust gets close to saturation at times during the maneuver. Yaw angle deviations are the largest in CA-1 case and the smallest in CA-3 case. The other three fuel mass configuration cases described in Table 6.1, [1 0.1 0.8 0.1], [1 0 1 0], and [0 1 0 1] are all asymmetric cases. The controller with all three control allocation cases can successfully complete the refueling maneuver despite the asymmetric mass distribution. The case [1 0.1 0.8 0.1] is one of the cases that was shown to fail before, when the control design was based on one fuel mass configuration. The other two, [1 0 1 0] and [0 1 0 1], has even greater asymmetry. Still the controller with only three nominal design cases included can control the aircraft in different mass distributions.

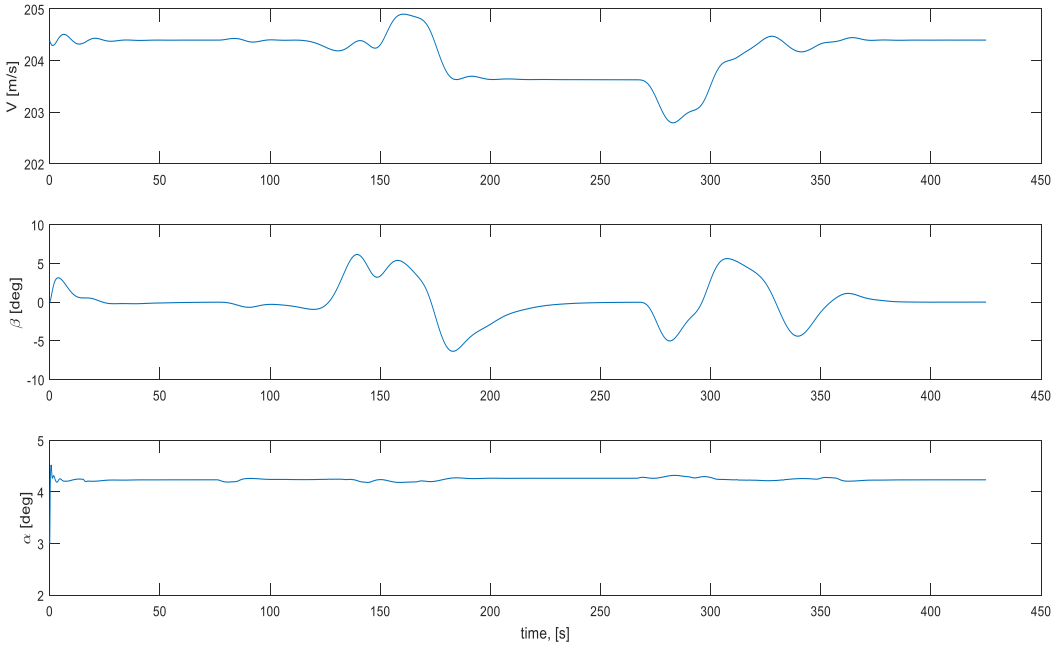

Figure 6.3. Airspeed, sideslip angle and angle of attack when fuel mass configuration in simulation is [0 0 0 0], (CA-1).

Figs. 6.13- 6.14, 6.15- 6.16, and 6.17- 6.18 present the responses of control variables, airspeed, sideslip angle, and angle of attack in CA-1 cases with mass configurations [1 0.1 0.8 0.1], [1 0 1 0], and [0 1 0 1], respectively.

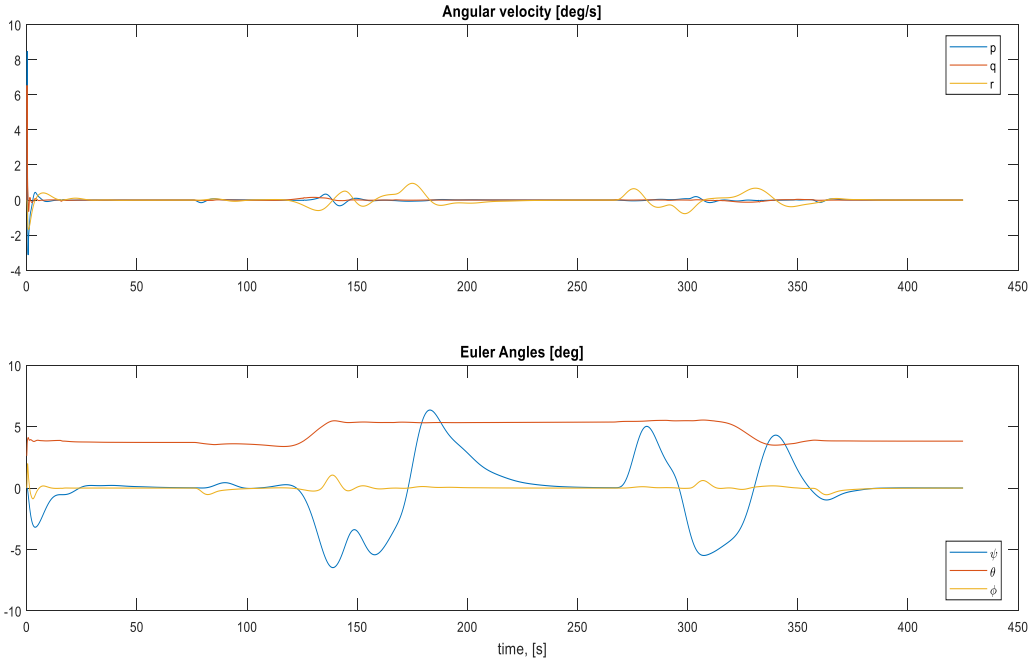

Figure 6.4. Angular velocity and Euler angles when fuel mass configuration in simulation is [0 0 0 0], (CA-1).

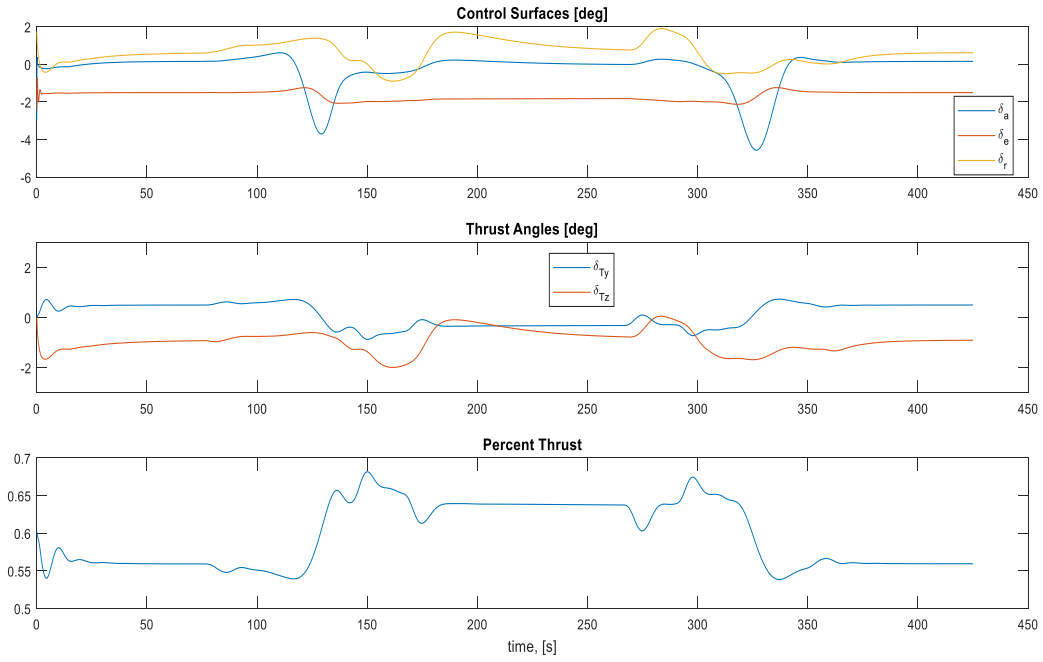

Figure 6.5. Control variables when fuel mass configuration in simulation is [0 0 0 0], (CA-2).

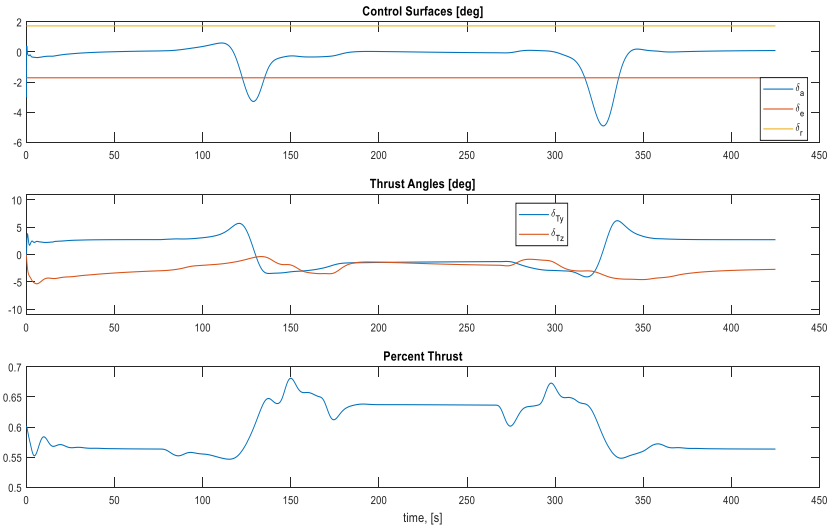

Figure 6.6. Control variables when fuel mass configuration in simulation is [0 0 0 0], (CA-3).

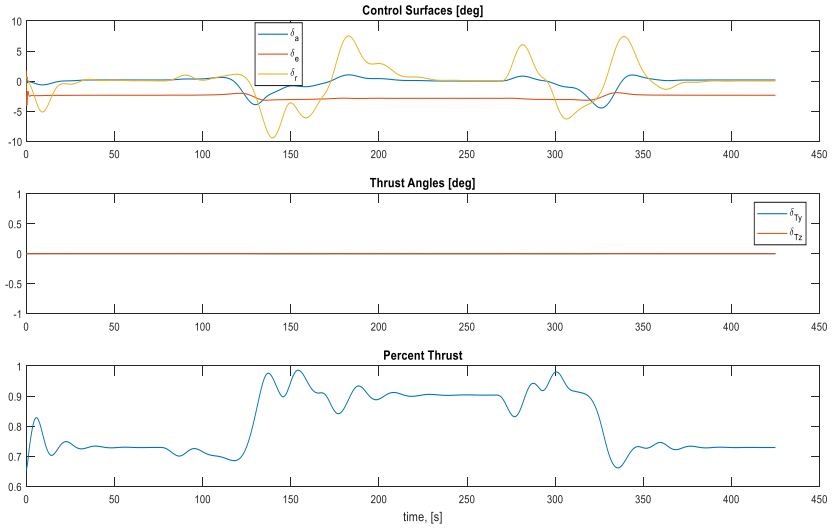

Figure 6.7. Control variables when fuel mass configuration in simulation is [1 1 1 1], (CA-1).

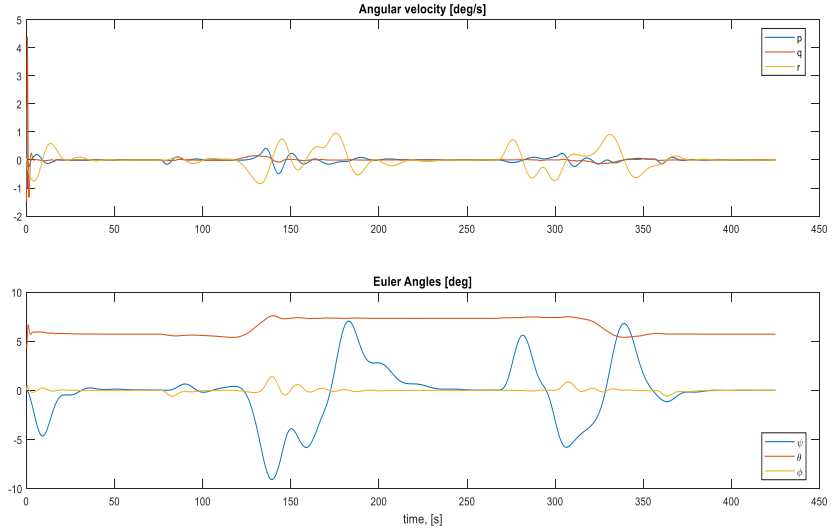

Figure 6.8. Angular velocity and Euler angles when fuel mass configuration in simulation is [1 1 1 1], (CA-1).

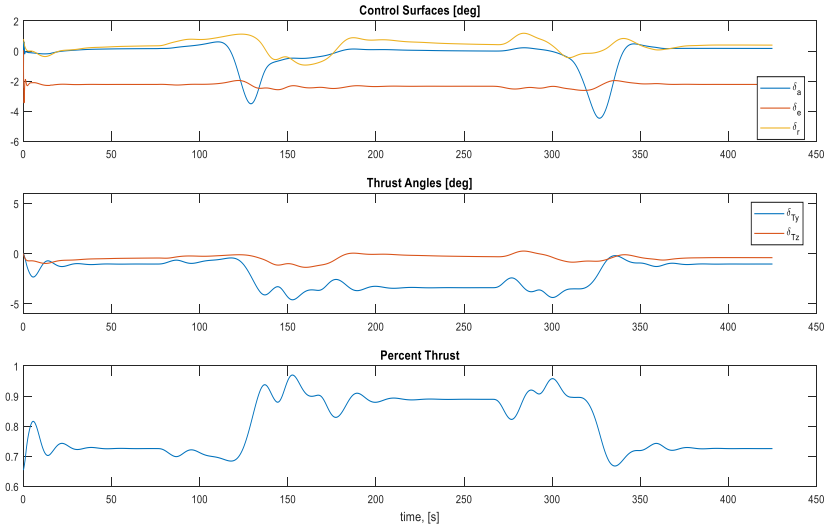

Figure 6.9. Control variables when fuel mass configuration in simulation is [1 1 1 1], (CA-2).

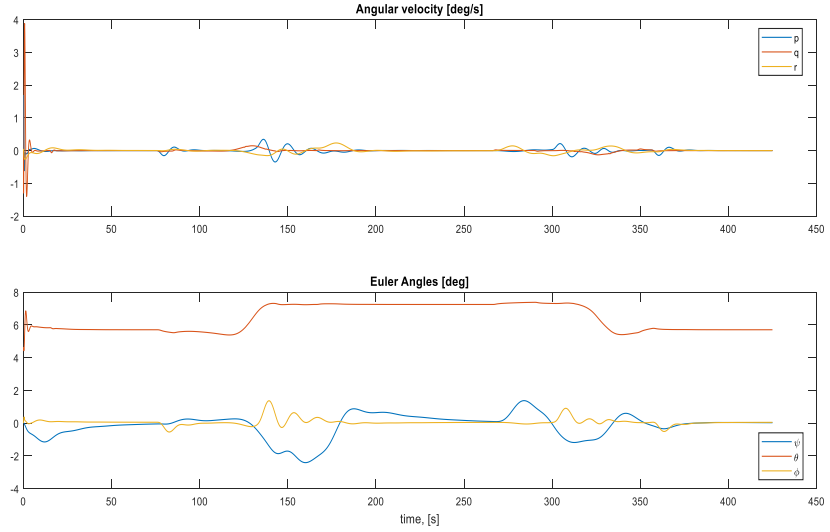

Figure 6.10. Angular velocity and Euler angles when fuel mass configuration in simulation is [1 1 1 1], (CA-2).

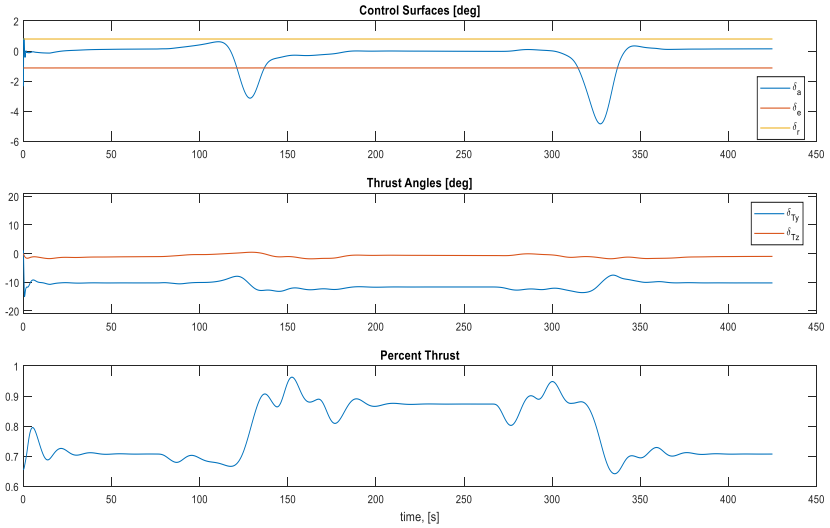

Figure 6.11. Control variables when fuel mass configuration in simulation is [1 1 1 1], (CA-3).

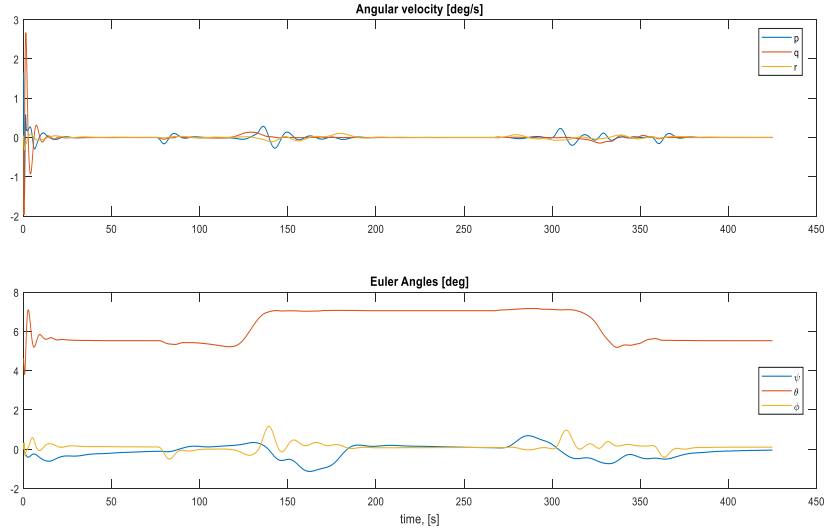

Figure 6.12. Angular velocity and Euler angles when fuel mass configuration in simulation is [1 1 1 1], (CA-3).

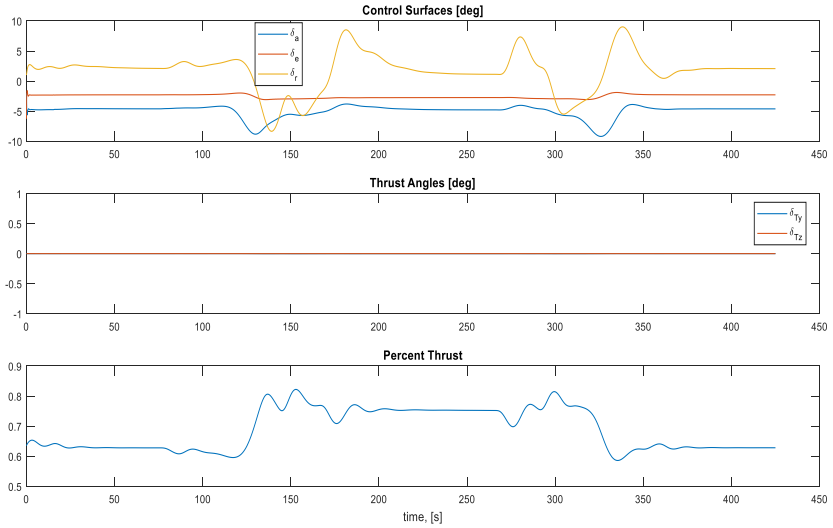

Figure 6.13. Control variables when fuel mass configuration in simulation is [1 0.1 0.8 0.1], (CA-1).

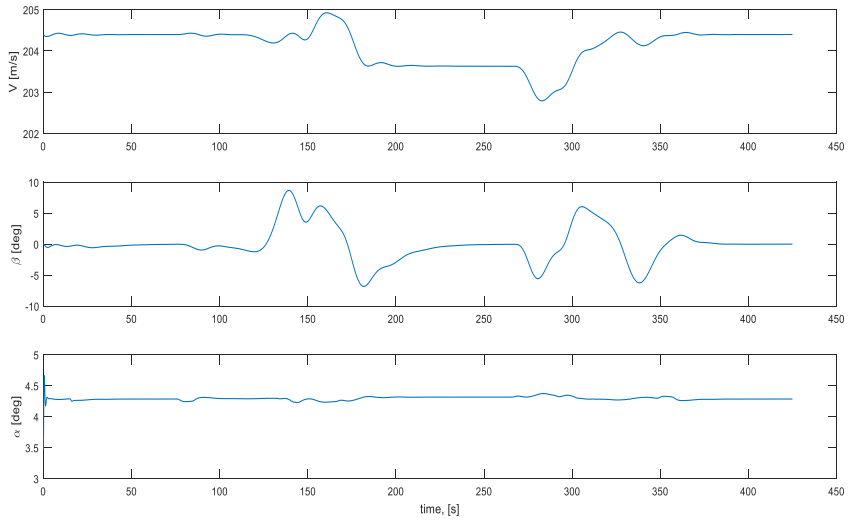

Figure 6.14. Airspeed, sideslip angle and angle of attack when fuel mass configuration in simulation is [1 0.1 0.8 0.1], (CA-1).

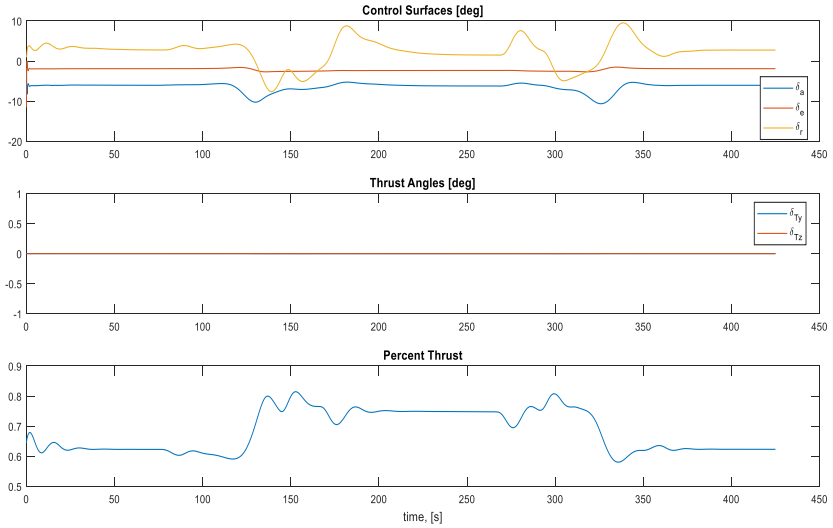

Figure 6.15. Control variables when fuel mass configuration in simulation is [1 0 1 0], (CA-1).

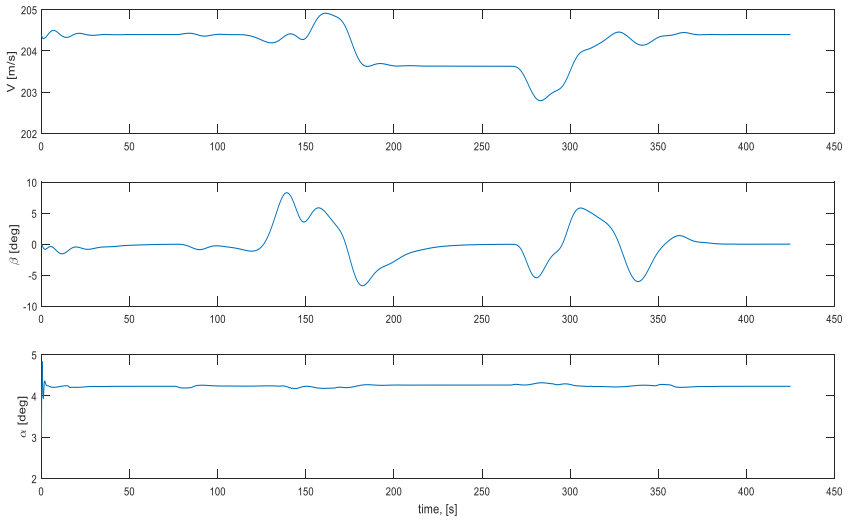

Figure 6.16. Airspeed, sideslip angle and angle of attack when fuel mass configuration in simulation is [1 0 1 0], (CA-1).

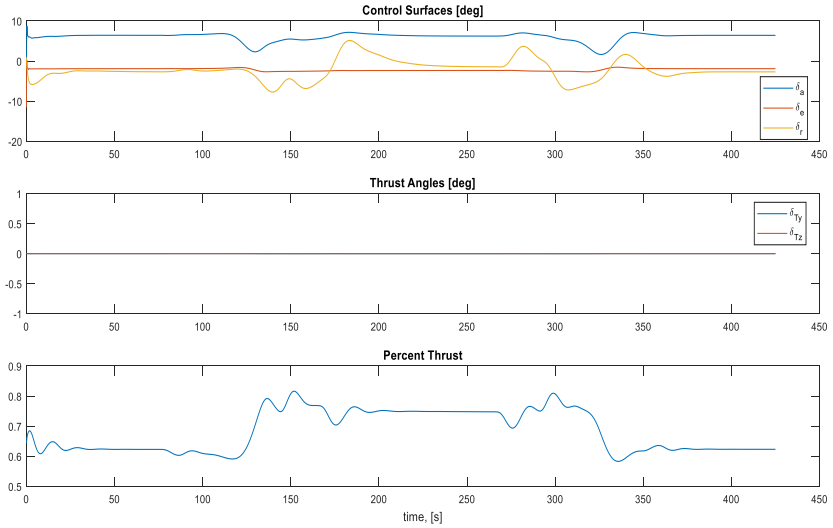

Figure 6.17. Control variables when fuel mass configuration in simulation is [0 1 0 1], (CA-1).

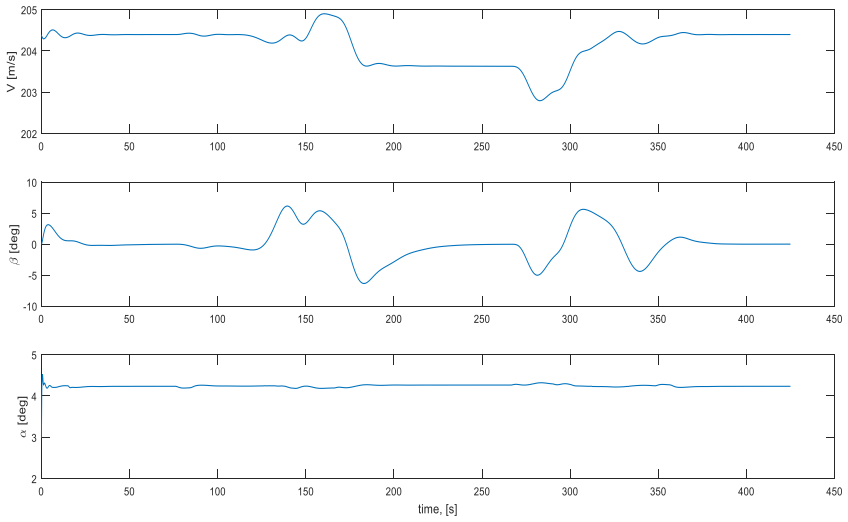

Figure 6.18. Airspeed, sideslip angle and angle of attack when fuel mass configuration in simulation is [0 1 0 1], (CA-1).

CHAPTER 7

CONCLUSION AND FUTURE WORK

This research effort focuses on addressing the issue of mass/inertia variation in aerial refueling and formation flight by expanding the gain scheduling scheme to include fuel mass in each fuel tank among the scheduling variables in addition to airspeed and turn rate. The fuel mass in each fuel tank is considered as state variable in addition to the standard states associated with aircraft dynamics. All possible fuel distributions, both symmetric and asymmetric, are considered in trim analyses of the aircraft in straight level and steady-turn flight conditions at constant altitude and constant airspeed. The gain scheduling controller design requires the definition of trim conditions in terms of the fuel amounts in fuel tanks for each set of turn rate and speed. The three turn rates (zero, right turn, and left turn) and two speed values result in six nominal flight conditions, as done with the tanker aircraft.

For the receiver aircraft, the number of mass/inertia configurations to be included in the set of trim conditions should be determined. The objective is to keep the number of such fuel tank configurations small while making sure that they will cover the whole span of the mass/inertia variation of the receiver aircraft. To reduce the number of cases included in the gain scheduling, similar cases are combined. In each possible case, the equations of motion are linearized to obtain the state and control matrices. From the state and control matrices, various transfer functions are computed. Similarity of the cases are determined based on the eigenvalue locations of the state matrix and Bode plots of the transfer functions. The specific aircraft considered is a tailless delta wing aircraft with thrust vectoring capability. The eigenvalue and

Bode analyses show that variations in the dynamics of the aircraft are not significant for fractional changes in the fuel amounts in each tank. This imply that only completely empty and completely full fuel tanks are sufficient to capture the variation in the dynamics. This specific aircraft has four fuel tanks, which imply that there are still $2^4 = 16$ fuel mass configurations per flight condition. Eigenvalue and Bode plot analyses further demonstrate that not all 16 mass configurations are needed. Two or three mass configurations for each flight conditions are eventually kept for the gain scheduling control design.

An LQR-based MIMO (Multi Input Multi Output) integral control is designed for each nominal flight and mass configuration. An interpolation scheme based on the "mass distance" is developed to combine this linear controllers into the gain scheduling controller. The "mass distance" is defined as the norm of the differences between the current fuel tank amounts and those of each nominal mass configuration. The Lagrange interpolation scheme, as commonly used in gain scheduling, assumes that all possible combinations of fuel mass configurations are included among the nominal conditions used in gain scheduling. However, as stated above, only a subset of possible mass configurations is included in gain scheduling. While this is done to reduce the computational complexity, it brings about a potential issue with the Lagrange interpolation. If the current mass configuration of the aircraft is one of the 16 fuel mass configurations stated above, but not included in the subset determined after eliminating "similar" cases, the Lagrange interpolation scheme computes all the coefficients of the cases included as zero. This would cause the gain scheduling controller to fail by simply generating zeros for all control variables. To avoid this issue, an alternative interpolation method is developed for mass configurations by employing the "mass distance" discussed above.

The receiver controller was tuned in three control allocation cases: (1) no thrust vectoring; only aerodynamic control effects in use, (2) both aerodynamic effectors and thrust vectoring in use, and (3) no elevator or rudder used; only thrust vectoring and aileron in use. The performance of the gain scheduling controller is evaluated through the aerial refueling maneuver when the receiver moves between the observation position, point on the side and behind the tanker, and the refueling position, a point right behind and slightly below the tanker. The simulation results first of all demonstrates that a linear controller designed based on a nominal flight condition and mass configuration cannot safely complete the refueling maneuver when the aircraft has a different mass configuration. The simulation results further shows that the gain scheduling controller employing mass configuration as additional scheduling variables can successfully carry out the refueling maneuver with various symmetric and asymmetric fuel tank configuration. All three control allocation schemes employing the mass-configuration-based gain scheduling perform similarly in terms of tracking the commanded trajectory while the control responses vary accordingly.

There are various directions for future research effort in this area. The location of Eigenvalues and Bode plots are used to determine whether two linear modes are close to each other. A more formal way of quantifying how close linear models should be developed in deciding whether to include in the gain scheduling scheme. The receiver aircraft considered is a tailless delta wing aircraft, which is a small aircraft geometrically and thus the fuel tanks are close to the origin of the body frame. It is expected that the effect of the fuel mass variation will be more profound when larger receiver aircraft is considered. The analyses and the design effort can be repeated for a larger aircraft, for example, another KC-135 flying behind the tanker KC-135 aircraft. In this research numerous simulations are carried out in evaluating the performance of the gain scheduling controller. However, in each simulation run, the

mass configuration is fixed. The performance of the gain scheduling can be evaluated when the mass configuration is varying during simulation.

APPENDIX A

NOMINAL CONDITIONS OF THE RECEIVER AIRCRAFT

Table A.1. Nominal Conditions (1-32) of the Receiver by Turn rate, Airspeed, and Receiver Fuel Tanks Status

Nominal Conditon	Flight Case	Tank 1	Tank 2	Tank 3	Tank 4
1	1	0	0	0	0
2	1	0	0	0	1
3	1	0	0	1	0
4	1	0	0	1	1
5	1	0	1	0	0
6	1	0	1	0	1
7	1	0	1	1	0
8	1	0	1	1	1
9	1	1	0	0	0
10	1	1	0	0	1
11	1	1	0	1	0
12	1	1	0	1	1
13	1	1	1	0	0
14	1	1	1	0	1
15	1	1	1	1	0
16	1	1	1	1	1
17	2	0	0	0	0
18	2	0	0	0	1
19	2	0	0	1	0
20	2	0	0	1	1
21	2	0	1	0	0
22	2	0	1	0	1
23	2	0	1	1	0
24	2	0	1	1	1
25	2	1	0	0	0
26	2	1	0	0	1
27	2	1	0	1	0
28	2	1	0	1	1
29	2	1	1	0	0
30	2	1	1	0	1
31	2	1	1	1	0
32	2	1	1	1	1

Table A.2. Nominal Conditions (33-64) of the Receiver by Turn rate, Airspeed, and Receiver Fuel Tanks Status

Nominal Conditon	Flight Case	Tank 1	Tank 2	Tank 3	Tank 4
33	3	0	0	0	0
34	3	0	0	0	1
35	3	0	0	1	0
36	3	0	0	1	1
37	3	0	1	0	0
38	3	0	1	0	1
39	3	0	1	1	0
40	3	0	1	1	1
41	3	1	0	0	0
42	3	1	0	0	1
43	3	1	0	1	0
44	3	1	0	1	1
45	3	1	1	0	0
46	3	1	1	0	1
47	3	1	1	1	0
48	3	1	1	1	1
49	4	0	0	0	0
50	4	0	0	0	1
51	4	0	0	1	0
52	4	0	0	1	1
53	4	0	1	0	0
54	4	0	1	0	1
55	4	0	1	1	0
56	4	0	1	1	1
57	4	1	0	0	0
58	4	1	0	0	1
59	4	1	0	1	0
60	4	1	0	1	1
61	4	1	1	0	0
62	4	1	1	0	1
63	4	1	1	1	0
64	4	1	1	1	1

Table A.3. Nominal Conditions (65-96) of the Receiver by Turn rate, Airspeed, and Receiver Fuel Tanks Status

Nominal Conditon	Flight Case	Tank 1	Tank 2	Tank 3	Tank 4
65	5	0	0	0	0
66	5	0	0	0	1
67	5	0	0	1	0
68	5	0	0	1	1
69	5	0	1	0	0
70	5	0	1	0	1
71	5	0	1	1	0
72	5	0	1	1	1
73	5	1	0	0	0
74	5	1	0	0	1
75	5	1	0	1	0
76	5	1	0	1	1
77	5	1	1	0	0
78	5	1	1	0	1
79	5	1	1	1	0
80	5	1	1	1	1
81	6	0	0	0	0
82	6	0	0	0	1
83	6	0	0	1	0
84	6	0	0	1	1
85	6	0	1	0	0
86	6	0	1	0	1
87	6	0	1	1	0
88	6	0	1	1	1
89	6	1	0	0	0
90	6	1	0	0	1
91	6	1	0	1	0
92	6	1	0	1	1
93	6	1	1	0	0
94	6	1	1	0	1
95	6	1	1	1	0
96	6	1	1	1	1

APPENDIX B

EIGENVALUES OF THE RECEIVER AIRCRAFT

Table B.1. Eigenvalues of Receiver Aircraft for Nominal Conditions from 1 to 8

Nominal Cond. 1	Nominal Cond. 2	Nominal Cond. 3	Nominal Cond. 4
$-0.7114 + 1.3278i$	$-1.4901 + 0.5805i$	$-1.4898 + 0.5887i$	-2.7864
$-0.7114 - 1.3278i$	$-1.4901 - 0.5805i$	$-1.4898 - 0.5887i$	1.8090
-1.4681	1.0454	1.0478	-1.0044
1.0143	-0.9398	-0.9481	0.8600
-0.8861	0.7265	0.7243	-0.4528
$-0.0065 + 0.0747i$	-0.0783	0.0896	0.0092
$-0.0065 - 0.0747i$	$0.0378 + 0.1025i$	$-0.0424 + 0.0986i$	$-0.0037 + 0.0724i$
0.0097	$0.0378 - 0.1025i$	$-0.0424 - 0.0986i$	$-0.0037 - 0.0724i$
$+0.0297i$	$+0.0297i$	$+0.0297i$	$+0.0297i$
$-0.0297i$	$-0.0297i$	$-0.0297i$	$-0.0297i$
0	0	0	0
0	0	0	0
Nominal Cond. 5	Nominal Cond. 6	Nominal Cond. 7	Nominal Cond. 8
$-0.5899 + 2.4090i$	$-0.5616 + 1.2809i$	$-0.7148 + 1.7744i$	-1.7700
$-0.5899 - 2.4090i$	$-0.5616 - 1.2809i$	$-0.7148 - 1.7744i$	-0.8783
-1.1915	-0.9536	-0.9573	$0.7407 + 0.0919i$
0.9131	0.8561	0.8541	$0.7407 - 0.0919i$
-0.9660	-0.7785	-0.3564	-0.2978
-0.0874	-0.1503	0.0725	$-0.0044 + 0.0751i$
$0.0419 + 0.0987i$	$0.0724 + 0.1241i$	$-0.0316 + 0.1112i$	$-0.0044 - 0.0751i$
$0.0419 - 0.0987i$	$0.0724 - 0.1241i$	$-0.0316 - 0.1112i$	0.0095
$+0.0297i$	$+0.0297i$	$+0.0297i$	0
$-0.0297i$	$-0.0297i$	$-0.0297i$	0
0	0	0	$+0.0297i$
0	0	0	$-0.0297i$

Table B.2. Eigenvalues of Receiver Aircraft for Nominal Conditions from 9 to 16

Nominal Cond. 9	Nominal Cond. 10	Nominal Cond. 11	Nominal Cond. 12
$-0.5916 + 2.4086i$	$-0.7142 + 1.7743i$	$-0.5690 + 1.2788i$	-1.7691
$-0.5916 - 2.4086i$	$-0.7142 - 1.7743i$	$-0.5690 - 1.2788i$	-0.8794
-1.1926	-0.9591	-0.9437	$0.7393 + 0.0882i$
-0.9641	0.8527	0.8563	$0.7393 - 0.0882i$
0.9117	-0.3370	-0.7903	-0.2977
0.0840	-0.0924	0.1232	$-0.0006 + 0.0588i$
$-0.0419 + 0.1080i$	$0.0421 + 0.0901i$	$-0.0560 + 0.1516i$	$-0.0006 - 0.0588i$
$-0.0419 - 0.1080i$	$0.0421 - 0.0901i$	$-0.0560 - 0.1516i$	0.0045
$+0.0297i$	$+0.0297i$	$+0.0297i$	$+0.0297i$
$-0.0297i$	$-0.0297i$	$-0.0297i$	$-0.0297i$
0	0	0	0
0	0	0	0
Nominal Cond. 13	Nominal Cond. 14	Nominal Cond. 15	Nominal Cond. 16
$-0.6548 + 3.1745i$	$-0.6096 + 2.4435i$	$-0.6098 + 2.4435i$	$-0.4470 + 1.3133i$
$-0.6548 - 3.1745i$	$-0.6096 - 2.4435i$	$-0.6098 - 2.4435i$	$-0.4470 - 1.3133i$
-0.8508	-0.8527	-0.8475	-0.7807
0.8332	0.7769	0.7776	0.7097
-0.7806	-0.4269	-0.4556	-0.3947
$-0.0065 + 0.0730i$	-0.1275	1.1031	0.0124
$-0.0065 - 0.0730i$	$0.0588 + 0.1091i$	$-0.0448 + 0.1308i$	$-0.0033 + 0.0760i$
0.0120	$0.0588 - 0.1091i$	$-0.0448 - 0.1308i$	$-0.0033 - 0.0760i$
$+0.0297i$	$+0.0297i$	$+0.0297i$	$+0.0297i$
$-0.0297i$	$-0.0297i$	$-0.0297i$	$-0.0297i$
0	0	0	0
0	0	0	0

Table B.3. Eigenvalues of Receiver Aircraft for Nominal Conditions from 17 to 24

Nominal Cond. 17	Nominal Cond. 18	Nominal Cond. 19	Nominal Cond. 20
$-0.7649 + 1.4286i$	$-1.6186 + 0.6284i$	$-1.6184 + 0.6367i$	-3.0003
$-0.7649 - 1.4286i$	$-1.6186 - 0.6284i$	$-1.6184 - 0.6367i$	1.9493
-1.6119	1.1326	1.1343	-1.0980
1.1162	-1.0024	-1.0102	0.9469
-0.9428	0.7985	0.7990	-0.4875
$-0.0072 + 0.0701i$	-0.0742	0.0817	$-0.0039 + 0.0671i$
$-0.0072 - 0.0701i$	$0.0353 + 0.0945i$	$-0.0402 + 0.0919i$	$-0.0039 - 0.0671i$
0.0083	$0.0353 - 0.0945i$	$-0.0402 - 0.0919i$	0.0075
$+0.0297i$	$+0.0297i$	$+0.0297i$	$+0.0297i$
$-0.0297i$	$-0.0297i$	$-0.0297i$	$-0.0297i$
0	0	0	0
0	0	0	0
Nominal Cond. 21	Nominal Cond. 22	Nominal Cond. 23	Nominal Cond. 24
$-0.6348 + 2.5938i$	$-0.6032 + 1.3790i$	$-0.7692 + 1.9069i$	-1.9090
$-0.6348 - 2.5938i$	$-0.6032 - 1.3790i$	$-0.7692 - 1.9069i$	-0.9645
-1.3600	-1.1007	-1.0523	$0.8110 + 0.0825i$
1.0141	0.9514	0.9447	$0.8110 - 0.0825i$
-0.9884	-0.7918	-0.3796	-0.3207
-0.0872	-0.1469	0.0720	0.0222
$0.0407 + 0.0951i$	$0.0700 + 0.1216i$	$-0.0334 + 0.1066i$	$-0.0114 + 0.0729i$
$0.0407 - 0.0951i$	$0.0700 - 0.1216i$	$-0.0334 - 0.1066i$	$-0.0114 - 0.0729i$
$+0.0297i$	$+0.0297i$	$+0.0297i$	$+0.0297i$
$-0.0297i$	$-0.0297i$	$-0.0297i$	$-0.0297i$
0	0	0	0
0	0	0	0

Table B.4. Eigenvalues of Receiver Aircraft for Nominal Conditions from 25 to 32

Nominal Cond. 25	Nominal Cond. 26	Nominal Cond. 27	Nominal Cond. 28
$-0.6365 + 2.5934i$	$-0.7684 + 1.9067i$	$-0.6114 + 1.3771i$	-1.9079
$-0.6365 - 2.5934i$	$-0.7684 - 1.9067i$	$-0.6114 - 1.3771i$	-0.9653
-1.3600	-1.0536	-1.0967	-0.3206
1.0130	0.9436	0.9513	$0.8105 + 0.0798i$
-0.9870	-0.3648	-0.7933	$0.8105 - 0.0798i$
0.0820	-0.0909	0.1216	-0.0218
$-0.0423 + 0.0134i$	$0.0411 + 0.0879i$	$-0.0572 + 0.1460i$	$0.0110 + 0.0569i$
$-0.0423 - 0.0134i$	$0.0411 - 0.0879i$	$-0.0572 - 0.1460i$	$0.0110 - 0.0569i$
$+0.0297i$	$+0.0297i$	$+0.0297i$	$+0.0297i$
$-0.0297i$	$-0.0297i$	$-0.0297i$	$-0.0297i$
0	0	0	0
0	0	0	0
Nominal Cond. 29	Nominal Cond. 30	Nominal Cond. 31	Nominal Cond. 32
$-0.7041 + 3.4165i$	$-0.6554 + 2.6296i$	$-0.6559 + 2.6296i$	$-0.4805 + 1.4135i$
$-0.7041 - 3.4165i$	$-0.6554 - 2.6296i$	$-0.6559 - 2.6296i$	$-0.4805 - 1.4135i$
-1.0258	-0.9537	-0.9504	-0.8726
0.9339	0.8692	0.8699	0.7955
-0.7618	-0.4552	-0.4759	-0.4182
$-0.0066 + 0.0679i$	-0.1203	-0.0984	0.0098
$-0.0066 - 0.0679i$	$0.0555 + 0.1045i$	$-0.0450 + 0.1235i$	$-0.0036 + 0.0708i$
0.0098	$0.0555 - 0.1045i$	$-0.0450 - 0.1235i$	$-0.0036 - 0.0708i$
$+0.0297i$	$+0.0297i$	$+0.0297i$	$+0.0297i$
$-0.0297i$	$-0.0297i$	$-0.0297i$	$-0.0297i$
0	0	0	0
0	0	0	0

Table B.5. Eigenvalues of Receiver Aircraft for Nominal Conditions from 33 to 40

Nominal Cond. 33	Nominal Cond. 34	Nominal Cond. 35	Nominal Cond. 36
0	0	0	0
0	0	0	0
0	0	0	0
-1.5279	$-1.5218 + 0.5860i$	$-1.5218 + 0.5860i$	0.8671
1.0293	$-1.5218 - 0.5860i$	$-1.5218 - 0.5860i$	-1.0505
-0.8405	1.0551	1.0551	-0.4153
0.0129	-0.8902	-0.8902	-2.7894
0	-0.7298	0.7298	0
$-0.7115 + 1.3280i$	0.0146	0.0146	0.0162
$-0.7115 - 1.3280i$	0	0	1.8128
$-0.0078 + 0.0732i$	$-0.0074 + 0.0714i$	$-0.0074 + 0.0714i$	$-0.0058 + 0.0719i$
$-0.0078 - 0.0732i$	$-0.0074 - 0.0714i$	$-0.0074 - 0.0714i$	$-0.0058 - 0.0719i$
Nominal Cond. 37	Nominal Cond. 38	Nominal Cond. 39	Nominal Cond. 40
0	0	0	0
0	0	0	0
0	0	0	0
$-0.5916 + 2.4109i$	$-0.5655 + 1.2815i$	$-0.7134 + 1.7718i$	-1.7767
$-0.5916 - 2.4109i$	$-0.5655 - 1.2815i$	$-0.7134 - 1.7718i$	-0.9169
-1.3206	-1.0842	-0.9992	$0.7489 + 0.0915i$
0.9320	0.8732	0.8677	$0.7489 - 0.0915i$
-0.8520	-0.6652	-0.3254	-0.2724
0.0150	0.0166	$+0.0167$	0.0185
0	0	0	0
$-0.0081 + 0.0726i$	$-0.0060 + 0.0738i$	$-0.0054 + 0.0736i$	$-0.0060 + 0.0686i$
$-0.0081 - 0.0726i$	$-0.0060 - 0.0738i$	$-0.0054 - 0.0736i$	$-0.0060 - 0.0686i$

Table B.6. Eigenvalues of Receiver Aircraft for Nominal Conditions from 41 to 48

Nominal Cond. 41	Nominal Cond. 42	Nominal Cond. 43	Nominal Cond. 44
0	0	0	0
0	0	0	0
0	0	0	0
$-0.5916 + 2.4109i$	$-1.7134 + 1.7718i$	$-0.5655 + 1.2815i$	-1.7767
$-0.5916 - 2.4109i$	$-1.7134 - 1.7718i$	$-0.5655 - 1.2815i$	-0.9169
-1.3206	-0.9992	-1.0842	$0.7489 + 0.0915i$
0.9320	0.8677	0.8732	$0.7489 - 0.0915i$
-0.8527	-0.3254	-0.6652	-0.2724
0.0150	0.0167	0.0166	0.0185
0	0	0	0
$-0.0081 + 0.0726i$	$-0.0054 + 0.0736i$	$-0.0060 + 0.0738i$	$-0.0060 + 0.0686i$
$-0.0081 - 0.0726i$	$-0.0054 - 0.0736i$	$-0.0060 - 0.0738i$	$-0.0060 - 0.0686i$
Nominal Cond. 45	Nominal Cond. 46	Nominal Cond. 47	Nominal Cond. 48
0	0	0	0
0	0	0	0
0	0	0	0
0.8571	$-0.6092 + 2.4444i$	$-0.6092 + 2.4444i$	0.7242
-1.0201	$-0.6092 - 2.4444i$	$-0.6092 - 2.4444i$	-0.8506
-0.6343	-0.9195	-0.9195	-0.3412
0.0174	0.7966	0.7966	0.0217
0	-0.3940	-0.3940	0
$-0.6546 + 3.1759i$	0.0192	0.0192	$-0.4470 + 1.3138i$
$-0.6546 - 3.1759i$	0	0	$-0.4470 - 1.3138i$
$-0.0082 + 0.0725i$	$-0.0063 + 0.0730i$	$-0.0063 + 0.0730i$	$-0.0056 + 0.0743i$
$-0.0082 - 0.0725i$	$-0.0063 - 0.0730i$	$-0.0063 - 0.0730i$	$-0.0056 - 0.0743i$

Table B.7. Eigenvalues of Receiver Aircraft for Nominal Conditions from 49 to 56

Nominal Cond. 49	Nominal Cond. 50	Nominal Cond. 51	Nominal Cond. 52
0	0	0	0
0	0	0	0
0	0	0	0
-1.6717	$-1.6509 + 0.6342i$	$-1.6509 + 0.6342i$	0.9550
1.1321	$-1.6509 - 0.6342i$	$-1.6509 - 0.6342i$	-1.1456
-0.8979	1.1427	1.1427	-0.4491
0.0110	-0.9522	-0.9522	-3.0031
0	0.8030	0.8030	0
$-0.7651 + 1.4287i$	$-0.0074 + 0.0657i$	$-0.0074 + 0.0657i$	0.0136
$-0.7651 - 1.4287i$	$-0.0074 - 0.0657i$	$-0.0074 - 0.0657i$	1.9528
$-0.0083 + 0.0689i$	0.0123	0.0123	$-0.0059 + 0.0667i$
$-0.0083 - 0.0689i$	0	0	$-0.0059 - 0.0667i$
Nominal Cond. 53	Nominal Cond. 54	Nominal Cond. 55	Nominal Cond. 56
0	0	0	0
0	0	0	0
0	0	0	0
$-0.6366 + 2.5957i$	$-0.6075 + 1.3797i$	$-0.7676 + 1.9039i$	-1.9158
$-0.6366 - 2.5957i$	$-0.6075 - 1.3797i$	$-0.7676 - 1.9039i$	-1.0038
-1.4682	-1.2094	-1.0951	$0.8199 + 0.0817i$
1.0340	0.9694	0.9594	$0.8199 - 0.0817i$
-0.8964	-0.6990	-0.3501	-0.2945
0.0126	0.0138	0.0139	0.0152
0	0	0	0
$-0.0083 + 0.0677i$	$-0.0062 + 0.0691i$	$-0.0057 + 0.0689i$	$-0.0058 + 0.0630i$
$-0.0083 - 0.0677i$	$-0.0062 - 0.0691i$	$-0.0057 - 0.0689i$	$-0.0058 - 0.0630i$

Table B.8. Eigenvalues of Receiver Aircraft for Nominal Conditions from 57 to 64

Nominal Cond. 57	Nominal Cond. 58	Nominal Cond. 59	Nominal Cond. 60
0	0	0	0
0	0	0	0
0	0	0	0
$-0.6366 + 2.5957i$	$-0.7676 + 1.9039i$	$-0.6075 + 1.3797i$	-1.9158
$-0.6366 - 2.5957i$	$-0.7676 - 1.9039i$	$-0.6075 - 1.3797i$	-1.0038
-1.4682	-1.0951	-1.2094	$0.8199 + 0.0817i$
1.0340	0.9594	0.9694	$0.8199 - 0.0817i$
-0.8964	-0.3501	-0.6990	-0.2945
0.0126	0.0139	0.0138	0.0152
0	0	0	0
$-0.0083 + 0.0677i$	$-0.0057 + 0.0689i$	$-0.0062 + 0.0691i$	$-0.0058 + 0.0630i$
$-0.0083 - 0.0677i$	$-0.0057 - 0.0689i$	$-0.0062 - 0.0691i$	$-0.0058 - 0.0630i$
Nominal Cond. 61	Nominal Cond. 62	Nominal Cond. 63	Nominal Cond. 64
0	0	0	0
0	0	0	0
0	0	0	0
0.9583	$-0.6551 + 2.6303i$	$-0.6551 + 2.6303i$	0.8110
-1.1460	$-0.6551 - 2.6303i$	$-0.6551 - 2.6303i$	-0.9414
-0.6649	-1.0198	-1.0198	-0.3663
0.0144	0.8897	0.8897	0.0175
0	-0.4200	-0.4200	0
$-0.7039 + 3.4178i$	0.0157	0.0157	$-0.4804 + 1.4141i$
$-0.7039 - 3.4178i$	0	0	$-0.4804 - 1.4141i$
$-0.0081 + 0.0675i$	$-0.0063 + 0.0680i$	$-0.0063 + 0.0680i$	$-0.0054 + 0.0693i$
$-0.0081 - 0.0675i$	$-0.0063 - 0.0680i$	$-0.0063 - 0.0680i$	$-0.0054 - 0.0693i$

Table B.9. Eigenvalues of Receiver Aircraft for Nominal Conditions from 65 to 72

Nominal Cond. 65	Nominal Cond. 66	Nominal Cond. 67	Nominal Cond. 68
$-0.7114 + 1.3278i$	$-1.4898 + 0.5887i$	$-1.4901 + 0.5805i$	-2.7864
$-0.7114 - 1.3278i$	$-1.4898 - 0.5887i$	$-1.4901 - 0.5805i$	1.8090
-1.4681	1.0478	1.0454	-1.0043
1.0143	-0.9481	-0.9398	0.8600
-0.8861	0.7243	0.7265	-0.4528
$-0.0065 + 0.0747i$	0.0896	-0.0783	0.0092
$-0.0065 - 0.0747i$	$-0.0424 + 0.0986i$	$0.0378 + 0.1025i$	$-0.0037 + 0.0724i$
0.0097	$-0.0424 - 0.0986i$	$0.0378 - 0.1025i$	$-0.0037 - 0.0724i$
$+0.0297i$	$+0.0297i$	$+0.0297i$	$+0.0297i$
$-0.0297i$	$-0.0297i$	$-0.0297i$	$-0.0297i$
0	0	0	0
0	0	0	0
Nominal Cond. 69	Nominal Cond. 70	Nominal Cond. 71	Nominal Cond. 72
$-0.5916 + 2.4086i$	$-0.5690 + 1.2788i$	$-0.7142 + 1.7743i$	-1.7691
$-0.5916 - 2.4086i$	$-0.5690 - 1.2788i$	$-0.7142 - 1.7743i$	-0.8794
-1.1926	-0.9437	-0.9591	$0.7394 + 0.0882i$
-0.9641	0.8563	0.8521	$0.7394 - 0.0882i$
0.9117	-0.7903	-0.3370	-0.2977
0.0840	0.1232	-0.0924	$-0.0006 + 0.0588i$
$-0.0419 + 0.1080i$	$-0.0560 + 0.1516i$	$0.0421 + 0.0901i$	$-0.0006 - 0.0588i$
$-0.0419 - 0.1080i$	$-0.0560 - 0.1516i$	$0.0421 - 0.0901i$	0.0045
$+0.0297i$	$+0.0297i$	$+0.0297i$	$+0.0297i$
$-0.0297i$	$-0.0297i$	$-0.0297i$	$-0.0297i$
0	0	0	0
0	0	0	0

Table B.10. Eigenvalues of Receiver Aircraft for Nominal Conditions from 73 to 80

Nominal Cond. 73	Nominal Cond. 74	Nominal Cond. 75	Nominal Cond. 76
$-0.5899 + 2.4090i$	$-0.7148 + 1.7744i$	$-0.5616 + 1.2809i$	-1.7700
$-0.5899 - 2.4090i$	$-0.7148 - 1.7744i$	$-0.5616 - 1.2809i$	-0.8783
-1.1915	-0.9573	-1.9536	$0.7407 + 0.0919i$
0.9131	0.8541	0.8561	$0.7407 - 0.0919i$
-0.9660	-0.3564	-0.7785	-0.2978
-0.0874	0.0725	-0.1503	$-0.0044 + 0.0751i$
$0.0419 + 0.0987i$	$-0.0316 + 0.1112i$	$0.0724 + 0.1241i$	$-0.0044 - 0.0751i$
$0.0419 - 0.0987i$	$-0.0316 - 0.1112i$	$0.0724 - 0.1241i$	0.0095
$+0.0297i$	$+0.0297i$	$+0.0297i$	0
$-0.0297i$	$-0.0297i$	$-0.0297i$	0
0	0	0	$+0.0297i$
0	0	0	$-0.0297i$
Nominal Cond. 77	Nominal Cond. 78	Nominal Cond. 79	Nominal Cond. 80
$-0.6548 + 3.1745i$	$-0.6098 + 2.4435i$	$-0.6096 + 2.4435i$	$-0.4470 + 1.3133i$
$-0.6548 - 3.1745i$	$-0.6098 - 2.4435i$	$-0.6096 - 2.4435i$	$-0.4470 - 1.3133i$
-0.8508	-0.8475	-0.8527	-0.7807
0.8332	0.7776	0.7769	0.7097
-0.7806	-0.4556	-0.4269	-0.3947
$-0.0065 + 0.0730i$	0.1031	-0.1275	0.0124
$-0.0065 - 0.0730i$	$-0.0448 + 0.1308i$	$0.0588 + 0.1091i$	$-0.0033 + 0.0760i$
0.0120	$-0.0448 - 0.1308i$	$0.0588 - 0.1091i$	$-0.0033 - 0.0760i$
$+0.0297i$	$+0.0297i$	$+0.0297i$	$+0.0297i$
$-0.0297i$	$-0.0297i$	$-0.0297i$	$-0.0297i$
0	0	0	0
0	0	0	0

Table B.11. Eigenvalues of Receiver Aircraft for Nominal Conditions from 81 to 88

Nominal Cond. 81	Nominal Cond. 82	Nominal Cond. 83	Nominal Cond. 84
$-0.7649 + 1.4286i$	$-1.6184 + 0.6367i$	$-1.6186 + 0.6284i$	-3.0003
$-0.7649 - 1.4286i$	$-1.6184 - 0.6367i$	$-1.6186 - 0.6284i$	1.9493
-1.6119	1.1343	1.1326	-1.0980
1.1162	-1.0102	-1.0024	0.9469
-0.9428	0.7990	0.7985	-0.4875
$-0.0072 + 0.0701i$	0.0817	-0.0742	$-0.0039 + 0.0671i$
$-0.0072 - 0.0701i$	$-0.0402 + 0.0919i$	$0.0353 + 0.0945i$	$-0.0039 - 0.0671i$
0.0083	$-0.0402 - 0.0919i$	$0.0353 - 0.0945i$	0.0075
$+0.0297i$	$+0.0297i$	$+0.0297i$	$+0.0297i$
$-0.0297i$	$-0.0297i$	$-0.0297i$	$-0.0297i$
0	0	0	0
0	0	0	0
Nominal Cond. 85	Nominal Cond. 86	Nominal Cond. 87	Nominal Cond. 88
$-0.6365 + 2.5934i$	$-0.6114 + 1.3771i$	$-0.7684 + 1.9067i$	-1.9079
$-0.6365 - 2.5934i$	$-0.6114 - 1.3771i$	$-0.7684 - 1.9067i$	-0.9653
-1.3600	-1.0967	-1.0536	-0.3206
1.0130	0.9513	0.9436	$0.8105 + 0.0798i$
-0.9870	-0.7933	-0.3648	$0.8105 - 0.0798i$
0.0820	0.1216	-0.0909	-0.0218
$-0.0423 + 0.1034i$	$-0.0572 + 0.1460i$	$0.0411 + 0.0879i$	$0.0110 + 0.0569i$
$-0.0423 - 0.1034i$	$-0.0572 - 0.1460i$	$0.0411 - 0.0879i$	$0.0110 - 0.0569i$
$+0.0297i$	$+0.0297i$	$+0.0297i$	$+0.0297i$
$-0.0297i$	$-0.0297i$	$-0.0297i$	$-0.0297i$
0	0	0	0
0	0	0	0

Table B.12. Eigenvalues of Receiver Aircraft for Nominal Conditions from 89 to 96

Nominal Cond. 89	Nominal Cond. 90	Nominal Cond. 91	Nominal Cond. 92
$-0.6348 + 2.5938i$	$-0.7692 + 1.9069i$	$-0.6032 + 1.3790i$	-1.9090
$-0.6348 - 2.5938i$	$-0.7692 - 1.9069i$	$-0.6032 - 1.3790i$	-0.9645
-1.3600	-1.0523	-1.1007	$0.8110 + 0.0825i$
1.0141	0.9447	0.9514	$0.8110 - 0.0825i$
-0.9884	-0.3796	-0.7918	-0.3207
-0.0872	0.0720	-0.1469	0.0222
$0.0407 + 0.0951i$	$-0.0334 + 0.1066i$	$0.0700 + 0.1216i$	$-0.0114 + 0.0719i$
$0.0407 - 0.0951i$	$-0.0334 - 0.1066i$	$0.0700 - 0.1216i$	$-0.0114 - 0.0719i$
$+0.0297i$	$+0.0297i$	0	$+0.0297i$
$-0.0297i$	$-0.0297i$	$+0.0297i$	$-0.0297i$
0	0	$-0.0297i$	0
0	0	0	0
Nominal Cond. 93	Nominal Cond. 94	Nominal Cond. 95	Nominal Cond. 96
$-0.7041 + 3.4165i$	$-0.6559 + 2.6296i$	$-0.6554 + 2.6296i$	$-0.4805 + 1.4135i$
$-0.7041 - 3.4165i$	$-0.6559 - 2.6296i$	$-0.6554 - 2.6296i$	$-0.4805 - 1.4135i$
-1.0258	-0.9504	-0.9537	-0.8726
0.9339	0.8699	0.8692	0.7955
-0.7618	-0.4759	-0.4552	-0.4182
$-0.0066 + 0.0679i$	0.0984	-0.1203	0.0098
$-0.0066 - 0.0679i$	$-0.0450 + 0.1235i$	$0.0555 + 0.1045i$	$-0.0036 + 0.0708i$
0.0098	$-0.0450 - 0.1235i$	$0.0555 - 0.1045i$	$-0.0036 - 0.0708i$
$+0.0297i$	$+0.0297i$	$+0.0297i$	$+0.0297$
$-0.0297i$	$-0.0297i$	$-0.0297i$	-0.0297
0	0	0	0
0	0	0	0

APPENDIX C

STRAIGHT LEVEL FLIGHT EIGENVALUES COMPARISON

Table C.1. Eigenvalues of Symmetrical Identity Cases for Straight Flight with $V_{T,2}$

Nominal Cond. 57	Nominal Cond. 53	Nominal Cond. 51	Nominal Cond. 50
Tank 1	Tank 2	Tank 3	Tank 4
0	0	0	0
0	0	0	0
0	0	0	0
$-0.6366 + 2.5957i$	$-0.6366 + 2.5957i$	$-1.6509 + 0.6342i$	$-1.6509 + 0.6342i$
$-0.6366 - 2.5957i$	$-0.6366 - 2.5957i$	$-1.6509 - 0.6342i$	$-1.6509 - 0.6342i$
-1.4682	-1.4682	1.1427	1.1427
1.0340	1.0340	-0.9522	-0.9522
-0.8964	-0.8964	0.8030	0.8030
0.0126	0.0126	$-0.0074 + 0.0657i$	$-0.0074 + 0.0657i$
0	0	$-0.0074 - 0.0657i$	$-0.0074 - 0.0657i$
$-0.0083 + 0.0677i$	$-0.0083 + 0.0677i$	0.0123	0.0123
$-0.0083 - 0.0677i$	$-0.0083 - 0.0677i$	0	0
Nominal Cond. 59	Nominal Cond. 54	Nominal Cond. 58	Nominal Cond. 55
Tank 1,3	Tank 2,4	Tank 1,4	Tank 2,3
0	0	0	0
0	0	0	0
0	0	0	0
$-0.6075 + 1.3797i$	$-0.6075 + 1.3797i$	$-0.7676 + 1.9039i$	$-0.7676 + 1.9039i$
$-0.6075 - 1.3797i$	$-0.6075 - 1.3797i$	$-0.7676 - 1.9039i$	$-0.7676 - 1.9039i$
-1.2094	-1.2094	-1.0951	-1.0951
0.9694	0.9694	0.9594	0.9594
-0.6990	-0.6990	-0.3501	-0.3501
0.0138	0.0138	0.0139	0.0139
0	0	0	0
$-0.0062 + 0.0691i$	$-0.0062 + 0.0691i$	$-0.0057 + 0.0689i$	$-0.0057 + 0.0689i$
$-0.0062 - 0.0691i$	$-0.0062 - 0.0691i$	$-0.0057 - 0.0689i$	$-0.0057 - 0.0689i$

Table C.2. Eigenvalues of Symmetrical Identity Cases for Straight Flight with $V_{T,2}$

Nominal Cond. 63	Nominal Cond. 62	Nominal Cond. 60	Nominal Cond. 56
Tank 1,2,3	Tank 1,2,4	Tank 1,3,4	Tank 2,3,4
0	0	0	0
0	0	0	0
0	0	0	0
$-0.6551 + 2.6303i$	$-0.6551 + 2.6303i$	-1.9158	-1.9158
$-0.6551 - 2.6303i$	$-0.6551 - 2.6303i$	-1.0038	-1.0038
-1.0198	-1.0198	$0.8199 + 0.0817i$	$0.8199 + 0.0817i$
0.8897	0.8897	$0.8199 - 0.0817i$	$0.8199 - 0.0817i$
-0.4200	-0.4200	-0.2945	-0.2945
0.0157	0.0157	0.0152	0.0152
0	0	0	0
$-0.0063 + 0.0680i$	$-0.0063 + 0.0680i$	$-0.0058 + 0.0630i$	$-0.0058 + 0.0630i$
$-0.0063 - 0.0680i$	$-0.0063 - 0.0680i$	$-0.0058 - 0.0630i$	$-0.0058 - 0.0630i$

Table C.3. Eigenvalues of Symmetrical Identity Cases for Straight Flight with $V_{T,1}$

Nominal Cond. 41	Nominal Cond. 37	Nominal Cond. 35	Nominal Cond. 34
Tank 1	Tank 2	Tank 3	Tank 4
0	0	0	0
0	0	0	0
0	0	0	0
$-0.5916 + 2.4109i$	$-0.5916 + 2.4109i$	$-1.5218 + 0.5860i$	$-1.5218 + 0.5860i$
$-0.5916 - 2.4109i$	$-0.5916 - 2.4109i$	$-1.5218 - 0.5860i$	$-1.5218 - 0.5860i$
-1.3206	-1.3206	1.0551	1.0551
0.9320	0.9320	-0.8902	-0.8902
-0.8527	-0.8520	0.7298	0.7298
0.0150	0.0150	0.0146	0.0146
0	0	0	0
$-0.0081 + 0.0726i$	$-0.0081 + 0.0726i$	$-0.0074 + 0.0714i$	$-0.0074 + 0.0714i$
$-0.0081 - 0.0726i$	$-0.0081 - 0.0726i$	$-0.0074 - 0.0714i$	$-0.0074 - 0.0714i$
Nominal Cond. 43	Nominal Cond. 38	Nominal Cond. 42	Nominal Cond. 39
Tank 1,3	Tank 2,4	Tank 1,4	Tank 2,3
0	0	0	0
0	0	0	0
0	0	0	0
$-0.5655 + 1.2815i$	$-0.5655 + 1.2815i$	$-0.7134 + 1.7718i$	$-0.7134 + 1.7718i$
$-0.5655 - 1.2815i$	$-0.5655 - 1.2815i$	$-0.7134 - 1.7718i$	$-0.7134 - 1.7718i$
-1.0842	-1.0842	-0.9992	-0.9992
0.8732	0.8732	0.8677	0.8677
-0.6652	-0.6652	-0.3254	-0.3254
0.0166	0.0166	0.0167	0.0167
0	0	0	0
$-0.0060 + 0.0738i$	$-0.0060 + 0.0738i$	$-0.0054 + 0.0736i$	$-0.0054 + 0.0736i$
$-0.0060 - 0.0738i$	$-0.0060 - 0.0738i$	$-0.0054 - 0.0736i$	$-0.0054 - 0.0736i$

Table C.4. Eigenvalues of Symmetrical Identity Cases for Straight Flight with $V_{T,1}$

Nominal Cond. 47	Nominal Cond. 46	Nominal Cond. 44	Nominal Cond. 40
Tank 1,2,3	Tank 1,2,4	Tank 1,3,4	Tank 2,3,4
0	0	0	0
0	0	0	0
0	0	0	0
$-0.6092 + 2.4444i$	$-0.6092 + 2.4444i$	-1.7767	-1.7767
$-0.6092 - 2.4444i$	$-0.6092 - 2.4444i$	-0.9169	-0.9169
-0.9195	-0.9195	$0.7489 + 0.0915i$	$0.7489 + 0.0915i$
0.7966	0.7966	$0.7489 - 0.0915i$	$0.7489 - 0.0915i$
-0.3940	-0.3940	-0.2724	-0.2724
0.0192	0.0192	0.0185	0.0185
0	0	0	0
$-0.0063 + 0.0730i$	$-0.0063 + 0.0730i$	$-0.0060 + 0.0686i$	$-0.0060 + 0.0686i$
$-0.0063 - 0.0730i$	$-0.0063 - 0.0730i$	$-0.0060 - 0.0686i$	$-0.0060 - 0.0686i$

APPENDIX D

TURNING FLIGHT EIGENVALUES COMPARISON

Table D.1. Eigenvalues of Turning Flight with $V_{T,2}$

Nominal Cond. 89	Nominal Cond. 21	Nominal Cond. 85	Nominal Cond. 25
Tank 1	Tank 2	Tank 2	Tank 1
$\dot{\psi}_{T,2} = 1.7$	$\dot{\psi}_{T,3} = -1.7$	$\dot{\psi}_{T,2} = 1.7$	$\dot{\psi}_{T,3} = -1.7$
$-0.6348 + 2.5938i$	$-0.6348 + 2.5938i$	$-0.6356 + 2.5934i$	$-0.6356 + 2.5934i$
$-0.6348 - 2.5938i$	$-0.6348 - 2.5938i$	$-0.6356 - 2.5934i$	$-0.6356 - 2.5934i$
-1.3600	-1.3600	-1.3600	-1.3600
1.0141	1.0141	1.0130	1.0130
-0.9884	-0.9884	-0.9870	-0.9870
-0.0872	-0.0872	0.0820	0.0820
$0.0407 + 0.0951i$	$0.0407 + 0.0951i$	$-0.0423 + 0.1034i$	$-0.0423 + 0.1034i$
$0.0407 - 0.0951i$	$0.0407 - 0.0951i$	$-0.0423 - 0.1034i$	$-0.0423 - 0.1034i$
$+0.0297i$	$+0.0297i$	$+0.0297i$	$+0.0297i$
$-0.0297i$	$-0.0297i$	$-0.0297i$	$-0.0297i$
0	0	0	0
0	0	0	0
Nominal Cond. 83	Nominal Cond. 18	Nominal Cond. 82	Nominal Cond. 19
Tank 3	Tank 4	Tank 4	Tank 3
$\dot{\psi}_{T,2} = 1.7$	$\dot{\psi}_{T,3} = -1.7$	$\dot{\psi}_{T,2} = 1.7$	$\dot{\psi}_{T,3} = -1.7$
$-1.6186 + 0.6284i$	$-1.6186 + 0.6284i$	$-1.6184 + 0.6367i$	$-1.6184 + 0.6367i$
$-1.6186 - 0.6284i$	$-1.6186 - 0.6284i$	$-1.6184 - 0.6367i$	$-1.6184 - 0.6367i$
1.1326	1.1326	1.1343	1.1343
-1.0024	-1.0024	-1.0102	-1.0102
0.7985	0.7985	0.7990	0.7990
-0.0742	-0.0742	0.0817	0.0817
$0.0353 + 0.0945i$	$0.0353 + 0.0945i$	$-0.0402 + 0.0919i$	$-0.0402 + 0.0919i$
$0.0353 - 0.0945i$	$0.0353 - 0.0945i$	$-0.0402 - 0.0919i$	$-0.0402 - 0.0919i$
$+0.0297i$	$+0.0297i$	$+0.0297i$	$+0.0297i$
$-0.0297i$	$-0.0297i$	$-0.0297i$	$-0.0297i$
0	0	0	0
0	0	0	0

Table D.2. Eigenvalues of Turning Flight with $V_{T,2}$

Nominal Cond. 93	Nominal Cond. 29	Nominal Cond. 91	Nominal Cond. 22
Tank 1,2	Tank 1,2	Tank 1,3	Tank 2,4
$\dot{\psi}_{T,2} = 1.7$	$\dot{\psi}_{T,3} = -1.7$	$\dot{\psi}_{T,2} = 1.7$	$\dot{\psi}_{T,3} = -1.7$
$-0.7041 + 3.4165i$	$-0.7041 + 3.4165i$	$-0.6032 + 1.3790i$	$-0.6032 + 1.3790i$
$-0.7041 - 3.4165i$	$-0.7041 - 3.4165i$	$-0.6032 - 1.3790i$	$-0.6032 - 1.3790i$
-1.0258	-1.0258	-1.1007	-1.1007
0.9339	0.9339	0.9514	0.9514
-0.7618	-0.7618	-0.7918	-0.7918
$-0.0066 + 0.0678i$	$-0.0066 + 0.0678i$	-0.1469	-0.1469
$-0.0066 - 0.0678i$	$-0.0066 - 0.0678i$	$0.0700 + 0.1216i$	$0.0700 + 0.1216i$
0.0098	0.0098	$0.0700 - 0.1216i$	$0.0700 - 0.1216i$
$+0.0297i$	$+0.0297i$	0	$+0.0297i$
$-0.0297i$	$-0.0297i$	$+0.0297i$	$-0.0297i$
0	0	$-0.0297i$	0
0	0	0	0
Nominal Cond. 90	Nominal Cond. 23	Nominal Cond. 87	Nominal Cond. 26
Tank 1,4	Tank 2,3	Tank 2,3	Tank 1,4
$\dot{\psi}_{T,2} = 1.7$	$\dot{\psi}_{T,3} = -1.7$	$\dot{\psi}_{T,2} = 1.7$	$\dot{\psi}_{T,3} = -1.7$
$-0.7692 + 1.9069i$	$-0.7692 + 1.9069i$	$-0.7684 + 1.9067i$	$-0.7684 + 1.9067i$
$-0.7692 - 1.9069i$	$-0.7692 - 1.9069i$	$-0.7684 - 1.9067i$	$-0.7684 - 1.9067i$
-1.0523	-1.0523	-1.0536	-1.0536
0.9447	0.9447	0.9436	0.9436
-0.3796	-0.3796	-0.3648	-0.3648
0.0720	0.0720	-0.0909	-0.0909
$-0.0334 + 0.1066i$	$-0.0334 + 0.1066i$	$0.0411 + 0.0879i$	$0.0411 + 0.0879i$
$-0.0334 - 0.1066i$	$-0.0334 - 0.1066i$	$0.0411 - 0.0879i$	$0.0411 - 0.0879i$
$+0.0297i$	$+0.0297i$	$+0.0297i$	$+0.0297i$
$-0.0297i$	$-0.0297i$	$-0.0297i$	$-0.0297i$
0	0	0	0
0	0	0	0

Table D.3. Eigenvalues of Turning Flight with $V_{T,2}$

Nominal Cond. 86	Nominal Cond. 27	Nominal Cond. 84	Nominal Cond. 20
Tank 2,4	Tank 1,3	Tank 3,4	Tank 3,4
$\dot{\psi}_{T,2} = 1.7$	$\dot{\psi}_{T,3} = -1.7$	$\dot{\psi}_{T,2} = 1.7$	$\dot{\psi}_{T,3} = -1.7$
$-0.6114 + 1.3771i$	$-0.6114 + 1.3771i$	-3.0003	-3.0003
$-0.6114 - 1.3771i$	$-0.6114 - 1.3771i$	1.9493	1.9493
-1.0967	-1.0967	-1.0980	-1.0980
0.9513	0.9513	0.9469	0.9469
-0.7933	-0.7933	-0.4875	-0.4875
0.1216	0.1216	$-0.0039 + 0.0671i$	$-0.0039 + 0.0671i$
$-0.0572 + 0.1460i$	$-0.0572 + 0.1460i$	$-0.0039 - 0.0671i$	$-0.0039 - 0.0671i$
$-0.0572 - 0.1460i$	$-0.0572 - 0.1460i$	0.0075	0.0075
$+0.0297i$	$+0.0297i$	$+0.0297i$	$+0.0297i$
$-0.0297i$	$-0.0297i$	$-0.0297i$	$-0.0297i$
0	0	0	0
0	0	0	0
Nominal Cond. 92	Nominal Cond. 24	Nominal Cond. 88	Nominal Cond. 28
Tank 1,3,4	Tank 2,3,4	Tank 2,3,4	Tank 1,3,4
$\dot{\psi}_{T,2} = 1.7$	$\dot{\psi}_{T,3} = -1.7$	$\dot{\psi}_{T,2} = 1.7$	$\dot{\psi}_{T,3} = -1.7$
-1.9090	-1.9090	-1.9079	-1.9079
-0.9645	-0.9645	-0.9653	-0.9653
$0.8110 + 0.0825i$	$0.8110 + 0.0825i$	-0.3206	-0.3206
$0.8110 - 0.0825i$	$0.8110 - 0.0825i$	$0.8105 + 0.0798i$	$0.8105 + 0.0798i$
-0.3207	-0.3207	$0.8105 - 0.0798i$	$0.8105 - 0.0798i$
0.0222	0.0222	-0.0218	-0.0218
$-0.0114 + 0.0719i$	$-0.0114 + 0.0719i$	$0.0110 + 0.0569i$	$0.0110 + 0.0569i$
$-0.0114 - 0.0719i$	$-0.0114 - 0.0719i$	$0.0110 - 0.0569i$	$0.0110 - 0.0569i$
$+0.0297i$	$+0.0297i$	$+0.0297i$	$+0.0297i$
$-0.0297i$	$-0.0297i$	$-0.0297i$	$-0.0297i$
0	0	0	0
0	0	0	0

Table D.4. Eigenvalues of Turning Flight with $V_{T,2}$

Nominal Cond. 96	Nominal Cond. 32	Nominal Cond. 81	Nominal Cond. 17
Tank 1,2,3,4	Tank 1,2,3,4	Tank empty	Tank empty
$\dot{\psi}_{T,2} = 1.7$	$\dot{\psi}_{T,3} = -1.7$	$\dot{\psi}_{T,2} = 1.7$	$\dot{\psi}_{T,3} = -1.7$
$-0.4805 + 1.4135i$	$-0.4805 + 1.4135i$	$-0.7649 + 1.4286i$	$-0.7649 + 1.4286i$
$-0.4805 - 1.4135i$	$-0.4805 - 1.4135i$	$-0.7649 + 1.4286i$	$-0.7649 + 1.4286i$
-0.8726	-0.8726	-1.6119	-1.6119
0.7955	0.7955	1.1162	1.1162
-0.4182	-0.4182	-0.9428	-0.9428
0.0098	0.0098	$-0.0072 + 0.0701i$	$-0.0072 + 0.0701i$
$-0.0036 + 0.0708i$	$-0.0036 + 0.0708i$	$-0.0072 - 0.0701i$	$-0.0072 - 0.0701i$
$-0.0036 - 0.0708i$	$-0.0036 - 0.0708i$	0.0083	0.0083
$+0.0297i$	$+0.0297i$	$+0.0297i$	$+0.0297i$
$-0.0297i$	$-0.0297i$	$-0.0297i$	$-0.0297i$
0	0	0	0
0	0	0	0

Table D.5. Eigenvalues of Turning Flight with $V_{T,1}$

Nominal Cond. 73	Nominal Cond. 5	Nominal Cond. 69	Nominal Cond. 9
Tank 1	Tank 2	Tank 2	Tank 1
$\dot{\psi}_{T,2} = 1.7$	$\dot{\psi}_{T,3} = -1.7$	$\dot{\psi}_{T,2} = 1.7$	$\dot{\psi}_{T,3} = -1.7$
$-0.5899 + 2.4090i$	$-0.5899 + 2.4090i$	$-0.5916 + 2.4086i$	$-0.5916 + 2.4086i$
$-0.5899 - 2.4090i$	$-0.5899 - 2.4090i$	$-0.5916 - 2.4086i$	$-0.5916 - 2.4086i$
-1.1915	-1.1915	-1.1926	-1.1926
0.9131	0.9131	-0.9641	-0.9641
-0.9660	-0.9660	0.9117	0.9117
-0.0874	-0.0874	0.0840	0.0840
$0.0419 + 0.0987i$	$0.0419 + 0.0987i$	$-0.0419 + 0.1080i$	$-0.0419 + 0.1080i$
$0.0419 - 0.0987i$	$0.0419 - 0.0987i$	$-0.0419 - 0.1080i$	$-0.0419 - 0.1080i$
$+0.0297i$	$+0.0297i$	$+0.0297i$	$+0.0297i$
$-0.0297i$	$-0.0297i$	$-0.0297i$	$-0.0297i$
0	0	0	0
0	0	0	0
Nominal Cond. 67	Nominal Cond. 2	Nominal Cond. 66	Nominal Cond. 3
Tank 3	Tank 4	Tank 4	Tank 3
$\dot{\psi}_{T,2} = 1.7$	$\dot{\psi}_{T,3} = -1.7$	$\dot{\psi}_{T,2} = 1.7$	$\dot{\psi}_{T,3} = -1.7$
$-1.4901 + 0.5805i$	$-1.4901 + 0.5805i$	$-1.4898 + 0.5887i$	$-1.4898 + 0.5887i$
$-1.4901 - 0.5805i$	$-1.4901 - 0.5805i$	$-1.4898 - 0.5887i$	$-1.4898 - 0.5887i$
1.0454	1.0454	1.0478	1.0478
-0.9398	-0.9398	-0.9481	-0.9481
0.7265	0.7265	0.7243	0.7243
-0.0783	-0.0783	0.0896	0.0896
$0.0378 + 0.1025i$	$0.0378 + 0.1025i$	$-0.0424 + 0.0986i$	$-0.0424 + 0.0986i$
$0.0378 - 0.1025i$	$0.0378 - 0.1025i$	$-0.0424 - 0.0986i$	$-0.0424 - 0.0986i$
$+0.0297i$	$+0.0297i$	$+0.0297i$	$+0.0297i$
$-0.0297i$	$-0.0297i$	$-0.0297i$	$-0.0297i$
0	0	0	0
0	0	0	0

Table D.6. Eigenvalues of Turning Flight with $V_{T,1}$

Nominal Cond. 77	Nominal Cond. 13	Nominal Cond. 75	Nominal Cond. 6
Tank 1,2	Tank 1,2	Tank 1,3	Tank 2,4
$\dot{\psi}_{T,2} = 1.7$	$\dot{\psi}_{T,3} = -1.7$	$\dot{\psi}_{T,2} = 1.7$	$\dot{\psi}_{T,3} = -1.7$
$-0.6548 + 3.1745i$	$-0.6548 + 3.1745i$	$-0.5616 + 1.2809i$	$-0.5616 + 1.2809i$
$-0.6548 - 3.1745i$	$-0.6548 - 3.1745i$	$-0.5616 - 1.2809i$	$-0.5616 - 1.2809i$
-0.8508	-0.8508	-0.9536	-0.9536
0.8332	0.8332	0.8561	0.8561
-0.7806	-0.7806	-0.7785	-0.7785
$-0.0065 + 0.0730i$	$-0.0065 + 0.0730i$	-0.1503	-0.1503
$-0.0065 - 0.0730i$	$-0.0065 - 0.0730i$	$0.0724 + 0.1241i$	$0.0724 + 0.1241i$
0.0120	0.0120	$0.0724 - 0.1241i$	$0.0724 - 0.1241i$
$+0.0297i$	$+0.0297i$	$+0.0297i$	$+0.0297i$
$-0.0297i$	$-0.0297i$	$-0.0297i$	$-0.0297i$
0	0	0	0
0	0	0	0
Nominal Cond. 74	Nominal Cond. 7	Nominal Cond. 71	Nominal Cond. 10
Tank 1,4	Tank 2,3	Tank 2,3	Tank 1,4
$\dot{\psi}_{T,2} = 1.7$	$\dot{\psi}_{T,3} = -1.7$	$\dot{\psi}_{T,2} = 1.7$	$\dot{\psi}_{T,3} = -1.7$
$-0.7148 + 1.7744i$	$-0.7148 + 1.7744i$	$-0.7142 + 1.7743i$	$-0.7142 + 1.7743i$
$-0.7148 - 1.7744i$	$-0.7148 - 1.7744i$	$-0.7142 - 1.7743i$	$-0.7142 - 1.7743i$
-0.9573	-0.9573	-0.9591	-0.9591
0.8541	0.8541	0.8521	0.8527
-0.3564	-0.3564	-0.3370	-0.3370
0.0725	0.0725	-0.0924	-0.0924
$-0.0316 + 0.1112i$	$-0.0316 + 0.1112i$	$0.0421 + 0.0901i$	$0.0421 + 0.0901i$
$-0.0316 - 0.1112i$	$-0.0316 - 0.1112i$	$0.0421 - 0.0901i$	$0.0421 - 0.0901i$
$+0.0297i$	$+0.0297i$	$+0.0297i$	$+0.0297i$
$-0.0297i$	$-0.0297i$	$-0.0297i$	$-0.0297i$
0	0	0	0
0	0	0	0

Table D.7. Eigenvalues of Turning Flight with $V_{T,1}$

Nominal Cond. 70	Nominal Cond. 11	Nominal Cond. 68	Nominal Cond. 4
Tank 2,4	Tank 1,3	Tank 3,4	Tank 3,4
$\dot{\psi}_{T,2} = 1.7$	$\dot{\psi}_{T,3} = -1.7$	$\dot{\psi}_{T,2} = 1.7$	$\dot{\psi}_{T,3} = -1.7$
$-0.5690 + 1.2788i$	$-0.5690 + 1.2788i$	-2.7864	-2.7864
$-0.5690 - 1.2788i$	$-0.5690 - 1.2788i$	1.8090	1.8090
-0.9437	-0.9437	-1.0043	-1.0043
0.8563	0.8563	0.8600	0.8600
-0.7903	-0.7903	-0.4528	-0.4528
0.1232	0.1232	0.0092	0.0092
$-0.0560 + 0.1516i$	$-0.0560 + 0.1516i$	$-0.0037 + 0.0724i$	$-0.0037 + 0.0724i$
$-0.0560 - 0.1516i$	$-0.0560 - 0.1516i$	$-0.0037 - 0.0724i$	$-0.0037 - 0.0724i$
$+0.0297i$	$+0.0297i$	$+0.0297i$	$+0.0297i$
$-0.0297i$	$-0.0297i$	$-0.0297i$	$-0.0297i$
0	0	0	0
0	0	0	0
Nominal Cond. 79	Nominal Cond. 14	Nominal Cond. 78	Nominal Cond. 15
Tank 1,2,3	Tank 1,2,4	Tank 1,2,4	Tank 1,2,3
$\dot{\psi}_{T,2} = 1.7$	$\dot{\psi}_{T,3} = -1.7$	$\dot{\psi}_{T,2} = 1.7$	$\dot{\psi}_{T,3} = -1.7$
$-0.6096 + 2.4435i$	$-0.6096 + 2.4435i$	$-0.6098 + 2.4435i$	$-0.6098 + 2.4435i$
$-0.6096 - 2.4435i$	$-0.6096 - 2.4435i$	$-0.6098 - 2.4435i$	$-0.6098 - 2.4435i$
-0.8527	-0.8527	-0.8475	-0.8475
0.7769	0.7769	0.7776	0.7776
-0.4269	-0.4269	-0.4556	-0.4556
-0.1275	-0.1275	0.1031	0.1031
$0.0588 + 0.1091i$	$0.0588 + 0.1091i$	$-0.0448 + 0.1308i$	$-0.0448 + 0.1308i$
$0.0588 - 0.1091i$	$0.0588 - 0.1091i$	$-0.0448 + 0.1308i$	$-0.0448 + 0.1308i$
$+0.0297i$	$+0.0297i$	$+0.0297i$	$+0.0297i$
$-0.0297i$	$-0.0297i$	$-0.0297i$	$-0.0297i$
0	0	0	0
0	0	0	0

Table D.8. Eigenvalues of Turning Flight with $V_{T,1}$

Nominal Cond. 76	Nominal Cond. 8	Nominal Cond. 72	Nominal Cond. 12
Tank 1,3,4	Tank 2,3,4	Tank 2,3,4	Tank 1,3,4
$\dot{\psi}_{T,2} = 1.7$	$\dot{\psi}_{T,3} = -1.7$	$\dot{\psi}_{T,2} = 1.7$	$\dot{\psi}_{T,3} = -1.7$
-1.7700	-1.7700	-1.7691	-1.7691
-0.8783	-0.8783	-0.8794	-0.8794
$0.7407 + 0.0919i$	$0.7407 + 0.0919i$	$0.7393 + 0.0882i$	$0.7393 + 0.0882i$
$0.7407 - 0.0919i$	$0.7407 - 0.0919i$	$0.7393 - 0.0882i$	$0.7393 - 0.0882i$
-0.2978	-0.2978	-0.2977	-0.2977
$-0.0044 + 0.0751i$	$-0.0044 + 0.0751i$	$-0.0006 + 0.0588i$	$-0.0006 + 0.0588i$
$-0.0044 - 0.0751i$	$-0.0044 - 0.0751i$	$-0.0006 - 0.0588i$	$-0.0006 - 0.0588i$
0.0095	0.0095	0.0045	0.0045
0	0	$+0.0297i$	$+0.0297i$
0	0	$-0.0297i$	$-0.0297i$
$+0.0297i$	$+0.0297i$	0	0
$-0.0297i$	$-0.0297i$	0	0
Nominal Cond. 80	Nominal Cond. 16	Nominal Cond. 65	Nominal Cond. 1
Tank 1,2,3,4	Tank 1,2,3,4	Tank empty	Tank empty
$\dot{\psi}_{T,2} = 1.7$	$\dot{\psi}_{T,3} = -1.7$	$\dot{\psi}_{T,2} = 1.7$	$\dot{\psi}_{T,3} = -1.7$
$-0.4470 + 1.3133i$	$-0.4470 + 1.3133i$	$-0.7114 + 1.3278i$	$-0.7114 + 1.3278i$
$-0.4470 - 1.3133i$	$-0.4470 - 1.3133i$	$-0.7114 - 1.3278i$	$-0.7114 - 1.3278i$
-0.7807	-0.7807	-1.4681	-1.4681
0.7097	0.7097	1.0143	1.0143
-0.3947	-0.3947	-0.8861	-0.8861
0.0124	0.0124	$-0.0065 + 0.0747i$	$-0.0065 + 0.0747i$
$-0.0033 + 0.0760i$	$-0.0033 + 0.0760i$	$-0.0065 - 0.0747i$	$-0.0065 - 0.0747i$
$-0.0033 - 0.0760i$	$-0.0033 - 0.0760i$	0.0097	0.0097
$+0.0297i$	$+0.0297i$	$+0.0297i$	$+0.0297i$
$-0.0297i$	$-0.0297i$	$-0.0297i$	$-0.0297i$
0	0	0	0
0	0	0	0

REFERENCES

[1] J. J. Kim and B. N. Agrawal, "System identification and automatic mass balancing of ground-based three-axis spacecraft simulator," in *Proc. of the AIAA Guidance, Navigation and Control Conference and Exhibit*, Keystone, CO, 2006, p. 6595.

[2] ——, "Automatic mass balancing of air-bearing-based three-axis rotational spacecraft simulator," *AIAA Journal of Guidance, Control, and Dynamics*, vol. 32, no. 3, pp. 1005–1017, 2009.

[3] M. Abraham and M. Costello, "In-flight estimation of helicopter gross weight and mass center location," *Journal of Aircraft*, vol. 46, pp. 1042–1049, 1995.

[4] Y. Bestaoui, "A lagrangian approach to modeling of an airship with wind and varying mass effects," in *Proc. of 48th AIAA Aerospace Sciences Meeting including the New Horizons Forum and Aerospace Exposition*, Orlando, Florida, 4-7 January 2010, p. 40.

[5] L. Chen and G. Zhou and X. J. Yan and D. P. Duan, "Composite control strategy of stratospheric airships with moving masses," *AIAA Journal of Aircraft*, vol. 49, no. 3, pp. 794–801, May-June 2012.

[6] P. Lin and J. Zhou, "Researching variable structure control of moving mass reentry-vehicles," in *Proc. of the IEEE International Conference on Computer Science and Information Technology*, Chengdu, China, 9-11 July 2010, pp. 126–129.

[7] Matt R. Jardin and Eric R. Mueller, "Optimized measurements of unmanned-air-vehicle mass moment of inertia with a bifilar pendulum," *AIAA Journal of Aircraft*, vol. 46, no. 3, pp. 763–775, May-June 2009.

[8] K. D. Kumar and A.-M. Zou, "Attitude control of miniature satellite using movable masses," in *Proc. of AIAA SpaceOps Conference Delivering on the Dream Hosted by NASA Mars*, Huntsville, Alabama, 25-31 April 2010, p. 1982.

[9] P. K. Menon and G. D. Sweriduk and E. J. Ohlmeyer and D. S. Malyevac, "Integrated guidance and control of moving-mass actuated kinetic warheads," *AIAA Journal of Guidance, Control, and Dynamics*, vol. 27, no. 1, pp. 118–126, January-February 2004.

[10] P. K. Menon and S. S. Vaddi, "Finite-horizon robust integrated guidance-control of a moving-mass actuated kinetic warhead," in *Proc. of AIAA Guidance, Navigation, and Control Conference and Exhibit*, Keystone, Colorado, 21-24 August 2006, p. 6787.

[11] Rudranarayan M. Mukherjee and J. (Bob) Balaram, "Attitude dynamics and control of moving mass multibody aeromaneuver vehicle," in *Proc. of AIAA Atmospheric Flight Mechanics Conference and Exhibit*, Honolulu, Hawaii, 18-21 August 2008, p. 6390.

[12] Y. Qianchen, Z. Qingzhen, and Z. Huiping, "A compound control system of axial moving mass and aerodynamic force for mass moment missile," in *Proc. of the IEEE International Conference on Instrumentation, Measurement, Computer, Communication and Control*, Beijing, China, 21-23 October 2011, pp. 945–948.

[13] L. Qin and M. Yang, "Moving mass attitude law based on neural networks."

[14] J. Rogers and M. Costello, "Flight dynamics and control authority of a projectile equipped with a controllable internal translating mass," in *Proc. of AIAA Atmo-*

spheric Flight Mechanics Conference and Exhibit, Hilton Head, South Carolina, 20-23 August 2007, p. 6492.

[15] ——, "A variable stability projectile using an internal moving mass," in *Proc. of AIAA Atmospheric Flight Mechanics Conference and Exhibit*, Honolulu, Hawaii, 18-21 August 2008, p. 7116.

[16] ——, "Control authority of a projectile equipped with a controllable internal translating mass," *AIAA Journal of Guidance, Control, and Dynamics*, vol. 31, no. 5, pp. 1323–1333, September-October 2008.

[17] D. Wang, J. S. Jiang, and W. H. Zhang, "Frequency optimization with respect to lumped mass position," *AIAA Journal*, vol. 41, no. 9, pp. 1780–1787, September 2003.

[18] S. Wang, M. Yang, and Z. Wang, "Moving-mass trim control system design for spinning vehicles."

[19] C. A. Woolsey and N. E. Leonard, "Moving mass control for underwater vehicles."

[20] Y. Jiang, F. He, and Y. Yao, "Hybrid control strategy for attitude stabilization of an underactuated spacecraft with two moving mass," in *Proc. of the IEEE International Conference on Automation and Logistics*, Jinan, China, 18-21 August 2007, pp. 389–393.

[21] P. K. Menon and S. S. Vaddi, "Finite-horizon robust integrated guidance-control of a moving-mass actuated kinetic warhead," in *Proc. of AIAA Guidance, Navigation, and Control Conference and Exhibit*, Keystone, Colorado, 21-24 August 2006, p. 6787.

[22] R. H. Byrne, B. R. Sturgis, and R. D. Robinett, "A moving mass trim control system for reentry vehicle guidance," in *Proc. of AIAA Atmospheric Flight Mechanics Conference*, San Diego, California, 29-31 July 1996, p. 3438.

[23] R. H. Byrne, R. D. Robinett, and B. R. Sturgis, "Moving mass trim control system design," in *Proc. of AIAA Guidance, Navigation and Control Conference*, San Diego, California, 29-31 July 1996, p. 3826.

[24] W. Okolo, A. Dogan, and W. Blake, "Aircraft lateral trim using internal fuel transfer and differential thrust in formation flight," in *Proc. of the AIAA Atmospheric Flight Mechanics Conference*, Portland, Oregon, 08-11 August 2011, p. 6613.

[25] C. S. Beaverstock, J. Fincham, M. I. Friswell, R. M. Ajaj, R. D. Breuker, and N. Werter, "Effect of symmetric and asymmetric span morphing on flight dynamics," in *Proc. of the AIAA Atmospheric Flight Mechanics Conference*, National Harbor, Maryland, 13-17 January 2014, p. 0545.

[26] Jayme Waiskek and Atilla Dogan and William Blake, "Derivation of the dynamics equations of receiver aircraft in aerial refueling," *AIAA Journal of Guidance, Control, and Dynamics*, vol. 32, no. 2, pp. 585–597, March-April 2009.

[27] M.-G. Yoon, V. A. Ugrinovskii, and M. Pszczel, "Gain-scheduling of minimax optimal state-feedback controllers for uncertain linear parameter-varying systems."

[28] D. Saussie, L. Saydy, O. Akhrif, and C. Berard, "Gain scheduling with guardian maps for longitudinal flight control," *Journal of Guidance, Control, and Dynamics*, vol. 34, no. 4, pp. 1045–1059, July-August 2011.

[29] D. Saussie, L. Saydy, and O. Akhrif, "Gain scheduling control design for a pitch-axis missile autopilot," in *Proc. of the AIAA Guidance, Navigation and Control Conference and Exhibit*, Honolulu, Hawaii, August 2008, p. 7000.

[30] Y. Hamada, T. Ohtani, T. Kida, and T. Nagashio, "Synthesis of a linearly interpolated gain scheduling controller for large flexible spacecraft ets-viii," *Control Engineering Practice*, vol. 19, no. 6, pp. 611–625, June 2011.

[31] S. Theodoulis and G. Duc., "Missile autopilot design: Gain-scheduling and the gap metric," *Journal of Guidance, Control, and Dynamics*, vol. 32, no. 3, pp. 986–996, May-June 2009.

[32] J. YU, G. LUO, and Y. MEI, "Surface-to-air missile autopilot design using lqg/ltr gain scheduling method," *Chinese Journal of Aeronautics*, vol. 24, no. 3, pp. 279–286, June 2011.

[33] S. McNamara, C. Restrepo, E. Medina, R. Whitley, R. Proud, and J. Madsen, "Gain scheduling for the orion launch abort vehicle controller," in *Proc. of the AIAA Guidance, Navigation and Control Conference*, Portland, Oregon, 08-11 August 2011, p. 6259.

[34] W. Yang, M. N. Hammoudi, G. Herrmann, M. Lowenberg, and X. Chen, "Two-state dynamic gain scheduling control applied to an f16 aircraft model," *International Journal of Non-Linear Mechanics*, vol. 47, no. 10, pp. 1116–1123, December 2012.

[35] R. Smith and A. Ahmed, "Robust parametrically varying attitude controller designs for the x-33 vehicle," in *Proc. of the AIAA Guidance, Navigation, and Control Conference*, Denver, Colorado, 14-17 August 2000, p. 4158.

[36] G.-H. Yang and K.-Y. Lum, "Gain-scheduled flight control via state feedback," in *Proc. of the American Control Conference*, Denver, Colorado, 04-06 June 2003, pp. 3484–3489.

[37] D. P. White, J. G. Wozniak, and D. A. Lawrence, "Missile autopilot design using a gain scheduling technique."

[38] A. Fujimori, Z. Wu, P. N. Nikiforuk, and M. M. Gupta, "A design of a flight control system using fuzzy gain-scheduling," in *Proc. of the AIAA Guidance, Navigation and Control Conference*, New Orleans, Louisiana, August 1997, p. 3760.

[39] C. D. C. Jones, M. H. Lowenberg, and T. S. Richardson, "Tailored dynamic gain-scheduled control," *Journal of Guidance, Control, and Dynamics*, vol. 29, no. 6, pp. 1271–1281, November-December 2006.

[40] B. CLEMENT and G. DUC, "An interpolation method for gain-scheduling," in *Proc. of the IEEE the 40th Conference on Decision and Control*, Orlando, Florida, December 2001, pp. 1310–1315.

[41] Pierre Apkarian and Richard J. Adams, "Advanced gain-scheduling techniques for uncertain systems," *IEEE Transactions on Control Systems Technology*, vol. 6, no. 1, pp. 21–32, January 1998.

[42] Jianying Gao and Hector M. Budman, "Design of robust gain-scheduled pi controllers for nonlinear processes," *Journal of Process Control*, vol. 15, no. 7, pp. 807–817, October 2005.

[43] S. Alepuz, J. Bordonau, and J. Peracaula, "A novel control approach of three-level vsis using a lqr-based gain-scheduling technique."

[44] Isaac Kaminer and Antonio M. Pascoal and Pramod P. Khargonekar and Edward E. Coleman, "A velocity algorithm for the implementation of gain-scheduled controllers," *Automatica*, vol. 31, no. 8, pp. 1185–1191, August 1995.

[45] D. A. Lawrence and W. J. Rugh, "Gain scheduling dynamic linear controllers," *Automatica*, vol. 31, no. 3, pp. 381–390, March 1995.

[46] Daniel J. Stilwell and Douglas A. Lawrence, "Sampled-data implementation of a gain scheduled controller," *International Journal of Robust and Nonlinear Control*, vol. 12, no. 9, pp. 855–868, July 2002.

[47] J. S. Shamma and M. Athans, "Gain scheduling: Potential hazards and possible remedies," *IEEE Control Systems*, vol. 12, no. 3, pp. 101–107, June 1992.

[48] ——, "Analysis of gain scheduled control for nonlinear plants," *IEEE Transactions on Automatic Control*, vol. 35, no. 8, pp. 898–907, August 1990.

[49] F. J. D. III, H. S. Kwatra, and J. S. Schwaber, "Dynamic gain scheduled process control," *Chemical Engineering Science*, vol. 53, no. 15, pp. 2675–2690, August 1998.

[50] S. R. Wells and R. A. Hess, "Multi-input/multi-output sliding mode control for a tailless fighter aircraft," *AIAA Journal of Guidance, Control, and Dynamics*, vol. 26, no. 3, pp. 463–473, May-June 2003.

[51] Gao C. and Hess R.A., "Inverse simulation of large amplitude aircraft maneuvers," *AIAA Journal of Guidance,Control,Dynamic*, vol. 16, no. 4, pp. 733–737, July 1993.

[52] F. Blanchini, "The gain scheduling and the robust state feedback stabilization problems," *IEEE Transactions on Automatic Control*, vol. 45, no. 11, pp. 2061–2070, November 2000.

[53] Eunyoung Kim, "Control and simulation of relative motion for aerial refueling in racetrack maneuver," Master's thesis, The University of Texas at Arlington, May 2007.

[54] Austin L. Smith and Donalad L. Kunz, "Dynamic coupling of the kc 135 tanker and boom for modeling and simulation," *AIAA Journal of Aircraft*, vol. 44, no. 3, pp. 1034–1039, May-June 2007.

[55] D. K.-J. Jackson, C. Tyler, and W. B. Blake, "Computational analysis of air-to-air refueling," in *Proc. of the 25th AIAA Applied Aerodynamics Conference*, Miami, Florida, 25-28 June 2007, p. 4289.

[56] A. F. Barfield and J. L. Hinchman, "An equivalent model for uav automated aerial refueling research," in *Proc. of the AIAA Modeling and Simulation Technologies Conference and Exhibit*, San Francisco, California, 15-18 August 2005, p. 6006.

BIOGRAPHICAL STATEMENT

EunYoung Kim was born in Seoul, Korea. She came to the U.S to join the university program in 2000 and pursued a bachelors degree in aerospace engineering with computer science as a double major at Iowa State University. After graduating from ISU in spring 2005, she joined the aerospace engineering graduate program at the University of Texas at Arlington in August 2005. While she worked on the Computer Aided Control Systems Design Lab with Dr. Atilla Dogan, she published a paper entitled Control of a Receiver Aircraft Relative to the Tanker in Racetrack Maneuver to the American Institute of Aeronautics and Astronautics (AIAA) in August 2006, and "Control of Simulation of Relative Motion for Aerial Refueling in Racetrack Maneuvers" to the Journal of Guidance, Control, and Dynamics (AIAA) in 2007. For her Master Thesis she published a paper entitled "Control and Simulation of Relative Motion for Aerial Refueling in Racetrack Maneuver" in May 2007. After pursuing Master degree in Aerospace Engineering from UTA she was continuing study in Doctoral program in Aerospace Engineering at UTA. After graduating from UTA she will go back to Korea and pursue fulltime research in the aerospace field.